EXPLORING UNCERTAINTIES IN THE RELATIONSHIP BETWEEN TEMPERATURE, ICE VOLUME, AND SEA LEVEL OVER THE PAST 50 MILLION YEARS

Edward Gasson,[1,2] Mark Siddall,[1] Daniel J. Lunt,[3,4] Owen J. L. Rackham,[5] Caroline H. Lear,[6] and David Pollard[7]

[1] Over the past decade, efforts to estimate temperature and sea level for the past 50 Ma have increased. In parallel, efforts to model ice sheet changes during this period have been ongoing. We review published paleodata and modeling work to provide insights into how sea level responds to changing temperature through changes in ice volume and thermal expansion. To date, the temperature to sea level relationship has been explored for the transition from glacial to interglacial states. Attempts to synthesize the temperature to sea level relationship in deeper time, when temperatures were significantly warmer than present, have been tentative. We first review the existing temperature and sea level data and model simulations, with a discussion of uncertainty in each of these approaches. We then synthesize the sea level and temperature data and modeling results we have reviewed to test plausible forms for the sea level versus temperature relationship. On this very long timescale there are no globally representative temperature proxies, and so we investigate this relationship using deep-sea temperature records and surface temperature records from high and low latitudes. It is difficult to distinguish between the different plausible forms of the temperature to sea level relationship given the wide errors associated with the proxy estimates. We argue that for surface high-latitude Southern Hemisphere temperature and deep-sea temperature, the rate of change of sea level to temperature has not remained constant, i.e., linear, over the past 50 Ma, although the relationship remains ambiguous for the available low-latitude surface temperature data. A nonlinear form between temperature and sea level is consistent with ice sheet modeling studies. This relationship can be attributed to (1) the different glacial thresholds for Southern Hemisphere glaciation compared to Northern Hemisphere glaciation and (2) the ice sheet carrying capacity of the Antarctic continent.

1. INTRODUCTION

[2] Understanding and predicting glacier and ice sheet dynamics is notoriously difficult [*Alley et al.*, 2005; *Allison et al.*, 2009], and as a result, in their fourth assessment report the Intergovernmental Panel on Climate Change did not provide sea level projections that accounted for rapid dynamical changes in ice flow [*Solomon et al.*, 2007]. The observational record contains worrying examples of nonlinear threshold type responses, such as the collapse of the Larsen B ice shelf and subsequent surging of glaciers [*De Angelis and Skvarca*, 2003; *Rignot et al.*, 2004]. However, the observational record does not help us constrain large changes to the ice sheets. Although there is no known analog to projected future warming in the paleoclimate record [*Crowley*, 1990; *Haywood et al.*, 2011], it does contain examples of large-scale changes to the ice sheets [*DeConto and Pollard*, 2003a; *Miller et al.*, 2005a]. The paleoclimate record can therefore aid understanding of ice sheet behavior and provide insight into the plausibility of large ice sheet changes in a warming world [*Scherer et al.*, 1998; *Pollard and DeConto*, 2009]. By looking to the paleoclimate record we can also attempt to better understand the relationship between different climate parameters, such as temperature, atmospheric CO_2, ice volume, and sea level [*Rohling et al.*, 2009].

[1]Department of Earth Sciences, University of Bristol, Bristol, UK.
[2]British Antarctic Survey, Cambridge, UK.
[3]BRIDGE, School of Geographical Sciences, University of Bristol, Bristol, UK.
[4]Also at British Antarctic Survey, Cambridge, UK.
[5]Bristol Centre for Complexity Sciences, University of Bristol, Bristol, UK.
[6]School of Earth and Ocean Sciences, Cardiff University, Cardiff, UK.
[7]Earth and Environmental Systems Institute, College of Earth and Mineral Sciences, Pennsylvania State University, University Park, Pennsylvania, USA.

[3] Over the past 50 million years, *eustatic sea level* has varied between ∼100 m above present in the early Eocene (∼56–49 Ma), when there was little or no land ice on Earth and the ocean basin volume was less than present [*Miller et al.*, 2005a; *Kominz et al.*, 2008; *Miller et al.*, 2009a], and 120–140 m below present [*Fairbanks*, 1989; *Yokoyama et al.*, 2000] during the *Last Glacial Maximum* (*LGM*; 19–23 ka), when there were large ice sheets in Antarctica, North America, Asia, and Europe [*Clark et al.*, 2009]. (Italicized terms are defined in the glossary, after the main text.) On this timescale, large (greater than 10 m) eustatic sea level variations have been caused predominately by changes in the volume of land ice [*Miller et al.*, 2005a]. Broadly, there have been four ice sheet states, these being (1) largely unglaciated conditions, (2) a glaciated East Antarctic, (3) interglacial conditions with additional ice sheets in the West Antarctic and Greenland (i.e., present-day conditions), and (4) glacial conditions with the additional growth of large ice sheets in the Northern Hemisphere [*de Boer et al.*, 2012]. The glaciation of the East Antarctic can also be further broken down into an intermediate state with ephemeral mountain ice caps and a fully glaciated state [*DeConto and Pollard*, 2003a; *Langebroek et al.*, 2009].

[4] The temperature range on this timescale is perhaps less well understood. Deep-sea paleoclimate proxies are commonly used to interpret past climate changes as much of the regional and seasonal changes present in surface ocean and terrestrial records are reduced by the large volume and slow recycling of the deep ocean [*Lear et al.*, 2000; *Lear*, 2007; *Sosdian and Rosenthal*, 2009]. Deep-sea temperatures (*DSTs*) in the early Eocene (50 Ma) may have been 7°C–15°C warmer than present, with a best estimate of ∼12°C [*Lear et al.*, 2000; *Zachos et al.*, 2001; *Billups and Schrag*, 2003; *Lear*, 2007]. The deep sea was ∼1.5°C–2°C cooler than present during the LGM, with further cooling limited as temperatures approached the freezing point for seawater [*Waelbroeck et al.*, 2002; *Elderfield et al.*, 2010; *Siddall et al.*, 2010a].

[5] Sea surface temperature (*SST*) proxies suggest that during the Eocene, the high latitudes were significantly warmer than present, approaching or even exceeding temperatures seen in the modern tropics [*Bijl et al.*, 2009; *Hollis et al.*, 2009; *Liu et al.*, 2009; *Bijl et al.*, 2010]. However, the lower latitudes were only a few degrees warmer than present in the Eocene [*Sexton et al.*, 2006; *Lear et al.*, 2008; *Keating-Bitonti et al.*, 2011], suggesting that there was a much reduced latitudinal temperature gradient [*Huber*, 2008; *Bijl et al.*, 2009]. During glacial conditions, the surface high latitudes show cooling [*Jouzel et al.*, 2007], with this cooling also extending to low latitudes, suggesting that there were additional feedbacks on the climate system, such as CO_2 feedbacks, in addition to orbital driven forcing [*Herbert et al.*, 2010; *Rohling et al.*, 2012].

[6] Over the past 50 Ma there have also been major tectonic changes, such as the uplift of the Himalayas following the collision of India with Asia, the opening of the Drake and Tasman passages, and the closing of the Panama seaway, which have all had an influence on the climate system [*Zachos et al.*, 2001].

1.1. Temperature to Sea Level Relationship

[7] Surface temperature is related to sea level through its control on the amount of ice stored on land and through thermal expansion. Sea level response to temperature forcing over the past 0.5 Ma has been studied using proxy data from ice cores, ocean sediments, and fossil corals [*Rohling et al.*, 2009; *Siddall et al.*, 2010a, 2010b]. However, for longer periods (10^6–10^7 years), only modeled estimates have been published, albeit constrained by data [*de Boer et al.*, 2010]. Here we use existing proxy records from the past 50 Ma to investigate the relationship and uncertainties between temperature and sea level during the transition to an "ice house" world. There are no globally representative temperature proxies on this timescale; instead, we investigate the relationship using DST and surface temperatures from high and low latitudes.

[8] When looking at this long time period, the proxy record of surface temperature is limited in both duration and spatial coverage, although records are improving with the continued development of new and existing proxies [*Lear et al.*, 2008; *Liu et al.*, 2009]. A limitation of using isolated surface temperature proxies is that there are inherent uncertainties as to whether regional and/or seasonal temperature fluctuations are being recorded [*Lear et al.*, 2000]. These potential biases are reduced in the DST record, although the DST record has other significant limitations [*Lear et al.*, 2000; *Billups and Schrag*, 2003]. DST is coupled to SST at regions of deep-water formation, which for the present day are predominantly, although not exclusively [*Gebbie and Huybers*, 2011], the high latitudes [*Zachos et al.*, 2001]. Therefore, DST proxies should not be seen as a record of past global temperature but should instead be viewed as analogous to past high-latitude surface temperature [*Zachos et al.*, 2001]. The DST record is useful when investigating the sea level to temperature relationship, as it is best coupled to the surface at regions of ice formation.

1.2. Review Outline

[9] The majority of this review is focused on the DST to sea level relationship for the past 50 Ma, as the DST record is more complete than the surface temperature record. Additionally, we investigate the surface temperature to sea level relationship over a key interval for sea level change, the *Eocene-Oligocene transition* (*EOT*). The direct translation between the DST to sea level relationship to the surface temperature to sea level relationship is dependent on the existence of a constant deep-sea to surface temperature gradient through time. We include a discussion of how the deep-sea to surface temperature gradient may have changed over the multimillion year timescale of this study because of changes in ocean circulation and changing sources of deep-water formation [*Cramer et al.*, 2009; *Katz et al.*, 2011].

[10] A number of explanations exist for the causes of glacial inception, when the first continental sized ice sheets formed on Antarctica (typically cited as occurring at the Eocene-Oligocene boundary ∼34 Ma [*Zachos et al.*, 2001]), such as regional cooling resulting from the opening of ocean gateways and the thermal isolation of Antarctica [*Kennett*,

1977; *Exon et al.*, 2001] or global cooling through declining atmospheric CO_2 [*DeConto and Pollard*, 2003a, 2003b; *Pagani et al.*, 2005]. However, a full discussion is beyond the scope of this review. Arguably, the more established hypothesis at present is that glacial inception on Antarctica resulted from global cooling, which was likely due to declining atmospheric CO_2 [*DeConto and Pollard*, 2003a, 2003b; *Huber et al.*, 2004; *Stickley et al.*, 2004; *Pagani et al.*, 2005; *Liu et al.*, 2009; *Pearson et al.*, 2009]. First we review the available sea level, temperature, and model data, then we give a synthesis of the sea level relationship with DST and the sea level relationship with SST from high and low latitudes, and finally, we explore how this has affected understanding of the evolution of ice sheets over the past 50 Ma.

2. PROXY RECORDS

[11] Long-duration (10^7 years) records of sea level, ice volume, and temperature over the past 50 Ma are limited to ocean sediment deposits. Although other proxy records exist (e.g., from isotope analysis of fossil tooth enamel [*Zanazzi et al.*, 2007] or sediment records from an incised river valley [*Peters et al.*, 2010]), these are of a too short duration to be included in this review. Long-term (10^7 years) records are presently limited to *sequence stratigraphy* records of sea level [*Miller et al.*, 2005a], *Mg/Ca* proxy records of DST [*Lear et al.*, 2000; *Billups and Schrag*, 2003], and records of oxygen isotopes ($\delta^{18}O$), which are a mixed climate signal [*Zachos et al.*, 2001]. Other proxies, such as the *tetraether index* (TEX_{86}) and the *alkenone unsaturation index* ($U^{k'}_{37}$), have been used to create intermediate-duration (10^6 years) SST records.

2.1. Sequence Stratigraphy: A Sea Level Proxy

[12] Sequence stratigraphy of *passive continental margin*s can provide a record of regional sea level over the past 50 Ma and even longer timescales [*Vail et al.*, 1977; *Haq et al.*, 1987; *Miller et al.*, 2005a; *Kominz et al.*, 2008]. Depositional sequences bounded by unconformities (periods of nondeposition and/or surfaces of erosion) show changes in regional sea level. By accurately dating sequences and inferring the past water depth during depositional phases from *lithofacies* and *biofacies* models, a quantitative estimate of sea level through time can be created (for a full discussion see *Miller et al.* [1998, 2005a], *Kominz et al.* [2008], and *Browning et al.* [2008]).

[13] *Vail et al.* [1977] developed a method for inferring global sea level by correlating sequences from multiple depositional basins. This work led to the production of the "Haq curve," which was claimed at the time to be a global eustatic record of sea level [*Haq et al.*, 1987]. *Miall* [1992] was critical of the approach used by *Haq et al.* [1987] as it assumes that the dating of sequences is accurate enough to allow for correlation across multiple depositional basins. However, the duration of some of the sequences is often less than the age error estimate. *Miall* [1992] demonstrated that sequences created using a random number generator with the same age errors could generate a good correlation with the Haq curve. It is unclear whether the sequences are the result of a global sea level signal or generated by regional processes, making correlation across multiple basins questionable [*Christie-Blick et al.*, 1988]. Other criticism has focused on the lack of availability of data that made up the Haq curve, meaning that independent verification of the record is not possible [*Miall*, 1992]. Given these fundamental weaknesses, *Miall* [1992] suggested that the Haq curve in particular should be abandoned and efforts should be focused on independent well-dated records, such as those discussed in the following.

[14] Within the last 15 years, multiple well-dated sediment cores from one region, the New Jersey (NJ) margin in the northeastern United States, have been used to create a sequence stratigraphy record of sea level over the past 10–100 Ma (sea level for 0–9 Ma in the study by *Miller et al.* [2005a] is estimated from a calibration of the $\delta^{18}O$ record as the NJ sequence stratigraphy record is incomplete from 0 to 7 Ma) [*Miller et al.*, 2005a; *Kominz et al.*, 2008] (see Figure 1). By taking into account compaction, loading, and subsidence of the sediment core (the *backstripping* method), a regional sea level record was created [*Browning et al.*, 2008]. The sequences are dated using a combination of *biostratigraphy*, *magnetostratigraphy*, and strontium isotope stratigraphy, providing age control better than ±0.5 Ma [*Kominz et al.*, 2008], which is a significant improvement on the ±3 Ma age errors of the Haq curve [*Miall*, 1992].

[15] When regional sea level drops below the level of the core hole site, there is a hiatus in the record, identified as an *unconformity*. This is a potential limitation of sequence stratigraphy because it means water depth information is restricted during *lowstands*. This is overcome in part by having multiple core hole locations from both onshore and offshore sites; however, there are still significant hiatuses in the composite record during lowstands. Although a quantitative record of water depth is limited during lowstands, it is likely that sea level was lower than surrounding highstands given the lack of sediment deposition. As shown in Figure 1, *Kominz et al.* [2008] provide "conceptual" lowstands, which highlight that sea level is lower during periods when there are no deposits; errors during these periods are significantly higher than during highstands. Here we assume generous errors of ±50 m during lowstands, based on the highest error estimate of *Miller et al.* [2005a]. The highstand sea level estimate has an associated water depth error. The errors generally increase with increasing water depth; highstand errors for the NJ sea level record are typically ±10–20 m [*Miller et al.*, 2005a].

[16] As shown in Figure 1, the NJ record shows a long-term fall in sea level of ∼100 m over the course of the past 50 Ma, which is greater than can be explained by the formation of the modern ice sheets [*Kominz et al.*, 2008; *Miller et al.*, 2009a]. Estimates of the total amount of ice stored in the modern ice sheets, in terms of sea level equivalence (ice volume divided by the ocean area and accounting for the change in volume with change in state from ice to seawater), vary from 64 to 80 m [*Lythe and Vaughan*, 2001; *Bamber et al.*, 2001; *Miller et al.*, 2005a; *Lemke et al.*,
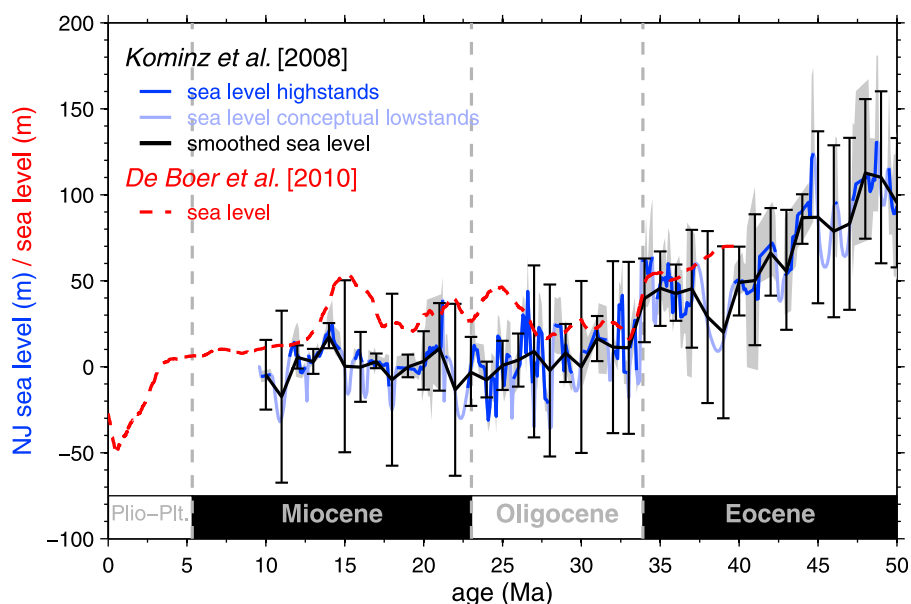
Figure 1. Sea level time series from 0 to 50 Ma. *Kominz et al.*'s [2008] regional sequence stratigraphy sea level data from the New Jersey margin (10–50 Ma), showing *highstand* data and "conceptual" low-stands (blue lines). Smoothed sea level data using a center-weighted running mean with a window size of ±0.5 Ma and interpolated to a 1 Ma temporal resolution (black line). Highstand errors (gray band) are from *Kominz et al.* [2008]; lowstand errors shown here are ±50 m, based on the highest error estimate of *Miller et al.* [2005a]. *De Boer et al.*'s [2010] sea level (red dashed line) was modeled using observation-constrained forward modeling with benthic foraminifera $\delta^{18}O$ data as input [*Zachos et al.*, 2008].

2007]. However, this is not directly relatable to the NJ sea level record. If this additional mass of water was added to the oceans, it would have an *isostatic* effect (hydroisostasy), meaning that the sea level rise visible from NJ may be ~33% less [*Pekar et al.*, 2002; *Miller et al.*, 2009a]. Therefore, assuming full isostatic adjustment (it should be noted that this hydroisostatic correction is not universally accepted [e.g., *Cramer et al.*, 2011]), only ~43–54 m of the long-term fall in the NJ record can be explained by the formation of the modern ice sheets [*Pekar et al.*, 2002; *Miller et al.*, 2005a]. Assuming that DSTs have cooled by ~12°C over the past 50 Ma (see below [*Lear et al.*, 2000; *Zachos et al.*, 2001]), ~12 m can be explained by *thermosteric* sea level fall [*Miller et al.*, 2009a]. This leaves an additional sea level fall, which by inference could be explained by an increase in ocean basin volume [*Miller et al.*, 2009a].

[17] Ocean crust production rates may have decreased since the early Cenozoic [*Xu et al.*, 2006]. Because seafloor becomes deeper as it ages, slower ocean crust production rate effectively increases ocean basin volume [*Xu et al.*, 2006]. This is not consistent with the results of *Rowley* [2002], which suggested ocean crust production rates, and therefore ocean basin volume, have not varied significantly over the past 180 Ma. *Müller et al.* [2008] reconstructed ocean basin volume using marine geophysical data. Their data did suggest a decrease in sea level caused by an increase in ocean basin volume since 50 Ma of ~20 m. It should be noted that their reconstruction significantly differs from the NJ record on longer timescales [*Müller et al.*, 2008], as discussed below. This combined total of ~75–86 m does

not close the long-term NJ sea level budget and may suggest that the record contains other components.

[18] For multiple reasons, a sea level record from any single coastal area should be viewed as a record of regional sea level rather than a record of global eustatic sea level [*Kominz et al.*, 2008]. This is because in addition to sea level changes resulting from the movement of water to and from storage as ice on land, the variation in the ocean basin volume, and the thermal expansion of water, there are regional effects that may be recorded [*Pekar et al.*, 2002]. If a continental plate moves vertically, e.g., as a result of ice loading, this will be seen as a sea level change in the record [*Peltier*, 1974]. Isostasy due to ice loading will not have affected the NJ record over the period of 10–100 Ma as it is unlikely that large-scale North American glaciation occurred prior to the Plio-Pleistocene. Even though the margin has subsequently been subject to isostasy, the preserved record of water depth was formed free from a glacioisostatic signal. However, there are other tectonic effects that may pose a challenge to the sequence stratigraphy method and that may be contained in the NJ sea level record [*Kominz et al.*, 2008].

[19] It has been suggested that northeast America has subsided since the Late Cretaceous, as the continent over-rode the subducted Farallon slab [*Conrad et al.*, 2004; *Spasojević et al.*, 2008]. This would have been synchronous with declining sea level since the Late Cretaceous highstand, having the effect of masking some of the sea level decline in the NJ record [*Müller et al.*, 2008]. This subduction could explain the discrepancy between the sea level estimates of *Müller et al.* [2008], based on the reconstruction of basin

volume from geophysical data, and the NJ record of *Miller et al.* [2005a]. If the NJ margin did subside because of this mechanism, it would only affect the sea level record on long timescales (10^7–10^8 years). This should be too slow to be confused with the more rapid glacioeustatic signal in the record [*Miller et al.*, 2005a], but it may still have contributed to the broad sea level trend of the last 50 Ma.

[20] More recently, *Petersen et al.* [2010] suggested that on intermediate timescales (2–20 Ma) small-scale convection in the mantle could generate vertical plate movements. Using a 2-D thermomechanical model, *Petersen et al.* [2010] demonstrated that vertical plate movements on the order of ~30 m were possible on intermediate timescales. Such convective cycles could generate sedimentary deposits, due to variations in water depth, which could be misinterpreted as being caused by eustatic sea level fluctuations [*Petersen et al.*, 2010].

[21] Another potential source of local sea level change in the NJ record is due to gravitational and Earth rotational effects. There is a gravitational effect between an ice sheet and the surrounding ocean that influences relative sea levels on a global scale [*Mitrovica et al.*, 2001, 2009; *Raymo et al.*, 2011]. Because of this gravitational effect, when a large ice sheet melts its mass is not evenly redistributed across the oceans. Sea level local to an ice sheet can therefore fall once the ice sheet has melted [*Mitrovica et al.*, 2001, 2009]. For the NJ region if the Antarctic ice sheet melted, the local sea level change would be greater than if the volume were evenly distributed across the oceans. In addition to the gravitational effect there are other feedbacks from this redistribution of mass, through influences on the Earth's rotation and solid Earth deformation [*Mitrovica et al.*, 2001, 2009]. As there have been large changes in the size of the ice sheets, this gravitational effect will be present in the NJ record and is another source of uncertainty.

[22] In order to test the NJ sequence stratigraphy record, additional sea level curves from well-dated deposits from multiple regions need to be generated. The NJ sequence stratigraphy record should be viewed as a regional sea level record that needs to be tested with additional data from other locations. Sequence stratigraphy data from the Russian platform agree well with the NJ record [*Sahagian and Jones*, 1993], although the Russian platform data are only for the Late Cretaceous and earlier. When applied to the late Pleistocene (10–130 ka), the sequence stratigraphy sea level record from NJ compares well against other sea level proxies, such as fossil corals [*Wright et al.*, 2009]. Additional sequence stratigraphy records are being assembled from expeditions to Australia and New Zealand, and this should provide further tests for the NJ record [*Kominz et al.*, 2008; *John et al.*, 2011]. Results from the northeastern Australian margin show large amplitude sea level changes in the Miocene, with events at 14.7 Ma and 13.9 Ma showing a larger sea level change than is evident in the NJ record [*John et al.*, 2011].

2.2. Temperature Proxies

[23] Proxy methods for calculating paleo-SSTs include the tetraether index (TEX_{86}) [*Wuchter et al.*, 2004], the alkenone unsaturation index ($U^{k'}_{37}$) [*Brassell et al.*, 1986], and the Mg/Ca ratio of planktic (surface-dwelling) *foraminifera*. The Mg/Ca proxy can also be used for benthic (bottom-dwelling) species of foraminifera to calculate DSTs [*Nürnberg et al.*, 1996]. Long-timescale (10^7 years) temperature records are currently limited to Mg/Ca records of benthic foraminifera [*Lear et al.*, 2000; *Billups and Schrag*, 2003]; for intermediate timescales (10^6 years) there are additional DST records using Mg/Ca and SST records using all of the proxies mentioned above for multiple regions over a variety of time periods. We do not cover all of the time periods where intermediate timescale records are available but focus on the EOT.

2.2.1. Mg/Ca Temperature Proxy

[24] Magnesium ions (Mg^{2+}) can be incorporated into the calcite ($CaCO_3$) tests of foraminifera, substituting for calcium; the amount incorporated shows a temperature-dependent relationship [*Nürnberg et al.*, 1996]. Both core top samples and culturing experiments show that the Mg/Ca ratio of foraminiferal calcite increases with water temperature [*Nürnberg et al.*, 1996; *Rosenthal et al.*, 1997; *Lea et al.*, 1999; *Anand et al.*, 2003]. The Mg/Ca ratios of suitable species of both benthic and planktic foraminifera can therefore be used as a proxy of DST and SST, respectively.

[25] A potential source of error in the Mg/Ca proxy, which is also relevant to other stable isotope proxies using foraminifera, is postmortem changes to the geochemical signal (diagenesis) [*Savin and Douglas*, 1973; *Brown and Elderfield*, 1996; *Rosenthal et al.*, 2000; *Sexton et al.*, 2006; *Lear*, 2007]. This source of error can be minimized by carefully selecting well-preserved samples, using multiple proxies, correcting for known effects, and rejecting samples that are at high risk to diagentic processes [*Rosenthal et al.*, 2000; *Rosenthal and Lohmann*, 2002; *Sexton et al.*, 2006; *Lear*, 2007]. *Billups and Schrag* [2003], however, suggest that perhaps the largest source of uncertainty in the Mg/Ca paleotemperature proxy is due to temporal changes in the seawater Mg/Ca ratios from changes in Mg^{2+} and Ca^{2+} cycling in the oceans, as discussed below.

[26] Because of the residence times of Mg^{2+} and Ca^{2+} ions in the oceans of ~10 Ma and ~1 Ma, respectively, when used on long timescales (10^7 years), the absolute Mg/Ca temperature estimates may contain errors [*Lear et al.*, 2000; *Billups and Schrag*, 2003; *Lear*, 2007]. To account for this, the Mg/Ca temperature estimates can be corrected for variations in seawater Mg/Ca [e.g., *Lear et al.*, 2000; *Lear*, 2007; *Creech et al.*, 2010].

[27] Reconstruction of past seawater Mg/Ca can be made through proxy measurements or modeling of the causes of variation in the ion concentrations. *Lowenstein et al.* [2001] reconstructed past seawater Mg/Ca using fluid inclusions in marine halites. Their data suggest that seawater Mg/Ca has increased over the past 50 Ma from initial values of 2.5–3.5 mol mol^{-1} to the present-day value of 5.2 mol mol^{-1}. This was slightly higher than the reconstructed estimate of ~2 mol mol^{-1} at 50 Ma using fossil enchinoderms [*Dickson*, 2002]. This lower estimate was supported by an alternative reconstruction using measurements of $CaCO_3$

veins recovered from oceanic crust. These estimates suggest seawater Mg/Ca was relatively constant prior to 24 Ma at 1.5–2.5 mol mol^{-1} before increasing toward the modern value [*Coggon et al.*, 2010]. Modeled estimates of past seawater Mg/Ca vary, with one model suggesting that ratios increased approximately linearly from a value of 3.85 mol mol^{-1} at 50 Ma [*Wilkinson and Algeo*, 1989]. To account for this variability, the Mg/Ca paleotemperatures can be calculated using these different seawater Mg/Ca scenarios [*Lear*, 2007].

[28] *Creech et al.* [2010] looked at multiple SST proxies in the early Eocene, including Mg/Ca and TEX$_{86}$. They used various seawater Mg/Ca scenarios and suggested a lower limit for seawater Mg/Ca of ~2 mol mol^{-1} in the early Eocene (with preferred scenarios ranging from 2.24 to 3.35 mol mol^{-1}) in order to reconcile the Mg/Ca SSTs with TEX$_{86}$ SSTs [*Creech et al.*, 2010]. Because of these uncertainties regarding the past seawater concentration of Mg/Ca, absolute Mg/Ca temperatures on long timescales (10^7 years) should be interpreted with caution [*Billups and Schrag*, 2003; *Lear*, 2007]. The Mg/Ca proxy is much more reliable when looking at relative Mg/Ca temperature changes over shorter (10^6 years) intervals [*Lear*, 2007].

[29] *Lear et al.* [2000] created a DST record from Mg/Ca ratios of benthic foraminifera from four sites. This provided a record of DSTs over the past 50 Ma, with an age resolution of ~1 Ma. *Lear* [2007] calculated a window of DST estimates, based on *Lear et al.*'s [2000] data (shown in Figure 2), using seawater Mg/Ca varying from 1.5 mol mol^{-1} to 5.2 mol mol^{-1} at 50 Ma, which then linearly increases to present day. The modeled seawater Mg/Ca estimate of *Wilkinson and Algeo* [1989, Figure 16f] produces Eocene DSTs that are in closest agreement with oxygen isotope records assuming an ice-free world, although this benthic δ^{18}O temperature estimate also contains an associated error due to uncertainties in estimating the δ^{18}O of seawater for an ice-free world. Since this early work, there have been numerous higher-resolution benthic Mg/Ca records published, spanning various portions of the Cenozoic. For example, *Billups and Schrag* [2003] used the Mg/Ca proxy to obtain DST records over the past 50 Ma from Ocean Drilling Program (ODP) Sites 757 and 689. Additional Paleogene (65.5–23 Ma) Mg/Ca records include those from Pacific ODP Sites 1218 and 1209 [*Lear et al.*, 2004; *Dutton et al.*, 2005; *Dawber and Tripati*, 2011], and additional Neogene (23–0.05 Ma) records include those from ODP Sites 761 and 1171 [*Shevenell et al.*, 2008; *Lear et al.*, 2010].

2.2.2. Surface Temperature Proxies: TEX$_{86}$ and U$^{k'}_{37}$

[30] Alkenones are highly resistant compounds found in sediments from all of the ocean basins and preserved in sediments spanning back to the Eocene and even earlier [*Boon et al.*, 1978; *Marlowe et al.*, 1990; *Müller et al.*, 1998]. They are synthesized by a very limited number of species of phytoplankton, such as the widespread *Emiliania huxleyi* in the modern ocean [*Volkman et al.*, 1980; *Marlowe et al.*, 1990]. The reason alkenones are synthesized by these species of phytoplankton remains unknown [*Conte et al.*, 1998; *Herbert*, 2003]. The degree of unsaturation in the

alkenone molecules, i.e., the number of double bonds, correlates with the temperature at synthesis [*Marlowe*, 1984]. The degree of alkenone unsaturation was used in a pioneering study to show late Pleistocene climate cycles [*Brassell et al.*, 1986]. A simplified alkenone unsaturation index (U$^{k'}_{37}$) was developed as a measure of the degree of alkenone unsaturation and then calibrated to temperature, from laboratory culturing studies and core top analysis [*Prahl and Wakeham*, 1987; *Sikes et al.*, 1991; *Müller et al.*, 1998]. The index can be used for temperatures ranging from ~1°C to 28°C, meaning that it cannot be used for extremely cool or warm regions and climates [*Herbert*, 2003]. As alkenones are well preserved in ocean sediments, the alkenone unsaturation index is a useful proxy for past SST, although we note that high temperatures at low latitudes might be particularly challenging [*Brassell et al.*, 1986; *Prahl and Wakeham*, 1987; *Müller et al.*, 1998; *Liu et al.*, 2009; *Herbert et al.*, 2010].

[31] The modern producers of alkenones have evolved relatively recently. For example, the species *E. huxleyi* evolved in the late Pleistocene, although alkenones are found in much older sediments [*Marlowe et al.*, 1990]. This has implications for using the U$^{k'}_{37}$ index further back in time, as the index is calibrated against alkenone samples produced by modern species of phytoplankton [*Herbert*, 2003]. A morphologic study suggested that modern alkenone producers share a common evolutionary pathway, evolving from, or belonging to, the same family, *Gephyrocapsaceae*, dating back to at least the Eocene, ~45 Ma. The relationship between producers of alkenones in even older sediments, from the Cretaceous, and modern species is less well understood [*Marlowe et al.*, 1990]. Furthermore, the form of alkenones found in these older sediments differs from modern alkenones [*Herbert*, 2003]. The U$^{k'}_{37}$ index has been used to estimate SST for the Eocene [*Bijl et al.*, 2010], although it is unlikely that the index would remain valid on even older sediments [*Herbert*, 2003].

[32] In addition to temperature, the degree of alkenone unsaturation also shows sensitivity to other factors, such as light [*Prahl et al.*, 2003]. Modern producers of alkenones live at various depths in the photic zone, and alkenones produced at greater depths could generate U$^{k'}_{37}$ temperatures cooler than the annual mean SST [*Prahl et al.*, 2001]. Additionally, the production rate of alkenones varies over an annual cycle, typically peaking in the spring or summer months, meaning that temperatures may not represent the mean annual temperature but may be slightly biased to warmer months [*Prahl et al.*, 1993; *Sprengel et al.*, 2000]. This seasonal bias generally increases with increasing latitude [*Sikes et al.*, 1997; *Ternois et al.*, 1998; *Herbert*, 2003; *Sikes et al.*, 2009]. The potential impacts of these external factors have been studied in detail through culturing studies, performing core top analysis, and using sediment traps (see *Herbert* [2003] for review).

[33] More recently, another organic paleothermometer has been developed, based on the composition of the membrane lipids of *Thaumarchaeota* (formerly classed as Crenarchaeota [*Brochier-Armanet et al.*, 2008]), a group of single
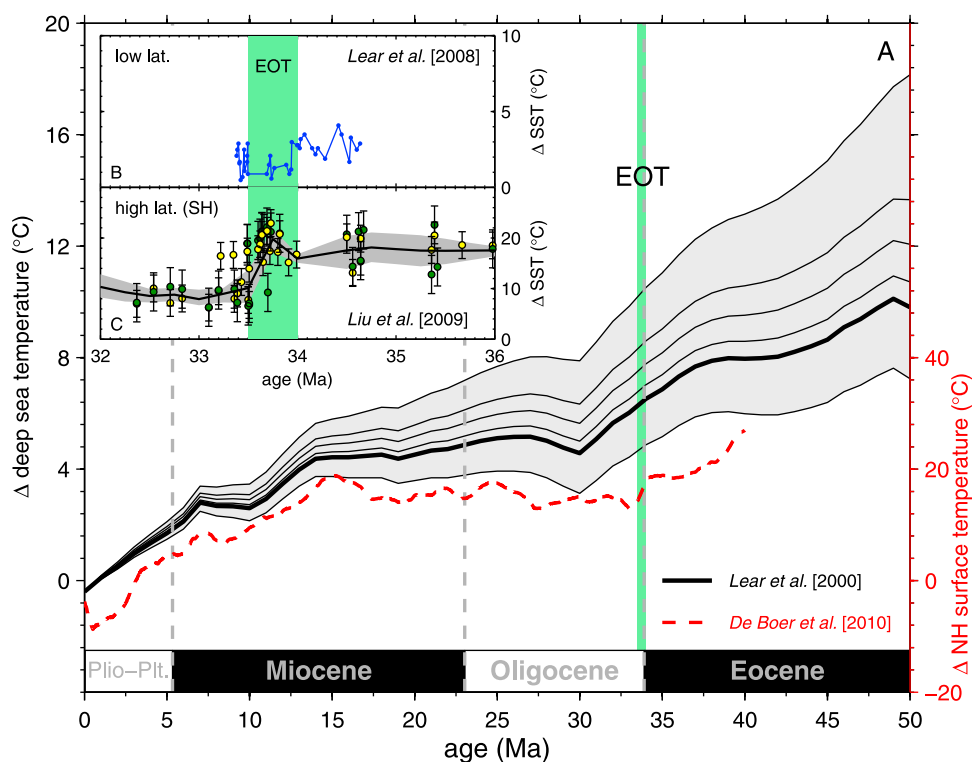
Figure 2. Temperature time series for both deep-sea and surface temperatures. (a) Both deep-sea temperature from Mg/Ca of benthic foraminifera [*Lear et al.*, 2000] (black lines) and Northern Hemisphere surface temperature from observation-constrained forward modeling [*de Boer et al.*, 2010] (red dashed line). *De Boer et al.*'s [2010] temperature is scaled so that it can be read on both axes using the deep-sea to Northern Hemisphere surface temperature parameter of *de Boer et al.* [2010]. The error envelope for *Lear et al.*'s [2000] data is for different seawater Mg/Ca scenarios from a constant scenario (low estimate) to a linearly increasing seawater Mg/Ca concentration from a value of 1.5 mol mol^{-1} at 50 Ma (high estimate) to present day. The thick line is the best estimate scenario of *Lear et al.* [2000] for a seawater Mg/Ca value at 50 Ma of 3.85 mol mol^{-1} linearly increasing to present. (b) EOT low-latitude sea surface temperature from Mg/Ca of planktic foraminifera from Tanzania [*Lear et al.*, 2008], shown here as an anomaly relative to a modern SST value of 27.1°C, taken from the coast immediately to the east of the core site. (c) EOT high-latitude Southern Hemisphere sea surface temperature, from TEX$_{86}$ (green dots) and U$^{k'}_{37}$ (yellow dots). Data are shown as an anomaly relative the modern SST for the paleolocation of each site [*Liu et al.*, 2009, supplementary information]; this differs from the work by *Liu et al.* [2009], where the data are presented as an anomaly relative to the pre-EOT mean for each site and includes additional Northern Hemisphere high-latitude sites. The best fit is calculated using a local weighted regression, with a weighting of 15%.

celled microorganisms. One group of membrane lipids biosynthesized by Thaumarchaeota are glycerol dialkyl glycerol tetraethers (GDGTs) [*Schouten et al.*, 2002]. The number of cyclopentane rings in the GDGTs shows a strong correlation with temperature at synthesis [*Schouten et al.*, 2002; *Wuchter et al.*, 2004]. It is thought that Thaumarchaeota can change the relative amounts of the different GDGTs (containing different numbers of cyclopentane rings) in their membranes, to allow changes to the membrane lipid fluidity, in response to changing temperature [*Sinninghe Damsté et al.*, 2002]. The TEX$_{86}$ index was developed as a measure of the relation between the distribution of GDGTs and the temperature at synthesis [*Schouten et al.*, 2002; *Wuchter et al.*, 2004]. The calibration has been further refined, although there is still debate as to what calibration is most appropriate, especially at extremely high (>30°C) and low

(<5°C) temperatures [*Kim et al.*, 2008; *Liu et al.*, 2009; *Kim et al.*, 2010]. The main advantages that the TEX$_{86}$ proxy has over the U$^{k'}_{37}$ proxy are that it can be used for higher temperatures than U$^{k'}_{37}$ and can be used further back in time, when low alkenone concentrations and uncertainties over the evolution of alkenone producers limit the use of the U$^{k'}_{37}$ proxy.

[34] Although the TEX$_{86}$ proxy has some advantages over the U$^{k'}_{37}$ proxy, it also has significant weaknesses. Thaumarchaeota are not restricted to the photic zone but are distributed throughout the ocean depths [*Karner et al.*, 2001]. Therefore, it seems unusual that the TEX$_{86}$ index shows such a strong correlation with SST [*Huguet et al.*, 2006]. The cells of Thaumarchaeota are too small to sink to the ocean floor postmortem; therefore, the TEX$_{86}$ signal must be transported to the ocean sediments in another way.

A likely mechanism is that Thaumarchaeota are consumed and the TEX_{86} signal is incorporated into marine snow. As most food webs are active in the upper ocean, this would also explain why TEX_{86} is well correlated with SST [*Wuchter et al.*, 2005, 2006; *Huguet et al.*, 2006]. Support for this interpretation comes from sediment traps set up at different depths, with measurements from deeper sediment traps reflecting SST rather than the ambient ocean temperature [*Wuchter et al.*, 2005, 2006]. A core top calibration using samples from multiple regions and ocean depths suggested that the TEX_{86} signal is strongly coupled to mixed layer temperatures, at depths of 0–30 m [*Kim et al.*, 2008]. However, another study suggested TEX_{86} temperatures cooler than actual SST, implying that for certain regions the TEX_{86} signal might originate in the subsurface [*Huguet et al.*, 2007].

[35] Potential seasonal biases affect the TEX_{86} proxy as well as the $U^{k'}_{37}$ proxy. Sediment trap studies suggest that the peak concentration of GDGTs occurs in the winter and spring months [*Wuchter et al.*, 2005], but when the TEX_{86} index is applied in sediment trap and core top studies the signal appears to be predominantly an annual mean [*Wuchter et al.*, 2005; *Kim et al.*, 2008]. Both TEX_{86} and $U^{k'}_{37}$ may be subject to alteration due to diagenesis [*Huguet et al.*, 2009] and contamination from secondary inputs [*Thomsen et al.*, 1998; *Weaver et al.*, 1999; *Weijers et al.*, 2006], although the diagenetic pathways differ [*Liu et al.*, 2009]. Alkenones can be transported laterally and can also be recycled from sediments, placing fossil alkenones or alkenones synthesized in different environments onto core tops and potentially biasing $U^{k'}_{37}$ temperature estimates [*Thomsen et al.*, 1998; *Weaver et al.*, 1999]. GDGTs are also found in soils and can be transported to ocean basins by rivers, potentially affecting the TEX_{86} proxy for sites near river outflow [*Weijers et al.*, 2006]. Enclosed settings may show calibration lines that are offset from open ocean calibration lines, which suggests that different source populations may exist [*Trommer et al.*, 2009, 2011]. To improve SST estimates and to reduce the impact of secondary effects on temperature signals, it is desirable to use multiple proxies whenever possible [*Liu et al.*, 2009].

2.2.3. Temperature Time Series

[36] Figure 2 shows different temperature records generated using the proxies discussed above, including the Mg/Ca DST record of *Lear et al.* [2000] and high- and low-latitude SST records for the EOT [*Lear et al.*, 2008; *Liu et al.*, 2009]. Although existing Mg/Ca DST records show a net cooling throughout the Eocene, at face value they show either no significant cooling or even warming at the EOT [*Lear et al.*, 2000; *Billups and Schrag*, 2003; *Lear et al.*, 2004; *Peck et al.*, 2010; *Pusz et al.*, 2011]. This is not consistent with the cooling that might be expected during a period of rapid ice growth [*Coxall and Pearson*, 2007]. The lack of cooling in the Mg/Ca records at the EOT initially led to the hypothesis that the majority of the oxygen isotope $\delta^{18}O$ shift at the EOT is due to an increase in ice mass [*Lear et al.*, 2000] (also see section 2.3 on $\delta^{18}O$). This would necessitate the growth of a greater ice mass than could be accommodated on

Antarctica, implying that Northern Hemisphere ice sheets formed much earlier in the Cenozoic than previously thought [*Coxall et al.*, 2005]. Additional evidence for Northern Hemisphere glaciation (albeit as isolated glaciers) much earlier in the Cenozoic was found in *ice-rafted debris* (*IRD*) deposits from the Arctic Ocean [*Moran et al.*, 2006] and off the coast of Greenland [*Eldrett et al.*, 2007]. However, it has also been shown that Antarctic land area at the EOT could have been greater than at present, meaning that more of the $\delta^{18}O$ increase can be explained by the growth of Antarctic ice in combination with cooling [*Wilson and Luyendyk*, 2009]. In addition, modeling studies suggest that atmospheric CO_2 concentrations were above the threshold for bipolar glaciation at this time [*DeConto et al.*, 2008].

[37] More recently, the lack of apparent cooling witnessed in the deep-sea EOT Mg/Ca records has been attributed to secondary effects in the Mg/Ca proxy related to the synchronous deepening of the *calcite compensation depth* (*CCD*) [*Lear et al.*, 2004; *Coxall et al.*, 2005]. In addition to the dominant control on Mg/Ca ratios recorded in foraminifera, changes in temperature, the ratio is also affected by the degree of carbonate saturation of seawater [*Martin et al.*, 2002]. This secondary control could become significant during large changes in carbonate saturation, such as the lowering of the CCD at the EOT [*Lear et al.*, 2004].

[38] Support for this hypothesis is found from Mg/Ca data from a shallow water site well above the paleo-CCD, which show a ~2.5°C cooling across the EOT, shown in Figure 2b [*Lear et al.*, 2008]. Additional evidence for this explanation is found in other deep-sea, surface, and terrestrial temperature proxies that also show a cooling across the EOT [*Dupont-Nivet et al.*, 2007; *Zanazzi et al.*, 2007; *Katz et al.*, 2008; *Liu et al.*, 2009; *Eldrett et al.*, 2009]. *Liu et al.* [2009] undertook a modeling study based on their surface temperature results in order to estimate deep-sea cooling. The model was able to reproduce the observed high-latitude surface cooling (~5°C), and their model generated a deep-sea cooling of ~4°C across the EOT. This deep-sea cooling could be even greater as *Liu et al.* [2009] suggest their (~5°C) high-latitude surface cooling may be a low estimate. Recent work attempting to correct for the simultaneous influence of changing seawater saturation state on the EOT deep-sea Mg/Ca records implies a deep-sea cooling on the order of 1.5°C, although this estimate will likely be refined as understanding of trace metal proxies advances [*Lear et al.*, 2010; *Pusz et al.*, 2011]. This 1.5°C of deep-sea cooling across the EOT is considerably less than the modeled deep-sea cooling suggested by *Liu et al.* [2009].

[39] Although the modeling study of *DeConto et al.* [2008] did not support bipolar glaciation at the EOT, it did suggest that, based on the proxy CO_2 records of *Pearson and Palmer* [2000] and *Pagani et al.* [2005], the CO_2 threshold for bipolar glaciation was crossed ~25 Ma, meaning that ephemeral Northern Hemisphere ice sheets may have been present much earlier than previously thought. This potentially means that some of the sea level variations during the Miocene could be explained by changes in Northern Hemisphere ice mass. However, this is not

consistent with the modeling work of *de Boer et al.* [2010, 2012], who suggested that the threshold for Northern Hemisphere glaciation was not reached in this period and that sea level variation in the Miocene was caused by the Antarctic ice sheets.

[40] The high-latitude SST record of *Liu et al.* [2009] is shown in Figure 2c. The cooling shown in Figure 2c at the EOT is greater than the ∼5°C of cooling suggested by *Liu et al.* [2009] in their original analysis. *Liu et al.* [2009] presented the data as a temperature anomaly relative to the mean temperature for each site prior to the EOT. The data are shown here as a temperature anomaly relative to modern temperatures at the paleolocation for the respective sites [*Liu et al.*, 2009, supplementary information]. Only Southern Hemisphere sites are included to allow comparison with Pleistocene Southern Hemisphere data in the later analysis.

[41] The surface temperature records in Figures 2b and 2c show pre-EOT temperatures significantly warmer than present in the Southern Hemisphere high latitudes and temperatures only a few degrees warmer in the low latitudes. This reduced latitudinal temperature gradient (which is even more pronounced in the early Eocene [*Bijl et al.*, 2009]) presents a paradox: to explain the very warm temperatures in the high latitudes suggests increased heat transport from the equator to the poles; however, the reduced temperature gradient evident from data implies a reduced transport of heat from the equator to the poles [*Huber*, 2008]. A full exploration of this paradox is beyond the scope of this review, but it should be noted that this reduced latitudinal temperature gradient in the Eocene remains a significant area of disagreement between data and climate models [*Hollis et al.*, 2009].

[42] *Lear et al.*'s [2000] DST record shows little temperature variation during the early Miocene, before a gradual cooling at ∼15 Ma that continues into the Pliocene. This is partly because the resolution of this record is particularly low in the Miocene and is unable to pick out the DST variations observed in higher-resolution Mg/Ca records [e.g., *Shevenell et al.*, 2008; *Lear et al.*, 2010]. Other paleoclimate proxies, notably the $\delta^{18}O$ record from benthic foraminifera (see section 2.3), suggest deep-sea warming and/or a decrease in ice volume into the Miocene followed by deep-sea cooling and/or an increase in ice volume from the middle to late Miocene [*Zachos et al.*, 2008]. Regional terrestrial paleoclimate proxies also show a return to a warmer climate in the middle Miocene followed by cooling in the late Miocene [*Utescher et al.*, 2007, 2009, 2011]. A prominent example of the effect of terrestrial warming into the Miocene is the change in distribution of crocodilians, which after being restricted to the lower latitudes during the Oligocene, returned to higher latitudes of North America in the Miocene. On the basis of modern climate distributions of crocodilians, the fossil crocodilian record suggests terrestrial warming in the Miocene following on from a cooler period in the Oligocene [*Markwick*, 1998]. Modeling studies, although not fully consistent with proxy data, have also simulated the warmth of the middle Miocene followed by cooling to the late Miocene [*Micheels et al.*, 2007; *You et al.*, 2009].

[43] The temporal resolution of *Lear et al.*'s [2000] data set is also too low to resolve the glacial-interglacial cycles of the Quaternary. In this review we will focus on the data set of *Lear et al.* [2000] for the period 10–50 Ma because of its long duration and as it appears to pick out the broad DST variations of the Cenozoic, although we acknowledge the limitations of this low-resolution multisite data set. Although *Lear et al.*'s [2000] record does not show a pronounced cooling at the EOT, it does not show a warming as *Billups and Schrag*'s [2003] record does, which subsequent records suggest is unlikely [*Dupont-Nivet et al.*, 2007; *Zanazzi et al.*, 2007; *Lear et al.*, 2008; *Liu et al.*, 2009; *Lear et al.*, 2010]. Additionally, *Billups and Schrag*'s [2003] data from the Indian Ocean (ODP 757) show little DST variation from the Miocene onward and generates unrealistically high DSTs for the Plio-Pleistocene. We supplement our analysis with the higher-resolution SST data sets [*Lear et al.*, 2008; *Liu et al.*, 2009] across the EOT.

2.2.4. Deep-Sea to Surface Temperature Gradient

[44] Surface temperature changes reach the deep sea primarily at regions of deep-water formation, which is predominantly in the high-latitude regions [e.g., *Zachos et al.*, 2001]. DST records are therefore suited to a review of the relationship between temperature and sea level as DST is strongly coupled to the surface climate at regions of ice formation. However, the coupling between the deep sea and the surface may not have remained constant through time. As previously discussed, there is a significant discrepancy between the DST records, based on Mg/Ca, and the surface records of temperature across the EOT due to secondary effects [*Lear et al.*, 2000, 2004; *Liu et al.*, 2009; *Eldrett et al.*, 2009]. In addition, changes in ocean circulation and stratification over the past 50 Ma may have affected the deep-sea to surface temperature gradient and may explain some of the changes in DST [*Cramer et al.*, 2009; *Katz et al.*, 2011].

[45] The Drake Passage opened and then gradually widened and deepened in the middle Eocene through the Oligocene as South America separated from Antarctica [*Kennett*, 1977; *Nong et al.*, 2000]. This opening, in addition to the opening of the Tasman gateway between Antarctica and Australia in the late Eocene to early Oligocene, led to the development of the Antarctic Circumpolar Current (ACC). Modeling studies suggest that the development of the ACC caused a reorganization of ocean currents, leading to a warming of ∼3°C–4°C of the high-latitude Northern Hemisphere surface waters and a cooling of a similar magnitude in the high-latitude Southern Hemisphere surface waters [*Toggweiler and Bjornsson*, 2000; *Nong et al.*, 2000; *Najjar et al.*, 2002]. These model results suggest that the deep sea also cooled by ∼2°C–3°C, a slightly lower magnitude than the surface southern high latitudes [*Nong et al.*, 2000; *Najjar et al.*, 2002].

[46] It is possible that feedbacks from the formation of a continental sized *East Antarctic Ice Sheet* (*EAIS*) across the EOT generated regional cooling and enhanced sea ice cover [*DeConto et al.*, 2007]. If this enhanced cooling were transmitted to the deep sea, this could explain why the $\delta^{18}O$

shift across the EOT is greater in deep-sea records than low-latitude surface records [*Pearson et al.*, 2008; *Lear et al.*, 2008]. This change in ocean currents due to the opening of gateways, and potentially the regional cooling due to the formation of the EAIS and enhanced sea ice cover, may have changed the surface to DST gradient. However, the coupling between the deep sea and the surface is still strongest with the regions of major ice formation during the study period, the high-latitude Southern Hemisphere. The ocean restructuring that occurred during this period may also have generated interbasinal divergence [*Cramer et al.*, 2009; *Katz et al.*, 2011], which is discussed in more detail in section 2.3 and has potential implications for multibasin composite proxy records such as the deep-sea Mg/Ca record of *Lear et al.* [2000].

2.3. Benthic Oxygen Isotopes and Ice Volume

[47] The oxygen isotope composition of foraminiferal calcite provides a record of climate changes throughout the Cenozoic. The three stable isotopes of oxygen, ^{16}O, ^{17}O, and ^{18}O, have natural abundances of 99.76%, 0.04%, and 0.20%, respectively [*Rohling and Cooke*, 1999]. The ratio of ^{18}O to ^{16}O is generally the more useful for climate research because of the higher natural abundance of ^{18}O compared to ^{17}O and the greater mass difference between ^{18}O and the predominant ^{16}O. A sample is analyzed using a mass spectrometer and conventionally presented using delta (δ) notation relative to an international standard, which is also analyzed [*Rohling and Cooke*, 1999]. During evaporation of water from the ocean, fractionation occurs because of preferential evaporation of the lighter ^{16}O isotope. Therefore, freshwater removed from oceans by evaporation has a low isotopic ratio relative to the source seawater. Fractionation also occurs during condensation, with the heavier ^{18}O isotope preferentially condensed. As atmospheric vapor is transported away from its source region, condensation during transport means the remaining vapor becomes more and more depleted in ^{18}O. Rainout from atmospheric vapor that has been transported a long way, i.e., from the low to high latitudes, will be very depleted in ^{18}O [*Dansgaard*, 1964]. The buildup of ice sheets from isotopically light (depleted in ^{18}O) precipitation, and subsequent storage of ^{16}O in ice sheets, will cause the oceans to become enriched in ^{18}O. The $\delta^{18}O$ values of seawater are therefore affected by storage of the lighter ^{16}O isotope in ice sheets [*Shackleton*, 1967]. In addition to this ice volume component, temperature-dependent fractionation occurs when the oxygen isotopes are incorporated into calcite tests of foraminifera [*Urey*, 1947]. Increases in benthic foraminiferal $\delta^{18}O$ suggest deep-sea cooling and increased ice storage on land [*Zachos et al.*, 2001].

[48] Benthic foraminiferal $\delta^{18}O$ data from multiple sites have been compiled to create $\delta^{18}O$ stacks [*Miller et al.*, 1987; *Zachos et al.*, 2001; *Lisiecki and Raymo*, 2005; *Zachos et al.*, 2008]. The compilation of *Zachos et al.* [2008] is shown in Figure 3. Starting in the early Eocene, Figure 3 shows a broad increase in benthic $\delta^{18}O$ throughout the Eocene with a rapid but brief reversal in the $\delta^{18}O$ trend at ∼40 Ma, a period known as the *Middle Eocene Climatic*

Optimum (MECO [*Zachos et al.*, 2008]). A significant transition at the EOT is seen as an abrupt increase in benthic $\delta^{18}O$ of ∼1.5‰, due to ice growth and/or declining DST [*Zachos et al.*, 2008; *Liu et al.*, 2009]. The most established view of the evolution of Cenozoic ice sheets places the first inception of a continent sized ice sheet on Antarctica at the EOT [*Zachos et al.*, 2001]. In older compilations there was a rapid ∼1.0‰ benthic $\delta^{18}O$ decrease during the late Oligocene, which had been interpreted as being due to warming and significant ice loss [*Miller et al.*, 1987; *Zachos et al.*, 2001]. More recent records suggest instead that this rapid decrease in benthic $\delta^{18}O$ was an artifact caused by data being combined from regions with contrasting thermal histories [e.g., *Pekar et al.*, 2006]. A later compilation with data from more regions removes this artifact [*Zachos et al.*, 2008]. The benthic $\delta^{18}O$ values remain relatively stable throughout the early Miocene before continuing to increase after the Middle Miocene Climatic Optimum (MMCO) across the middle Miocene climate transition (∼14 Ma) [*Zachos et al.*, 2008].

[49] Although a climate trend can be interpreted from the raw benthic $\delta^{18}O$ data, separating the signal into a quantitative record of ice volume or DST, until recently, has required an independent record of one of the components from which the other component can then be calculated [e.g., *Lear et al.*, 2000; *Waelbroeck et al.*, 2002]. However, this leads to the errors in the independent DST or ice volume record being translated to the calculated component. Alternatively, the relative contributions from these components can be estimated using ice sheet models constrained by the $\delta^{18}O$ observational data that solve changes in the ice volume and change in DST simultaneously [*de Boer et al.*, 2010]. In principle, the $\delta^{18}O$ data can also be used as a test for independent sea level and DST data, which can be combined to create a *synthetic $\delta^{18}O$* record using a simple calibration (see section 5.3).

[50] The benthic $\delta^{18}O$ record is also susceptible to the changes in ocean circulation discussed in section 2.2, which occurred during the Eocene and Oligocene with the opening of ocean gateways. *Cramer et al.* [2009] created a new benthic $\delta^{18}O$ compilation separated by ocean basin, in contrast to the *Zachos et al.* [2001, 2008] multibasin compilation. This showed interbasinal homogeneity from ∼65 Ma to ∼35 Ma shifting to heterogeneity from ∼35 Ma to present. This was attributed to the development of the ACC and ocean current reorganization at the EOT [*Cramer et al.*, 2009]. *Katz et al.* [2011] suggest that the modern four-layer ocean structure also developed in the early Oligocene because of the development of the ACC. Interbasinal heterogeneity is clearly a potential source of uncertainty in multibasin paleoclimate compilations [i.e., *Lear et al.*, 2000; *Zachos et al.*, 2008] and brings into question how representative multibasin compilations are of the global climate [*Cramer et al.*, 2009].

3. MODELING

[51] Modeling approaches to estimating Cenozoic ice volume and temperature can be broadly divided into physics
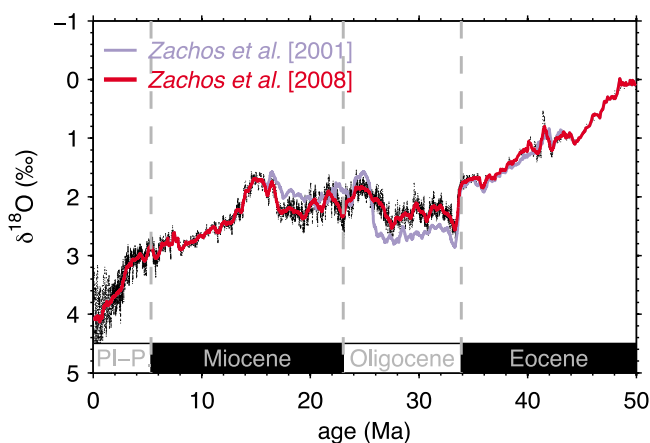
Figure 3. Stack of benthic foraminifera δ^{18}O data, showing *Zachos et al.*'s [2001] stack (light blue) and *Zachos et al.*'s [2008] updated stack with more data (red line and black dots). The additional data remove the artifact of a rapid decrease in benthic δ^{18}O toward the end of the Oligocene in *Zachos et al.*'s [2001] compilation. Raw data (black points) are smoothed with a 5-point running mean, as per *Zachos et al.* [2001], and curves are calculated using the smoothed data with an additional center-weighted running mean with a constant window size of ± 0.2 Ma.

based approximations using *general circulation models* (GCMs) and ice sheet models [*Pollard and DeConto*, 2005; *Huybrechts*, 1993] and observation-constrained modeling, which also uses ice sheet models [*Bintanja et al.*, 2005a; *de Boer et al.*, 2010].

3.1. Observation-Constrained Forward Modeling

[52] As the δ^{18}O record is a mixed climate signal, an alternative method of separating the components of the δ^{18}O signal has been developed, which uses ice sheet models constrained by the input δ^{18}O data [*Bintanja et al.*, 2005a, 2005b; *de Boer et al.*, 2010]. In summary, this approach uses 1-D models (and 3-D models for 0–3 Ma) of the North American, Eurasian, Greenland, West Antarctic, and East Antarctic ice sheets in a routine that is forced to follow the input benthic δ^{18}O observational data. The work of *de Boer et al.* [2010] is based on earlier work by *Bintanja et al.* [2005a, 2005b] but extended over the past 40 Ma. This method creates modeled estimates of Northern Hemisphere surface temperature, DST, ice volume, sea level, and benthic δ^{18}O. The Northern Hemisphere surface temperature and sea level data are shown in Figures 1 and 2, and the Northern Hemisphere surface temperature and sea level data are plotted against each other in Figure 4.

[53] *De Boer et al.* [2010] use ice sheet models to calculate the separate ice volume and DST components of the benthic δ^{18}O signal. For each time step, the ice sheet models require a temperature anomaly as input. The temperature anomaly is calculated from the difference between the modeled δ^{18}O ($\delta^{18}O_b$) at the current time step and the observed δ^{18}O ($\delta^{18}O_{obs}$) 100 years later (the *inverse routine*). This δ^{18}O anomaly over the 100 year interval is converted to a Northern Hemisphere temperature anomaly using a Northern

Hemisphere temperature to benthic δ^{18}O response parameter. An assumption of this approach is that Northern Hemisphere temperature is the predominant control on the benthic δ^{18}O record through its coupling with DST and forcing of ice growth. With this input, the ice sheet models can calculate a new ice volume, DST, and $\delta^{18}O_b$ signal for the next 100 years. The inverse routine is optimized to minimize the difference between the modeled and observed δ^{18}O signals and to satisfy independent climate constraints [*Bintanja et al.*, 2005a, 2005b; *de Boer et al.*, 2010].

[54] The inverse routine is sensitive to multiple parameters that can be tuned to satisfy independent sea level and temperature data. Northern Hemisphere temperatures are translated to DSTs using a response parameter. Northern Hemisphere temperatures are averaged over 3000 years to take into account the slow response of the oceans to atmospheric temperature change [*Bintanja et al.*, 2005a]. To represent changes in the Greenland and Antarctic ice sheets, the Northern Hemisphere temperature is linearly related to these regions by taking into account the different geographical location and altitude of these ice sheets. A sensitivity test suggested that changing these parameters can affect the long-term (3–35 Ma) sea level and Northern Hemisphere temperature averages by $\sim\pm 6$ m and $\sim\pm 2°$C. *De Boer et al.* [2010] select optimum values of these parameters based on agreement with the tuning parameters, such as LGM sea level ~ 120 m lower than present [*Rohling et al.*, 2009] and a sea level fall of ~ 40 m in the earliest Oligocene [*DeConto and Pollard*, 2003a].

[55] The study by *de Boer et al.* [2010] uses 1-D ice sheet models. This method has also been applied using a 3-D model over the past 3 Ma [*Bintanja and van de Wal*, 2008], and the 1-D results are similar over this period [*de Boer et al.*, 2010]. Equilibrium studies using both 1-D and 3-D models over North America suggest that the oversimplified geometry in the 1-D model means *hysteresis* effects seen in the 3-D results are not replicated [*Wilschut et al.*, 2006].
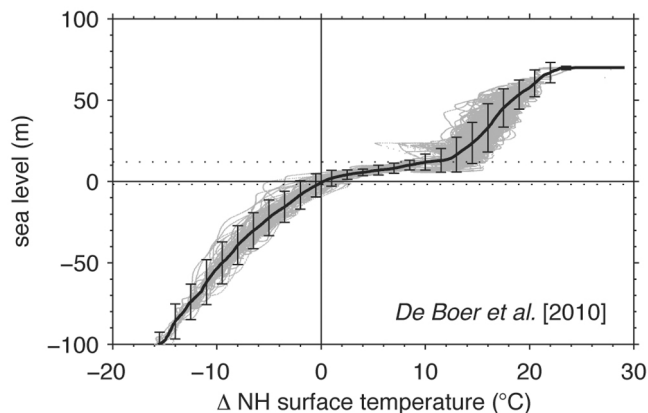

Figure 4. *De Boer et al.*'s [2010] observation-constrained forward modeled sea level and Northern Hemisphere surface air temperature. Solid line is smoothed using a center-weighted running mean with a window size of $\pm 0.05°$C. Error bars are calculated as 2 standard deviations of the data range $\pm 0.25°$C of each data point.

Indeed, *de Boer et al.* [2010] suggested that the use of 3-D models was possible scope for a future study. The hysteresis in the study of *Wilschut et al.* [2006] using 3-D models means that a certain temperature can be related to several sea level stands depending on the evolution of the system over time.

[56] *De Boer et al.* [2010, 2012] explore the relationship between sea level and Northern Hemisphere surface temperature in their observation-constrained model results; this is reproduced in Figure 4 for Northern Hemisphere surface temperature against sea level. Clearly present in their results are the broad climate states of the past 35 Ma, going from unglaciated conditions to partial glaciation with an East Antarctic Ice Sheet, then going to interglacial conditions with the additional growth of the Greenland Ice Sheet and the *West Antarctic Ice Sheet* (*WAIS*), and finally, going to glacial conditions with additional Northern Hemisphere ice sheets [*de Boer et al.*, 2012]. Their results suggest that the relationship between sea level and temperature (both deep sea and Northern Hemisphere surface) has not remained constant (i.e., linear) over the past 35 Ma. Sea level appears less sensitive to temperature for sea levels approximately between −2 m and 12 m relative to present (see Figure 4). This suggests that interglacial periods, when sea level is similar to present, are relatively stable in the context of variation over the past 35 Ma [*de Boer et al.*, 2010]. This is seen in the relative contributions to the $\delta^{18}O$ signal from DST and ice volume. From the middle Miocene (12–13 Ma) until ~3 Ma, when sea level in *de Boer et al.*'s [2010] reconstruction is ~10 m above present, the dominant contribution is from DST, with very little contribution from changing ice volume. It is likely that the lack of ice volume contribution is due to the EAIS being bound by the limits of the continent and Northern Hemisphere temperatures being above the threshold for widespread Northern Hemisphere glaciation. For temperatures warmer than present, the relationship between Northern Hemisphere surface temperature and sea level (and also DST and sea level, not shown here) shows a single-stepped, sigmoidal form [*de Boer et al.*, 2010].

[57] As this modeling approach is based on the global compilation of benthic $\delta^{18}O$ data, it is also susceptible to potential errors from interbasinal divergence, discussed in the work by *Cramer et al.* [2009] and in section 2.3. This modeling approach also assumes a constant deep-sea to surface temperature ratio [*de Boer et al.*, 2010]; for reasons discussed in sections 2.2 and 2.3, the deep-sea to surface temperature gradient may have changed on this long timescale [*Nong et al.*, 2000; *Najjar et al.*, 2002], and this may be a potential source of error in the results of *de Boer et al.* [2010].

3.2. GCM–Ice Sheet Modeling

[58] There are various methods of modeling past ice volume using GCMs and ice sheet models [*Pollard*, 2010]. This review is interested in how ice sheets have evolved in response to changes in temperature forcing and therefore will focus on modeling studies with transient forcing rather than time slice studies. Ice sheet models can be coupled with general circulation models to simulate long-term climate changes, with approximate feedbacks between the ice and climate systems. Although a full coupling between a GCM and an ice sheet model would be desirable, for multimillion year integrations this is currently not feasible given the high computational expense of running GCMs. Because of the discrepancy between the time taken for the climate system to approach equilibrium and for ice sheets to reach equilibrium, an *asynchronous coupling* can be used [e.g., *DeConto and Pollard*, 2003a, 2003b]. The climate system can be perturbed by slowly changing the atmospheric CO_2 concentration with the climate system in quasi-equilibrium and the ice sheets slowly varying because of orbital and greenhouse gas forcing [*Pollard and DeConto*, 2005].

[59] *DeConto and Pollard* [2003a, 2003b] used an asynchronous method to study the thresholds for inception of the EAIS at the EOT. Their method is split into two stages: (1) The GCM is used to provide extrapolated forcings for a much longer ice sheet simulation for different orbital configurations and CO_2 concentrations. An initial GCM run provides a mass balance for a 10 ka ice sheet simulation. At the end of the ice sheet run, and at subsequent 10 ka intervals, the GCM is run again with the updated ice sheet extent and a new orbital configuration. The ice sheet model provides feedback over each 10 ka interval because of albedo and topography changes. The orbital configurations are idealized representations of precession, obliquity, and eccentricity. This is completed for atmospheric CO_2 concentrations of 560 and 840 ppm (2 × and 3 × preindustrial CO_2). The GCM data are stored for the next stage [*Pollard and DeConto*, 2005]. (2) In the next stage, a 10 Ma ice sheet model simulation is completed. This is updated every 200 years with a new mass balance calculated using linear extrapolation of the GCM data. This creates an approximation of orbital cycles at a high temporal resolution. The extrapolation includes a linearly declining CO_2 concentration. The calculations take into account the logarithmic effect of CO_2 forcing on temperature change via radiation theory. The mass balance calculations correct for changing elevation due to changes in the size of the ice sheet, so height–mass balance feedback is represented. Albedo feedbacks on timescales longer than the first integration (10 ka) are not represented [*Pollard and DeConto*, 2005]. This method can be modified to investigate the effect of ocean gateways being opened or closed, the effect of mountain uplift, and the effect of orbital variations [*DeConto and Pollard*, 2003a; *Pollard and DeConto*, 2005].

[60] Modeling studies of the forcings required to form an ice sheet on Antarctica suggest that ice growth responds nonlinearly to changing temperature [*Oerlemans*, 2004]. This nonlinearity is caused by feedbacks such as height–mass balance feedback (the additional cooling caused by the temperature gradient in the atmosphere as an ice sheet grows vertically), precipitation feedback, and ice-albedo feedback [*Oerlemans*, 2002; *Notz*, 2009]. The initiation of glaciation displays a threshold response, with growth starting as the descending snow line intercepts high topographic regions [*Oerlemans*, 1982; *Pollard*, 1982; *DeConto and Pollard*, 2003a].

[61] In Figure 5, the model output from *Pollard and DeConto* [2005] for the formation and melting of the East Antarctic Ice Sheet is shown. The original CO_2 axis is converted to a temperature (average global surface) axis using the climate sensitivity of their GCM (2.5°C per doubling of CO_2 [*Thompson and Pollard*, 1997]) and accounting for the logarithmic dependence of temperature to CO_2. The data are reversed on both axes for consistency with the other figures shown here. Ice volumes are converted to sea levels assuming an ice-free sea level of 64 m above present [*Lythe and Vaughan*, 2001; *Bamber et al.*, 2001; *Lemke et al.*, 2007] and adjusting for the change in volume with change in state from ice to seawater. The original CO_2 forcing and model time is included but converted to a logarithmic scale.

[62] The results of *DeConto and Pollard* [2003a, 2003b] show the formation of ice on Antarctica in multiple stages under various atmospheric CO_2 concentrations. With a high atmospheric CO_2 concentration of 8 × preindustrial CO_2 (PIC), equal to 2240 ppmv, ice is limited to mountain glaciers in the Transantarctic Mountains and Dronning Maud Land. Isolated ice caps first form in the high-elevation regions of Dronning Maud Land and the Gamburtsev and Transantarctic Mountains as atmospheric CO_2 decreases to 3–4 × PIC (1120–840 ppmv). In the model, as CO_2 falls to ∼2.7 × PIC (∼760 ppmv) a threshold is crossed and height-mass balance feedback leads to the three isolated ice caps coalescing into a continent sized ice sheet. Although there are multiple "steps" in their results, there are two major steps marking (1) the transition from no ice to isolated mountain ice caps and (2) the transition to a full ice sheet (see Figure 5a). The total sea level shift in this two-step model of *Pollard and DeConto* [2005] is on the order of 50 m (∼33 m after accounting for hydroisostasy for comparison with the NJ record [*Pekar et al.*, 2002]); Figure 5 does not include other causes of sea level change, such as thermosteric sea level change.

[63] A study of forward (inception) and reverse (deglaciation) model runs investigated ice sheet hysteresis (reproduced in Figure 5) [*Pollard and DeConto*, 2005]. Starting with no ice, a descending snow line generates rapid ice mass gains as it meets the mountain regions. Once a full continental ice sheet has formed, the snow line must rise considerably higher to achieve negative net mass balance and initiate broad-scale retreat. This is because the steep outer slopes of the ice sheet and the atmospheric lapse rate require much warmer conditions to produce enough surface melt area around the margins to overcome the net interior snowfall (which at present is balanced by Antarctic iceberg and shelf discharge) [*Oerlemans*, 2002; *Pollard and DeConto*, 2005]. In the model runs for the EAIS, this hysteresis equates to a difference of 0.5 × PIC between forward and reverse runs. Although the forward run required atmospheric CO_2 to descend past ∼2.7 × PIC for inception to begin, the reverse run required atmospheric CO_2 to rise above ∼3.2 × PIC (∼900 ppmv) for deglaciation to begin. These runs include orbital variations; without orbital variations, the hysteresis is greater. The model shows formation of ice in a series of steps between multiple quasi-stable states. There is

a stable state just after the formation of ice in mountain regions as further growth is limited by the extent of the mountain ranges. The snow line has to descend further with additional cooling before there is additional growth. With the continent fully glaciated, further growth is inhibited when the ice sheet reaches the coastline [*Pollard and DeConto*, 2005].

[64] As noted in the work by *Pollard and DeConto* [2005], the asynchronous coupling method used for Figure 5 poorly represents albedo feedback on longer than orbital timescales. Ongoing work with improved coupling schemes suggests that the major no-ice to continental ice transitions are steeper than in Figure 5, and the hysteresis (i.e., difference between CO_2 levels of inception and deglaciation) is considerably more pronounced.

[65] The observation-constrained modeling work of *de Boer et al.* [2010] displays a single-step form for temperatures warmer than present, not a two-step form seen in the work of *Pollard and DeConto* [2005]. The two-stepped hypothesis is based on isolated ice caps initially forming in mountain regions prior to coalescing into a continental sized ice sheet with further cooling [*Pollard and DeConto*, 2005]. A possible reason that the work of *de Boer et al.* [2010] does not show this form is that the ice sheets used in their initial study used 1-D ice sheet models, with a simplified geometry. It is possible that if this work were completed with 3-D ice sheet models then a two-stepped form could be apparent, with the inclusion of the initial isolated ice cap phase.

4. SEA LEVEL VERSUS TEMPERATURE: METHODS

[66] Here we consider the possible forms for the relationships between DST to sea level and SST to sea level over the past 50 Ma. For the period 10–50 Ma the DST data used are *Lear et al.*'s [2000] benthic Mg/Ca record, and the sea level data used are *Kominz et al.*'s [2008] NJ sequence stratigraphy record. For the SST relationship with sea level, we use the same sea level record of *Kominz et al.* [2008] and additional SST records for the high-latitude Southern Hemisphere [*Liu et al.*, 2009] and low latitudes [*Lear et al.*, 2008] for the EOT. Additional Plio-Pleistocene data are shown on the plots. We test three functions, a linear function and single- and double-stepped nonlinear functions, which are based on previous publications exploring the relationship between temperature and sea level [*Pollard and DeConto*, 2005; *Archer*, 2006; *de Boer et al.*, 2010]. As this review is focused on the deep-time relationship between temperature and sea level, the Plio-Pleistocene data are shown as a guide and are not used when fitting the different functions. As the DST record is more complete, the majority of this review focuses on the relationship between DST and sea level, with the SST to sea level relationship investigated over the EOT. These changes are for the long-term response of sea level to SST or DST, with ice sheets approaching equilibrium with climate over 10^5–10^6 years.

4.1. Interpolation

[67] The temporal resolutions of the different records used in this synthesis vary. The Mg/Ca data set of *Lear et al.*
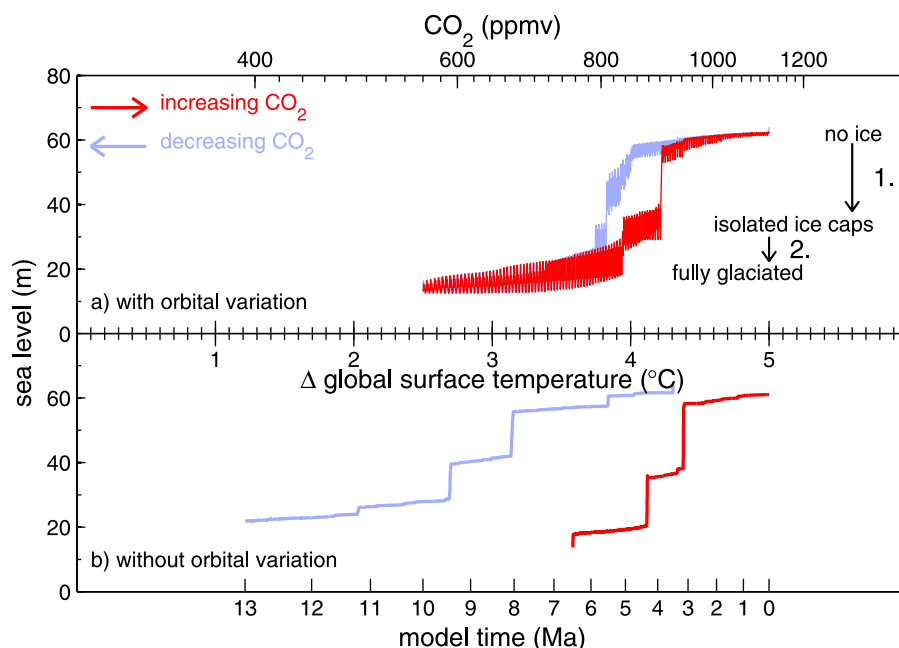
Figure 5. *Pollard and DeConto*'s [2005] GCM–ice sheet modeled results, for the East Antarctic Ice Sheet only (the WAIS is not fully represented). Data are converted to a temperature scale from the original CO_2 scale using the climate sensitivity of their model (2.5°C for a doubling of CO_2 [*Thompson and Pollard*, 1997]) and accounting for the logarithmic relationship between temperature and CO_2. The original axes of *Pollard and DeConto* [2005] are included but converted to an appropriate logarithmic scale. The ice volumes of the original figure are converted to sea level assuming ice-free sea level of 64 m above present [*Lemke et al.*, 2007] and accounting for the change in volume with change in state from ice to seawater. The high-frequency oscillations in the data in Figure 5a are due to idealized Milankovitch orbital forcing.

[2000] has a resolution of ∼1 Ma and does not resolve shorter climatic events. *Kominz et al.*'s [2008] sea level record has a temporal resolution of 0.1 Ma, although the age control is significantly worse, at ∼±0.5 Ma [*Kominz et al.*, 2008]. To compare these two data sets, the sea level data are first reduced to the same lower temporal resolution of *Lear et al.*'s [2000] data set. The higher-resolution sea level data are smoothed using a center-weighted running mean and a window size of ±0.5 Ma; the data are then interpolated with a 1 Ma frequency. Smoothing in this manner leads to the loss of some of the high-frequency sea level variability in the record, but major transitions, such as the EOT sea level fall, are preserved. For the SST records, the sea level data are interpolated using the same method but to a 0.1 Ma resolution for the low-latitude record and to a 0.25 Ma resolution for the high-latitude Southern Hemisphere record.

[68] The different records all span the EOT, a period of major sea level change; however, they all have different durations. *Kominz et al.*'s [2008] sequence stratigraphy data are not available from 10 Ma to present, so data are shown from 10 to 50 Ma, which is the maximum age of *Lear et al.*'s [2000] data set. The high-latitude Southern Hemisphere SST data of *Liu et al.* [2009] are shown from 32 to 36.5 Ma, which is the period of peak data density in their record. The low-latitude SST data of *Lear et al.* [2008] cover the period from 33.4 to 34.5 Ma. Therefore, there are significant data

gaps on the plots; in particular, the Miocene is not covered for the SST to sea level synthesis.

[69] *Lear et al.* [2000] used four core locations for their compilation. The site from which the most recent samples (exclusively for period 0–6 Ma) were obtained was DSDP Site 573. Modern DST for this site is 1.4°C (from NODC_ WOA98 provided by the NOAA/OAR/ESRL PSD, Boulder, Colorado, http://www.esrl.noaa.gov/psd/). The Mg/Ca DST data are shown as an anomaly relative to this modern-day value. *Liu et al.* [2009] provide modern paleolocation temperatures for all of their sites. The high-latitude Southern Hemisphere SST data are presented here as anomalies relative to the modern value for each site. *Lear et al.*'s [2008] record comes from an exposed shelf; the data are shown here as anomalies relative to a modern SST value of 27.1°C (*NODC_WOA98*), taken from the coast immediately to the east of the core site.

[70] A best and a low and high estimate are provided with the NJ highstand data. The low and high estimate is calculated as being 60% and 150% of the best estimate, respectively. Therefore, the best estimate is not the midpoint of the estimate range; the skewed errors are a result of using foraminifera habitat ranges as a water depth indicator, the errors of which increase with increasing water depth [*Kominz et al.*, 2008]. In order to carry out the regression, we require a symmetric error distribution. We calculate a midpoint from the asymmetrical (triangular) error distribution
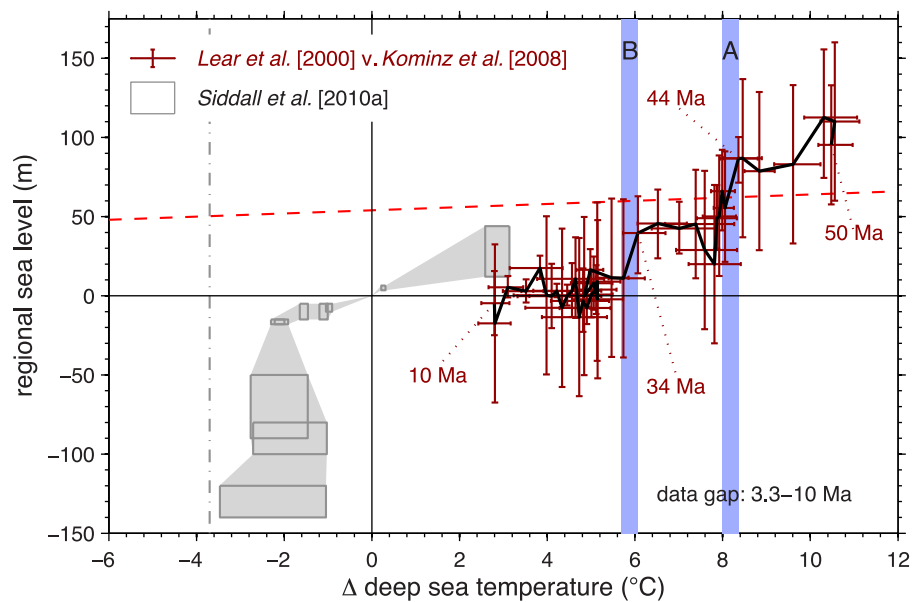
Figure 6. Deep-sea temperature against regional sea level crossplot. Dark red error bars are for *Kominz et al.*'s [2008] New Jersey regional sea level against *Lear et al.*'s [2000] Mg/Ca deep-sea temperature anomaly (this review). Shown connected in time order (black line). Blue bars highlight the two steps discussed in the text. Grey boxes are Plio-Pleistocene deep-sea temperature and sea level data from the Red Sea [*Siddall et al.*, 2010a]; the vertical gray dot-dashed line is the freezing point for water for the deep-sea temperature data used in the work by *Siddall et al.* [2010a], showing decreased deep-sea temperature variability as the freezing point is approached. The sloped red dashed line is the ice-free thermal expansion gradient, assuming an ice-free NJ sea level of 54 m and a thermal expansion of 1 m per °C [*Miller et al.*, 2009a].

and create a synthetic data set that has symmetric errors (see Figure 1). Errors are not provided for the conceptual lowstand data [*Kominz et al.*, 2008], although lowstand errors are likely to be larger than the highstand errors; here we use lowstand errors of ±50 m. The Mg/Ca DST curve is calculated using a weighted local regression of the raw data [*Lear et al.*, 2000]. Here we repeat this regression and obtain an error estimate from the raw data. Errors on the DST data are also unevenly distributed, and again we create a synthetic data set with a symmetric distribution.

4.2. Sea Level Versus Temperature Crossplots

[71] For each of the crossplots, additional data for the Plio-Pleistocene are shown to provide a reference for the relationship between the relevant temperatures and sea level for cooler climates. Figure 6 includes DST and Red Sea sea level data [*Siddall et al.*, 2003] compiled by *Siddall et al.* [2010a]. This highlights that as DSTs approach the freezing point for seawater (also highlighted in Figure 6) they show very little variation [*Siddall et al.*, 2010a]. Figure 7 includes Antarctic air temperature and sea level data for the last 500 ka [*Rohling et al.*, 2009]; again the sea level data come from the Red Sea record [*Siddall et al.*, 2003; *Rohling et al.*, 2009]. The proxy Antarctic air temperatures come from deuterium isotope (δD) data from EPICA Dome C [*Jouzel et al.*, 2007] and are presented as an anomaly relative to average temperature over the past 1 ka [*Rohling et al.*, 2009]. Figure 8 uses temperature data from a low-latitude SST stack from five tropical sites in the major ocean basins

using the $U^{k'}_{37}$ proxy [*Herbert et al.*, 2010] and Mg/Ca of planktic foraminifera [*Medina-Elizalde and Lea*, 2005]. We repeat the stacking method outlined by *Herbert et al.* [2010, supplementary information] but calculate temperatures as an anomaly relative to the average of the past 3 ka. Again the Plio-Pleistocene sea level data come from the Red Sea record [*Siddall et al.*, 2003; *Rohling et al.*, 2009].

[72] All of the plots of sea level against temperature exhibit a positive correlation. This relationship is expected because of thermal expansion and changing land ice volumes with changing temperature. There is an additional component to the sea level record that may not be directly related to temperature: the change in ocean basin volume. However, it is possible that there is a common driving mechanism: decreased seafloor spreading could cause a decline in atmospheric CO_2, resulting in increased basin volume (i.e., lower sea level) and decreased temperature [*Larson*, 1991; *Miller et al.*, 2009a]. The sea level record may contain regional tectonic influences, which are not related to temperature change (see section 2.1). The thermal expansion gradient assuming ice-free conditions (54 m above present at NJ margin for present temperature [*Pekar et al.*, 2002; *Miller et al.*, 2005a]) is shown on all of the plots (Figures 6–8) as a guide to how much of the NJ sea level variability is likely due to thermal expansion and glacioeustasy.

[73] In Figure 6 when the data are connected in time series (black line in Figure 6), it is possible that there is a two-stepped relationship between the DST data of *Lear et al.*
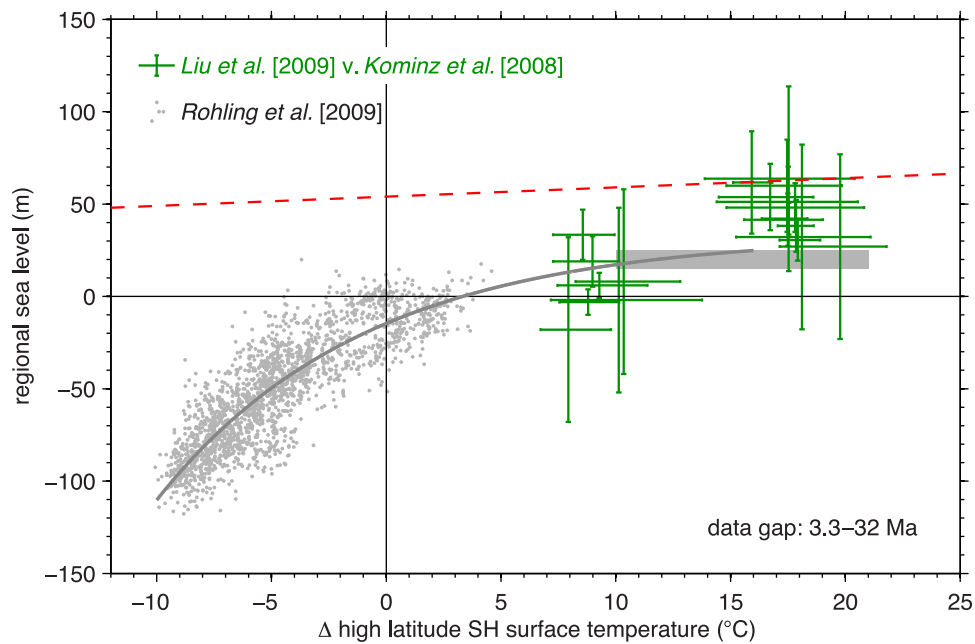
Figure 7. High-latitude Southern Hemisphere surface temperature against regional sea level. Dark green error bars are for *Kominz et al.*'s [2008] New Jersey regional sea level against *Liu et al.*'s [2009] TEX$_{86}$ and U$^{k'}_{37}$ SST for high-latitude Southern Hemisphere sites, shown as an anomaly relative to modern SST. The dark green data cover the EOT, with data from 32 to 36.5 Ma with a 0.25 Ma resolution. There is a data gap from the end of the dark green data at 32 Ma to the Plio-Pleistocene data. The gray dots show Pleistocene data (0–500 ka); the gray box is for the mid-Pliocene [*Rohling et al.*, 2009]. The gray dots from *Rohling et al.* [2009] are for Antarctic air temperature based on δD and sea level data from the Red Sea [*Siddall et al.*, 2003]. The gray line is the preferred exponential fit between temperature and sea level of *Rohling et al.* [2009]. The sloped red dashed line is the ice-free thermal expansion gradient, assuming ice-free NJ sea level of 54 m and a reduced thermal expansion gradient of 0.5 m per °C, to account for polar amplification [e.g., *Siddall et al.*, 2010a].

[2000] and the sea level data of *Kominz et al.* [2008]. This is potentially in agreement with the modeling work of *Pollard and DeConto* [2005] although the total sea level shift is greater than the ∼50 m (∼33 m after accounting for hydro-isostasy) shift seen in the work by *Pollard and DeConto* [2005] (Figure 5) as the sea level record used here includes thermosteric and ocean basin volume components. The two-step form seen in the study by *Pollard and DeConto* [2005] is solely due to glacioeustasy from the formation of the EAIS. An additional difference between the two-step form seen in the work of *Pollard and DeConto* [2005] and that seen here is the time scale. The two steps occurring in *Pollard and DeConto*'s [2005] study take place over a duration of ∼200 ka as their study is interested in glacial inception at the EOT. The two steps in this review are separated by ∼10 Ma. A first step occurs at 42–44 Ma (hereafter step A), and there is a second step (hereafter step B) at 33–34 Ma coinciding with the EOT. The lack of cooling in the DST record at the EOT should be taken into consideration when interpreting these steps. The lack of cooling accentuates step B at the EOT. Other temperature proxies suggest that there was cooling at the EOT [*Dupont-Nivet et al.*, 2007; *Zanazzi et al.*, 2007; *Lear et al.*, 2008; *Liu et al.*, 2009; *Lear et al.*, 2010], and deep-sea cooling may have been on the order of 1.5°C [*Lear et al.*, 2010; *Pusz et al.*, 2011]. In Figure 9, the DST data prior to the EOT are shifted by +1.5°C to take

into account cooling at the EOT. This results in the steepness of step B, as seen in Figure 6, being reduced. The SST plots, Figures 7 and 8, also span the EOT. The steep step B seen in the DST plot (Figure 6) is not evident in the SST plots. This again suggests that the steepness of step B in the DST plot is an artifact of the lack of cooling in the DST data across the EOT.

[74] Because the Mg/Ca temperature proxy is affected by past variations in seawater Mg/Ca [*Lear et al.*, 2000; *Billups and Schrag*, 2003] (see section 2.2), the absolute DST values can vary depending on the seawater Mg/Ca scenario used. DSTs using the favored scenario of *Lear et al.* [2000] and the extreme scenarios of *Lear* [2007] are shown in Figure 10 plotted against NJ sea level. It is unlikely that seawater Mg/Ca has remained constant over the past 50 Ma [*Wilkinson and Algeo*, 1989; *Lowenstein et al.*, 2001; *Dickson*, 2002; *Coggon et al.*, 2010], as per Figure 10a. However, it is possible that seawater Mg/Ca was lower than the preferred scenario of 3.85 mol mol^{-1} at 50 Ma [*Lear et al.*, 2000; *Lowenstein et al.*, 2001; *Dickson*, 2002; *Coggon et al.*, 2010], as per Figure 10c, where a value of 1.5 mol mol^{-1} at 50 Ma, linearly increasing to present, is used; although it is difficult to reconcile this Mg/Ca temperature scenario with the benthic $\delta^{18}O$ records assuming early Cenozoic ice-free conditions. As such, the absolute Mg/Ca DST values should be interpreted with caution.
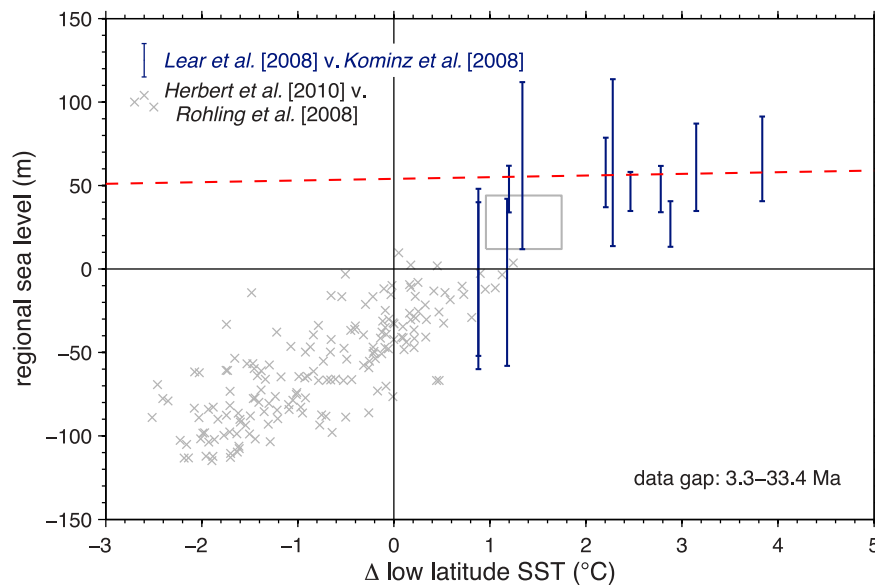
Figure 8. Low-latitude sea surface temperature against regional sea level. The dark blue error bars are for *Kominz et al.*'s [2008] New Jersey regional sea level against *Lear et al.*'s [2008] Mg/Ca sea surface temperature from Tanzania for the EOT. The dark blue data cover the period from 33.4 to 34.5 Ma, with a resolution of 0.1 Ma. Plio-Pleistocene data are shown in gray, with low-latitude SST data from the stack by *Herbert et al.* [2010] and sea level data from the Red Sea record [*Siddall et al.*, 2003; *Rohling et al.*, 2009]. Pleistocene data for 0–500 ka are shown as gray crosses; a mid-Pliocene data point is shown as a gray box. The sloped red dashed line is the ice-free thermal expansion gradient, assuming an ice-free NJ sea level of 54 m and a thermal expansion of 1 m per °C [*Miller et al.*, 2009a].

[75] The Cenozoic temperature trend is dominated by cooling, with shorter warm reversals. Hysteresis effects mean that the sea level thresholds may be at different temperatures for warming compared to cooling (see section 3.2 and Figure 5). Because of the long response time of the ice sheets, the relationship shown represents sea level in approximate equilibrium with temperature. The very long-term relationship between DST or SST and sea level investigated in this review is therefore not directly relatable to potential future surface warming on centennial timescales.

4.3. Function Selection

[76] The first function we test against the temperature and sea level data is a linear function. A linear form for the
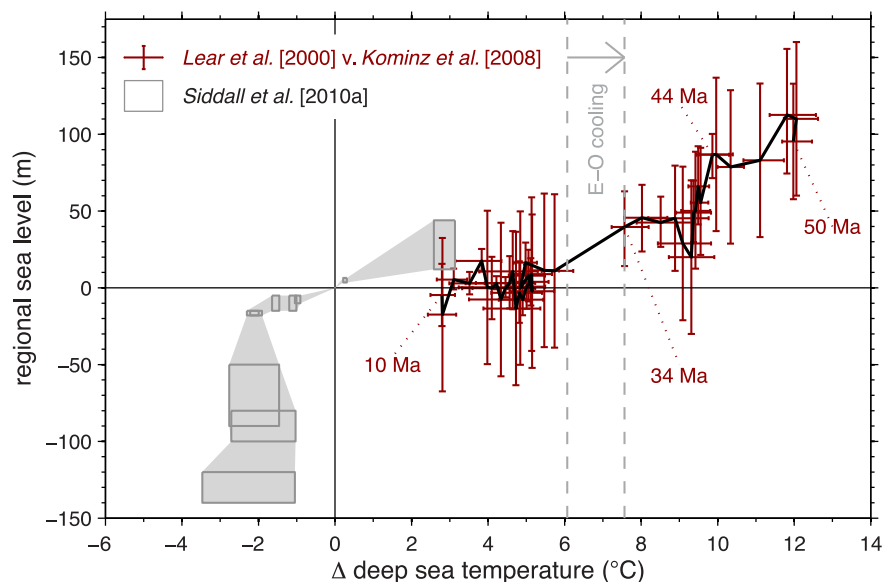

Figure 9. Deep-sea temperature against regional sea level. Data as per Figure 6 but with data prior to the EOT shifted by +1.5°C [*Lear et al.*, 2010; *Pusz et al.*, 2011] to account for EOT cooling not seen in *Lear et al.*'s [2000] record.
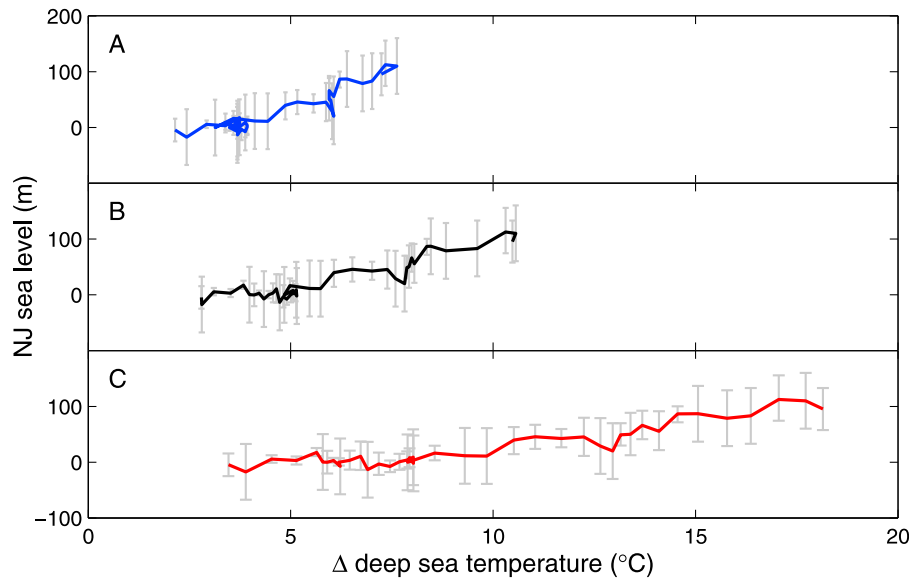
Figure 10. Impact of different past seawater Mg/Ca scenarios on crossplots of *Kominz et al.*'s [2008] New Jersey regional sea level against *Lear et al.*'s [2000] DST. (a) For constant seawater Mg/Ca scenario. (b) Best estimate scenario of *Lear et al.* [2000] for seawater Mg/Ca linearly increasing from 50 Ma value of 3.85 mol mol^{-1} [*Wilkinson and Algeo*, 1989] to present-day concentration of 5.2 mol mol^{-1}. (c) High estimate for seawater Mg/Ca linearly increasing from 50 Ma value of 1.5 mol mol^{-1} [*Lear*, 2007].

temperature to sea level relationship is suggested by *Archer* [2006] and also reproduced by *Jaeger et al.* [2008]. This is based on LGM, middle Pliocene, and Eocene temperature and sea level estimates, periods when temperature and sea level were significantly different to present. *Archer* [2006] uses LGM sea level of ~120 m lower than present [*Fairbanks*, 1989] and temperatures of 4°C–7°C colder than present [*Waelbroeck et al.*, 2002; *Schneider von Deimling et al.*, 2006; *Rahmstorf*, 2007]. In the middle Pliocene (~3 Ma), *Archer* [2006] suggests that temperatures were 2°C–3°C warmer than present and sea level was 25–35 m higher than present [*Dowsett et al.*, 1994]. In the late Eocene (40 Ma), *Archer* [2006] suggests that temperatures may have been 4°C–5°C warmer than present and sea level was 70 m higher than present, i.e., assuming ice-free conditions but not correcting for isostatic effects [e.g., *Miller et al.*, 2009a]. This temperature estimate, comparable to *Covey et al.*'s [1996] estimate, is lower than more recent Eocene temperature estimates. *Covey et al.*'s [1996] Eocene surface temperature estimate was based on an integration of a temperature anomaly against latitude profile. This included Eocene low-latitude temperatures that were cooler than present, based on δ^{18}O of planktic foraminifera [*Zachos et al.*, 1994]. It is acknowledged that the planktic δ^{18}O values, on which these cool low-latitude SSTs are based, are affected by diagenesis, meaning that the signal is contaminated with cooler deeper ocean temperatures [*Zachos et al.*, 1994; *Pearson et al.*, 2007]. Therefore, it is likely that this Eocene temperature estimate is too low.

[77] The approach of *Archer* [2006] is recreated in the insets of Figures 11–13 with a linear function that is forced through the origin, i.e., constrained to modern sea level and temperature. Their approach is intended as a tentative

approximation only and is not based on physical insights or modeling work. Although a linear model may be a fair approximation of the present-day temperature to sea level relationship, when the greatest contributor to sea level rise is thermal expansion [*Vermeer and Rahmstorf*, 2009], on longer timescales or for larger temperature changes when the greater contribution comes from glaciers and ice sheets it may be less applicable [*Pollard and DeConto*, 2005; *Vermeer and Rahmstorf*, 2009; *de Boer et al.*, 2010].

[78] In addition to linear functions, both forced (equation (1)) and unforced (equation (2)) through the origin, nonlinear functions are used to describe the relationship between temperature and sea level. The nonlinear relationship is based on both GCM–ice sheet modeling and observation-constrained modeling [*Huybrechts*, 1993; *Pollard and DeConto*, 2005; *de Boer et al.*, 2010]. The proposed nonlinear relationship varies from a single-stepped relationship [*Huybrechts*, 1993; *de Boer et al.*, 2010] to a two-step relationship [*Pollard and DeConto*, 2005].

$$S = mT \qquad (1)$$

$$S = mT + c \qquad (2)$$

The linear models to be used are shown in equations (1) and (2), where S is sea level, T is temperature, m is the rate of change of sea level with change in temperature, and c is the intercept on the sea level axis. An inverse *hyperbolic sine function* can be used to describe the single-stepped form (equation (3)).

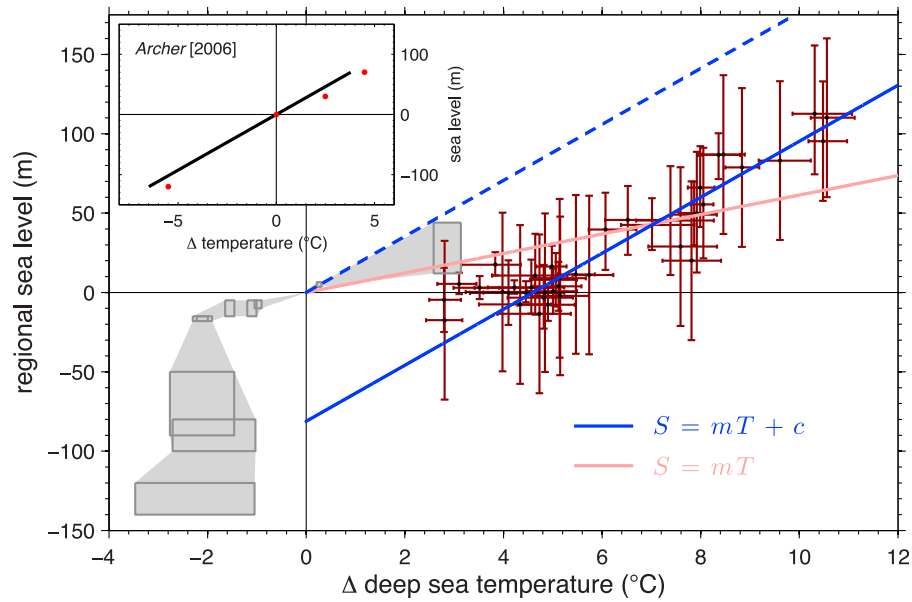$$S = a\sinh^{-1}\left(\frac{T-b}{c}\right) + d \qquad (3)$$

Figure 11. Data as per Figure 6, showing deep-sea temperature against regional sea level, with *Archer*'s [2006] linear trend shown inset. Linear functions are fit to the data of *Kominz et al.* [2008] and *Lear et al.* [2000] using orthogonal regression; functions are not constrained by additional Plio-Pleistocene data (gray boxes) [*Siddall et al.*, 2010a]. The pink line is forced through the origin. The dashed line is "corrected" for potential isostatic offset by shifting on the *y* axis so that it is consistent with modern temperature and sea level (see text).

In equation (3), *a* is the magnitude of the sea level change, *b* is the midpoint on the temperature axis, *c* is the peak rate of change in sea level with change in temperature, and *d* is the midpoint on the sea level axis [*Siddall et al.*, 2010b]. This function can replicate the form of the modeled results of

de Boer et al. [2010], showing the increased sea level to temperature response out of the quasi-stable interglacial state and also how the sea level response asymptotes as ice-free conditions are approached. This function is not based on ice dynamics, but is chosen because it is a sigmoid (s-shaped)
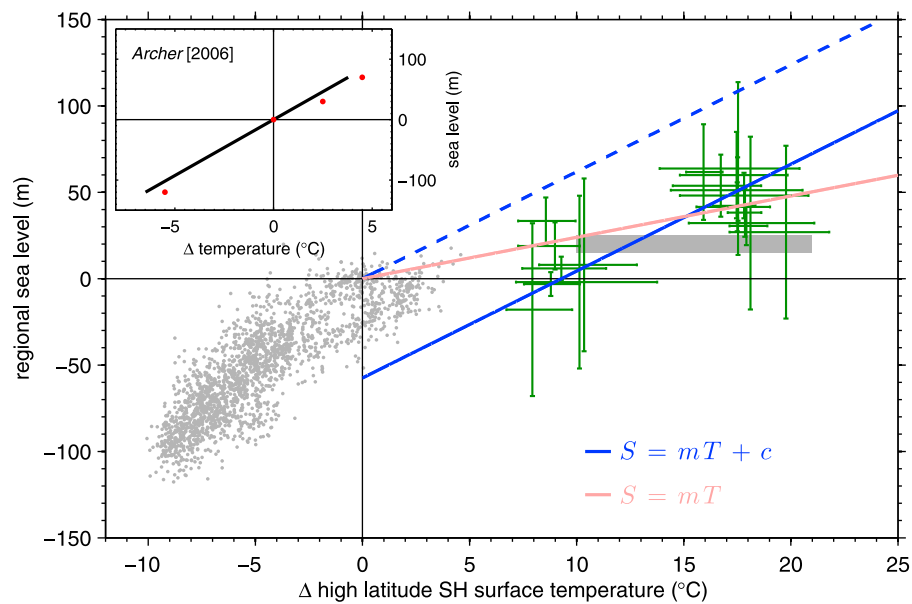

Figure 12. Data as per Figure 7, showing high-latitude Southern Hemisphere surface temperature against regional sea level, with *Archer*'s [2006] linear trend shown inset. Linear functions are fit to the data of *Kominz et al.* [2008] and *Liu et al.* [2009] using orthogonal regression; the functions are not constrained by the additional Plio-Pleistocene data shown in gray. The pink line is forced through the origin. The dashed blue line is "corrected" for potential isostatic offset in the NJ sea level data by shifting on the *y* axis so that it is consistent with modern temperature and sea level (see text).

Figure 13. Data as per Figure 8, showing low-latitude SST against regional sea level, with *Archer*'s [2006] linear trend shown inset. Linear functions are fit to the data of *Kominz et al.* [2008] and *Lear et al.* [2008] using orthogonal regression; the functions are not constrained by the additional Plio-Pleistocene data shown in gray. The pink line is forced through the origin. The dashed blue line is "corrected" for potential isostatic offset in the NJ sea level data by shifting on the y axis so that it is consistent with modern temperature and sea level (see text).
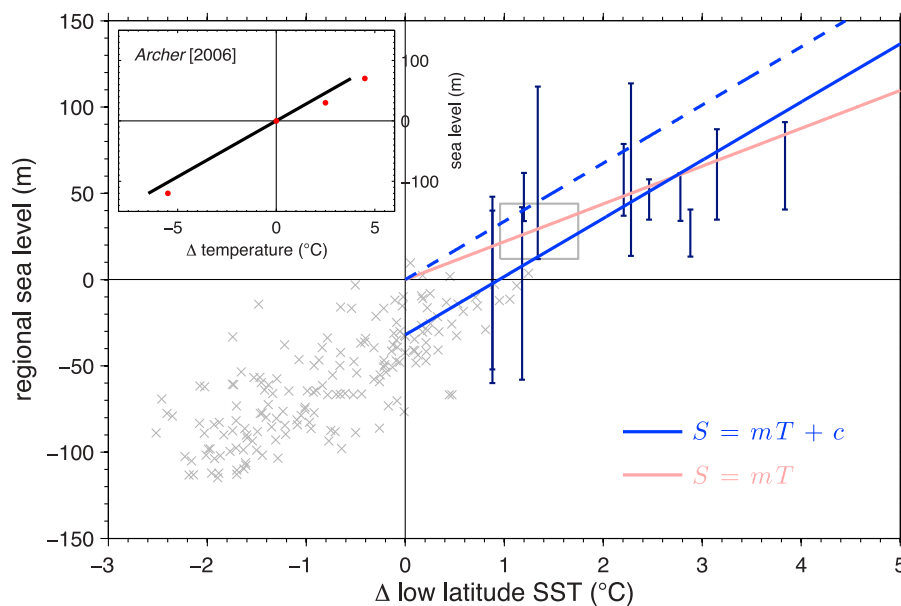
function that can replicate the form of the relationships in the data. The single-step model is also consistent with early GCM ice sheet modeling work of *Huybrechts* [1993].

[79] A double inverse hyperbolic sine function can replicate the two-stepped form (equation (4)).

$$S = \left[a_1 \sinh^{-1}\left(\frac{T - b_1}{c_1}\right)\right] + \left[a_2 \sinh^{-1}\left(\frac{T - b_2}{c_2}\right)\right] + d \quad (4)$$

Again this nonlinear function is not based on ice sheet dynamics but is chosen because it can replicate the two-stepped form seen in the modeling work of *Pollard and DeConto* [2005]. The double inverse hyperbolic sine function can also take a single-stepped form if it is present in the data.

4.4. Fitting Method

[80] Because there are significant errors in both the proxy sea level and temperature data, when fitting the functions to the data, *orthogonal regression* is used. Least squares regression attempts to minimize the sum of squared errors on the y axis (response) and assumes that errors on the x axis (predictor) are minimal. However, in this instance the predictor, DST or SST, contains significant error. It is likely that this is a common instance when performing regression within paleoclimatology, which is often ignored. Prior to fitting the data are nondimensionalized, by dividing by the standard deviation, to avoid overfitting to one axis. Orthogonal errors can be calculated for a linear function from the slope of the line. An optimum fit can then be found using an optimization algorithm [e.g., *Krystek and Anton*, 2007]. For a nonlinear function the orthogonal errors are

not as easily calculated, as the closest point on the curve to each data point is unknown.

[81] Here we approximate the orthogonal errors using a finite difference approach. The fit is optimized using a *genetic algorithm* (*GA*). The GA used is similar to that described by *Gulsen et al.* [1995]. This "global solver" is used in combination with a "local solver," which is better suited to finding a local minimum (MATLAB fminunc function). As the GA contains a random element, it may not find the same minimum every time it is run, although in practice if the GA is run for long enough the fits are very similar. In summary, the GA contains a population of coefficients. The population members are randomly mixed in each generation, with the worst members in terms of goodness of fit then being culled. This allows the best members of the population to remain and keep improving the fit until there is either no further improvement or the maximum number of generations is reached.

[82] The GA is given the coefficients from a least squares fit as a starting point. Random starting coefficients for the population size are then selected from a normal distribution with the starting coefficient as a mean. The goodness of fit, calculated from the sum of squared orthogonal errors, is calculated for the entire population. The population is ranked by goodness of fit and the bottom half culled. The remaining half are randomly sorted into pairs, and a crossover mechanism creates new members, which are the mean of the parent coefficients. Additionally, a mutation mechanism creates new coefficients from a uniform distribution of 2 times the range of all the parent coefficients. The goodness of fit is calculated for the new members and the cycle repeated. The
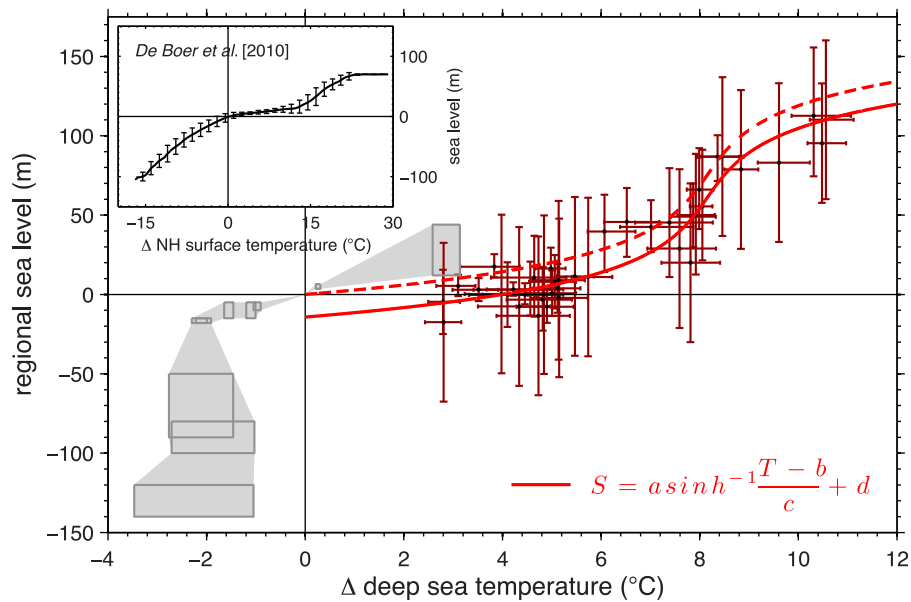
Figure 14. Data as per Figure 6, showing deep-sea temperature against regional sea level, with *de Boer et al.*'s [2010] observation-constrained modeled results inset. Single inverse hyperbolic sine function fit to *Kominz et al.*'s [2008] New Jersey regional sea level data and *Lear et al.*'s [2000] Mg/Ca deep-sea temperature. Dashed line is "corrected" for potential isostatic offset by shifting function on *y* axis so that it is consistent with modern deep-sea temperature and sea level (see text).

GA is run for 200 generations but can be terminated earlier if there is no improvement after 50 generations.

5. SYNTHESIS

[83] The linear function is fitted to all of the temperature versus sea level plots for high-latitude Southern Hemisphere SST, low-latitude SST, and DST. The single sinh^{-1} function is fitted to the high-latitude Southern Hemisphere SST and DST plots, and the double sinh^{-1} function is fitted to the DST plot only. Independent data show the relationship between the relevant temperatures and sea level at several intervals in the Plio-Pleistocene [*Rohling et al.*, 2009; *Herbert et al.*, 2010; *Siddall et al.*, 2010a]. These additional Plio-Pleistocene data are included in the figures as a guide; the functions are not constrained by these additional data.

5.1. Testing Linear Functions

[84] The linear function (Figures 11–13) highlights the positive correlation between sea level and DST or SST. However, there are important constraints that mean a linear model is not necessarily appropriate here. The y-intercept of the linear models suggests that for modern DSTs sea level would be approximately −81 m (Figure 11), for high-latitude Southern Hemisphere SST it would be −57 m (Figure 12), and for low-latitude SST it would be −32 m (Figure 13). Alternatively the linear function can be forced through the origin, i.e., be constrained to modern sea level and temperature, but this produces a poor fit to the DST and high-latitude Southern Hemisphere SST data, although it produces a reasonable fit to the low-latitude SST data.

[85] It is possible that the NJ sea level data contain a systematic offset due to isostatic effects during the Pleistocene.

Sea level on the NJ margin continued to rise throughout the Holocene and is presently on the order of ~10 m lower than equilibrium, assuming an exponential curve to equilibrium [see *Miller et al.*, 2009b, Figure 3; *Raymo et al.*, 2011]. Sea level records from other regions suggest Holocene stabilization, following a large sea level increase due to the melting of the major glacial period ice sheets, from 6 to 9 ka [*Siddall et al.*, 2003]. A crude "correction" for this potential systematic isostatic effect is to shift the data set on the *y* axis so that the function passes through the origin (dashed line in Figures 11–13). However, this would imply an offset due to postglacial isostasy of 81, 57, or 32 m for the DST, high-latitude Southern Hemisphere SST, and low-latitude SST data, respectively. This is significantly larger than the ~10 m from equilibrium previously mentioned [*Raymo et al.*, 2011]. This simple offsetting approach is also applied to the nonlinear functions in Figures 14–16.

[86] A second constraint that means a linear function may be a poor representation of the data is that once ice-free conditions are reached the function should asymptote to the thermal expansion gradient. The linear function is also not consistent with the independent Plio-Pleistocene data, except for the low-latitude SST data (Figure 13). Conceptually, a linear fit is not consistent with the modeling work of *de Boer et al.* [2010], which clearly showed different temperature thresholds for Northern Hemisphere and Southern Hemisphere glaciation.

5.2. Testing Nonlinear Functions

[87] An inverse hyperbolic sine function can describe a single-stepped form, similar to the work of *de Boer et al.* [2010], for temperatures warmer than present (Figure 4).
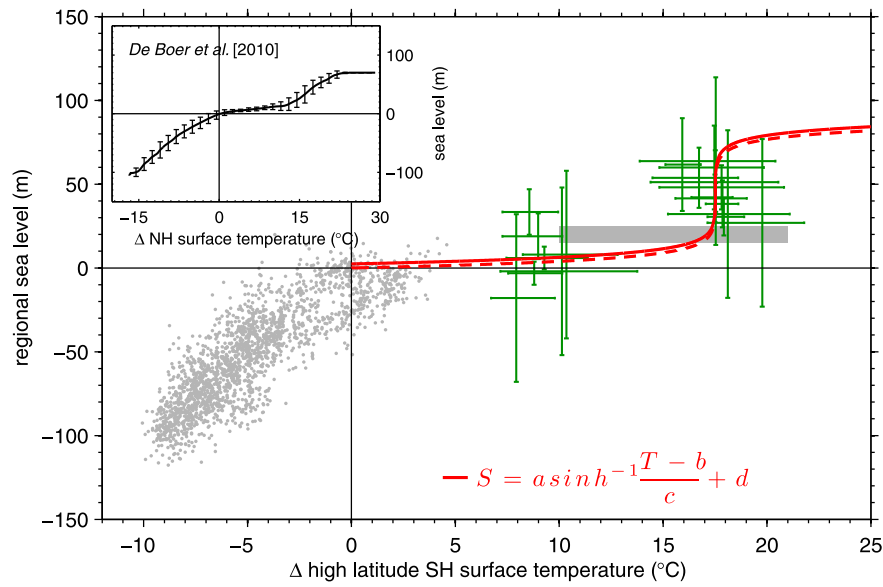
Figure 15. Data as per Figure 7, showing high-latitude Southern Hemisphere surface temperature against regional sea level, with *de Boer et al.*'s [2010] observation-constrained modeled results inset. Single inverse hyperbolic sine function fit to *Kominz et al.*'s [2008] New Jersey regional sea level data and *Liu et al.*'s [2009] high-latitude Southern Hemisphere SST data. Dashed line is "corrected" for potential isostatic offset by shifting function on y axis so that it is consistent with modern temperature and sea level (see text).

This function is not fitted to the low-latitude SST data, as a single-stepped form is not apparent in these data. This function can partially satisfy the independent constraints highlighted above. For modern DSTs this function predicts

sea level of -14 m (Figure 14). If there is a sea level offset due to Holocene isostasy then it could conceivably be of this magnitude [*Raymo et al.*, 2011], although for the high-latitude Southern Hemisphere SST data, the function predicts
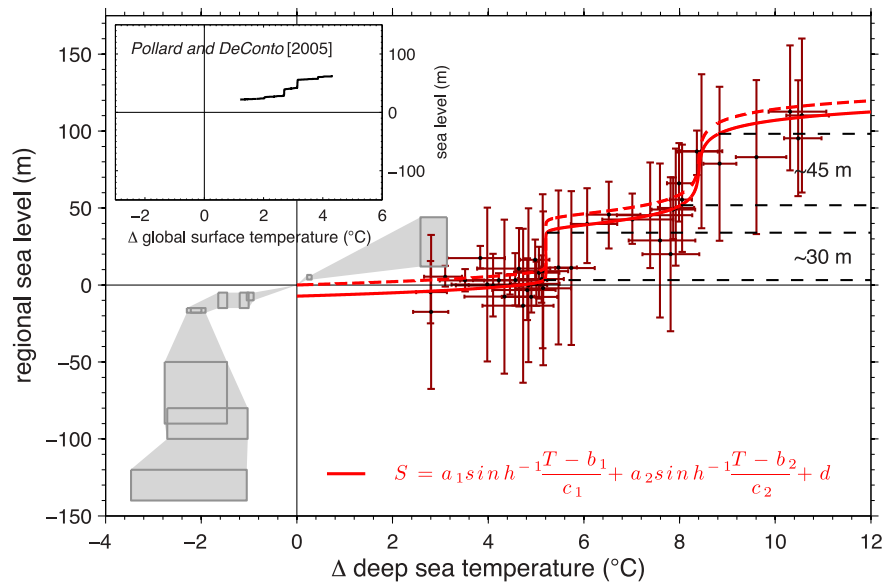

Figure 16. Data as per Figure 6, showing deep-sea temperature against regional sea level, with *Pollard and DeConto*'s [2005] ice sheet modeled results, for cooling direction without orbital variation, shown inset. Double inverse hyperbolic sine function fit to *Kominz et al.*'s [2008] New Jersey regional sea level data and *Lear et al.*'s [2000] Mg/Ca deep-sea temperature. Dashed line is "corrected" for potential isostatic offset by shifting function on y axis so that it is consistent with modern temperature and sea level (see text). The magnitude of the sea level changes occurring in the steps is highlighted, showing a total sea level change of $\sim$75 m, which is greater than for the two-step model of *Pollard and DeConto* [2005], suggesting that the NJ sea level record contains other effects (see text).
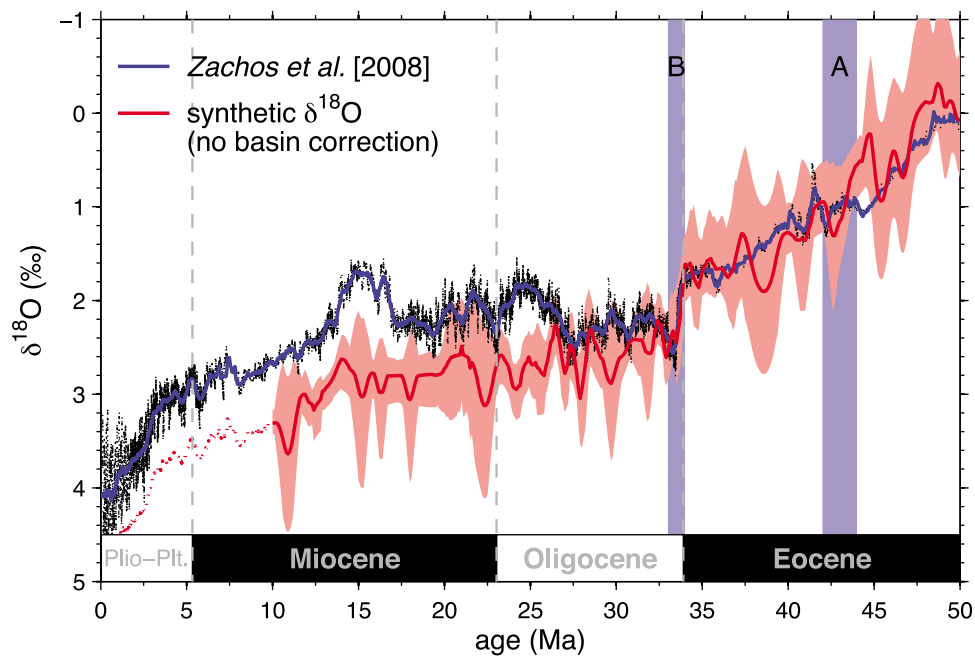
Figure 17. Synthetic $\delta^{18}O$ (red line) plotted against benthic $\delta^{18}O$ stack (blue line) [*Zachos et al.*, 2008]. The synthetic record is created using *Kominz et al.*'s [2008] sea level record and *Lear et al.*'s [2000] temperature record. The sea level data are first multiplied by 1.48 to account for hydroisostasy [*Pekar et al.*, 2002], thermal expansion is removed using the temperature record of *Lear et al.* [2000] and a factor of 1 m per °C, and sea level is then converted to $\delta^{18}O$ using a 0.01‰ per m calibration [*Pekar et al.*, 2002; *Miller et al.*, 2009a]. Ocean basin changes are not removed from the sea level record, and this is a potential source of error. *Lear et al.*'s [2000] temperature record is converted to $\delta^{18}O$ using a 0.25‰ per °C calibration [*Zachos et al.*, 2001]. These two signals are combined to create the synthetic $\delta^{18}O$ curve. From 0 to 10 Ma there are no sea level data, so the synthetic $\delta^{18}O$ curve (dotted red line) tracks the benthic $\delta^{18}O$ stack for the period 0–10 Ma.

modern sea level of +2 m (Figure 15). For temperatures cooler than present, the sea level to high-latitude Southern Hemisphere surface temperature relationship has been suggested by *Rohling et al.* [2009] to represent an exponential curve. The single-stepped function asymptotes toward modern temperature, which could join an exponential curve for temperatures cooler than present. The single-stepped form joining an exponential curve is similar to the relationship seen in the modeling work of *de Boer et al.* [2010].

[88] The upper asymptote for the single-step function suggests a sea level of 110 m for DSTs of +10°C and a sea level of 80 m for high-latitude Southern Hemisphere SSTs of +20°C. This is well above the ice-free thermal expansion gradient, as shown in Figures 6 and 7. This again highlights that the NJ sea level record contains other drivers of sea level change, such as ocean basin volume changes and potential isostatic changes. The high-latitude Southern Hemisphere SST plot against sea level (Figure 15) shows a steep transition, with the step occurring in the second cluster of data. It is likely that this is caused by discrepancies in the age models of the two data sets, as the sea level fall in *Kominz et al.*'s [2008] record at the EOT precedes the EOT temperature fall in the record of *Liu et al.* [2009]. It is important to bear in mind the ±0.5 Ma age error estimate of *Kominz et al.*'s [2008] record. If the age models were better matched,

the relationship between high-latitude Southern Hemisphere SST and sea level may be different.

[89] In addition to the single-stepped nonlinear function, a two-stepped nonlinear function is fitted to the DST data (Figure 16). The function identifies the two steps seen in the time-ordered data. As previously mentioned, this two-stepped form shows some consistencies with the modeling work of *Pollard and DeConto* [2005], although the sea level change in the steps of ∼75 m is greater than the ∼50 m (∼33 m after accounting for hydroisostasy for comparison with the NJ record) shift shown by *Pollard and DeConto* [2005], and the timescales are significantly different. The function produces extremely rapid rates of sea level change at the thresholds of the steps. Step B is due to the rapid formation of ice at the EOT. As previously discussed, step B is likely to be overly steep because of the lack of temperature change in *Lear et al.*'s [2000] Mg/Ca data set at the EOT. The origin of step A (∼42–44 Ma) is discussed in more detail below. The function is offset on the *y* axis by ∼4 m (dashed line in Figure 16) to account for the possible isostatic error.

5.3. Synthetic $\delta^{18}O$

[90] An alternative way to test the sea level and DST data is to create a synthetic $\delta^{18}O$ record using a simple calibration and compare it with the benthic $\delta^{18}O$ stack (Figure 17). Here

we convert the NJ sea level record and Mg/Ca DST record to a $\delta^{18}O$ signal using a calibration of 0.01‰ per m [*Pekar et al.*, 2002; *Miller et al.*, 2009a] and 0.25‰ per °C [*Zachos et al.*, 2001], respectively. Prior to this conversion, the NJ sea level record is adjusted for hydroisostasy by multiplying by 1.48 [*Pekar et al.*, 2002]. We remove thermal expansion from the sea level record using the DST record and a calibration of 1 m per °C. This sea level calibration is possibly an oversimplification when used on such a long timescale. It is possible that the first ice caps to form on Antarctica would have had a different isotopic composition to the present-day ice sheets [*DeConto et al.*, 2008; *Katz et al.*, 2008]. The modeling work of *de Boer et al.* [2012] shows that the scaling factor of seawater $\delta^{18}O$ to sea level has not remained constant over the last 40 Ma, although they suggest that the constant calibration, as used here, is a reasonable approximation. Additionally, the NJ sea level data set contains a signal from ocean basin changes and may include regional tectonic effects, which are not related to $\delta^{18}O$. We do not attempt to remove these effects from the NJ record and acknowledge that this is a limitation of this very simple approach. The synthetic record is tied to the benthic $\delta^{18}O$ stack [*Zachos et al.*, 2008] at 50 Ma. From 0 to 10 Ma, sea level data are not available [*Kominz et al.*, 2008]; in the work by *Miller et al.* [2005a] sea level in the late Miocene and Plio-Pleistocene is based on a calibration of the benthic $\delta^{18}O$ record. We extend the synthetic $\delta^{18}O$ from 0 to 10 Ma using the actual benthic $\delta^{18}O$ stack, with the dotted line in Figure 17.

[91] The synthetic record follows the general trend of the benthic $\delta^{18}O$ stack (Figure 17). The ∼1.6‰ increase in the benthic $\delta^{18}O$ stack from 50 Ma to the EOT is reproduced in the synthetic $\delta^{18}O$ record, with ∼1.1‰ due to temperature and ∼0.5‰ due to sea level. However, the large increase in the synthetic $\delta^{18}O$ record at ∼42–44 Ma, which is responsible for step A in the temperature and sea level crossplots, is not seen in the benthic $\delta^{18}O$ stack. The large increase in $\delta^{18}O$ at the EOT is seen in the synthetic record (step B), although it is of a slightly lower magnitude than the increase in the benthic $\delta^{18}O$ stack. This is probably due to the lack of apparent cooling in the uncorrected Mg/Ca DST record. The synthetic $\delta^{18}O$ record diverges from the benthic $\delta^{18}O$ stack in the Miocene, in particular during the middle Miocene. Both the DST and sea level records used in the synthetic $\delta^{18}O$ record have poor data coverage during the Miocene.

6. DISCUSSION

[92] The sea level and temperature synthesis generates several points for discussion; the majority of this discussion focuses on the DST to sea level relationship as the DST record is more complete than the SST record. The additional surface temperature records for the EOT are useful in determining whether there is a nonlinear response to temperature forcing across this boundary, as may be suggested by the uncorrected (for carbonate saturation effects) DST data. If the two-step function is appropriate, and if the first step (step A) is due to glacioeustasy, then it implies the

formation of significant land ice in the Eocene. Not all of the sea level variability is due to the formation of land ice; there are thermosteric and ocean basin volume components and potential regional tectonic effects. However, the rate and magnitude of the sea level decline in the raw NJ sea level record may suggest glacioeustasy as a cause [*Miller et al.*, 2008]. The significance of these steps should be considered in combination with the multiple sources of error in the data discussed in sections 2.1 and 2.2. Finally, we discuss the types of nonlinearity that might be expected when looking at the temperature to sea level relationship from ice-free conditions to full Northern Hemisphere glaciation. Broadly, the expected nonlinearity can be divided into two types: (1) as seen in some ice sheet modeling studies [*Huybrechts*, 1993; *Pollard and DeConto*, 2005; *Langebroek et al.*, 2009], where a small temperature forcing, near the glacial threshold, generates a large change in ice volume, and (2) nonlinearity caused by the different glacial thresholds for Northern and Southern Hemisphere glaciation. This second nonlinearity occurs as the ice sheet carrying capacity of the Antarctic continent is reached before the glacial threshold for Northern Hemisphere glaciation [*de Boer et al.*, 2012].

6.1. Eocene Ice and the Origins of Step A

[93] The extent of Antarctic glaciation prior to the EOT and whether Northern Hemisphere ice sheets existed before the Pliocene are two questions still subject to much debate [*Miller et al.*, 2005a; *Pekar et al.*, 2005; *Moran et al.*, 2006; *Eldrett et al.*, 2007; *Coxall and Pearson*, 2007; *Cox et al.*, 2010; *Dawber and Tripati*, 2011; *Dawber et al.*, 2011]. *Shackleton and Kennett* [1975] used the $\delta^{18}O$ record to hypothesize that a continent-sized ice sheet first formed on Antarctica ∼15 Ma. *Matthews and Poore* [1980] proposed an alternative theory, which suggested that there was an earlier ice formation event between the Eocene and Oligocene. As previously discussed (sections 2.3 and 5.3), the $\delta^{18}O$ record of benthic foraminifera shows a rapid increase in $\delta^{18}O$ at the EOT [*Zachos et al.*, 2008].

[94] The sequence stratigraphy record of sea level from the NJ margin shows large changes earlier than the Oligocene [*Miller et al.*, 2005a]. The rate and magnitude of these sea level changes may imply that they are due to changes in ice volume. In the raw NJ sea level data, step A is seen as a sea level fall of ∼35 m over ∼0.7 Ma (Figure 1) [*Kominz et al.*, 2008]. The relatively fast rate of these sea level changes has been suggested to rule out other factors that could cause a sea level change of this magnitude, such as variations in ocean basin volume [*Miller et al.*, 2005a]. A thermosteric response could explain the rate of sea level change but not the magnitude. This points to at least ephemeral ice sheets on Antarctica during the Eocene. This is controversial, as this same argument used to justify ice mass changes in the Eocene can be extended for the whole of the 100 Ma NJ record and would imply that ephemeral ice sheets were present during the whole of the Cenozoic and into the Late Cretaceous, a time that was thought to be ice free [*Miller et al.*, 2005b].

[95] *Miller et al.* [2008] used the modeled ice sheet maps of *DeConto and Pollard* [2003a] to estimate how large an

ice sheet would be required to explain each of the transitions in *Miller et al.*'s [2005a] sea level record. Clearly, a larger sea level transition would require the formation or loss of a larger ice sheet than a smaller sea level transition. Smaller ice sheets could form under the higher atmospheric CO_2 concentrations of the Eocene in the Antarctic mountain regions [*DeConto and Pollard*, 2003a; *Pagani et al.*, 2005]. A larger ice sheet would require a lower atmospheric CO_2 concentration than that shown in the Eocene proxy CO_2 records. All of the pre-Oligocene transitions in *Miller et al.*'s [2005a] record are of a small enough magnitude to be explained by the formation or loss of isolated ice caps in the Antarctic mountain regions [*Miller et al.*, 2008]. Only the larger sea level transition at the EOT would require growth of a continental sized Antarctic ice sheet.

[96] A potential problem with this hypothesis is that it is dependent on the existence of high-topographic regions during the Late Cretaceous and Eocene. However, the paleotopography of Antarctica is poorly known. Although some authors suggest that uplift of the trans-Antarctic mountains began in the Cretaceous [*Fitzgerald*, 2002], others place uplift much later, in the Eocene [*ten Brink et al.*, 1997]. The hypothesis of *Miller et al.* [2008] partially breaks down if trans-Antarctic mountain uplift did indeed occur more recently. However, even if the trans-Antarctic mountains were not uplifted, the other high-elevation regions of the Gamburtsev Mountains and Dronning Maud Land could have harbored isolated ice caps; indeed, the Gamburtsevs are considered to be the major early ice nucleation center for ice growth [*Huybrechts*, 1993; *DeConto and Pollard*, 2003a, 2003b] and to have formed considerably before the Cenozoic [e.g., *Cox et al.*, 2010].

[97] *Browning et al.* [1996] looked at links between $\delta^{18}O$ data in the Eocene with an earlier version of the NJ sequence stratigraphy sea level record. They suggested that increases in benthic and planktonic $\delta^{18}O$ correlate well with hiatuses in the sea level record from the late to middle Eocene onward (later than 42–43 Ma) and may suggest a glacioeustatic control. There is little correlation in the earlier Eocene (49–43 Ma) between the sea level record and the $\delta^{18}O$ record, meaning that a glacioeustatic control is unlikely. Therefore, they suggest that the late to middle Eocene (42–43 Ma) could mark the onset of Antarctic glaciation. This is consistent with the timing of the first step (~42–44 Ma) in the two-step model. This is slightly earlier than proposed by *Billups and Schrag* [2003] as the possible onset of glaciation. They suggested that the good agreement between their Mg/Ca record and the benthic $\delta^{18}O$ record in the early Eocene implied DST as a sole control on benthic $\delta^{18}O$. From ~40 Ma the Mg/Ca record diverges from the $\delta^{18}O$ record, suggesting that ice growth may have started to affect the benthic $\delta^{18}O$ ratios [*Billups and Schrag*, 2003].

[98] If ephemeral glaciation did begin in the late to middle Eocene and ice caps were present in Antarctica, then it would seem likely that the rapid increase in atmospheric CO_2 during the MECO (~40 Ma) [*Bijl et al.*, 2010] would have had an impact on ice volumes. This event is characterized by a rapid and large decrease in benthic $\delta^{18}O$ [*Zachos*

et al., 2008]. This benthic $\delta^{18}O$ shift suggests a rapid increase in DSTs, which may have been combined with decreasing ice volume. If this shift in benthic $\delta^{18}O$ was due to surface warming alone then it would require an increase in DST of ~4°C–5°C [*Bijl et al.*, 2010]. *Bijl et al.* [2010] using both TEX_{86} and $U^{k'}_{37}$ inferred a surface warming of 3°C and 6°C, respectively. This means that if this surface warming reached the deep sea, a reduction in ice volume is not needed to explain the large benthic $\delta^{18}O$ shift at the MECO [*Bijl et al.*, 2010]. This would suggest that either ice sheets were not present prior to this event or that they were not significantly affected by this rapid but brief warm interval.

[99] *Dawber et al.* [2011] suggested that stratigraphic sequences from the Hampshire Basin, United Kingdom, show large amplitude regional water depth changes in the middle Eocene. A negative benthic $\delta^{18}O$ excursion at the same site, comparable to the MECO $\delta^{18}O$ excursion seen in open ocean sites [*Bohaty et al.*, 2009], correlates with a large regional increase in water depth [*Dawber et al.*, 2011]. Although it is difficult to determine the cause of this regional change in water depth at the MECO, glacioeustasy is a possibility [*Dawber et al.*, 2011]. *Dawber and Tripati* [2011] could not precisely identify the MECO in their high-resolution middle Eocene benthic $\delta^{18}O$ record from Site 1209 in the Pacific. However, they did identify multiple $\delta^{18}O$ excursions in the middle Eocene (at ~44–43 Ma, ~42–40 Ma and ~39–38 Ma), which could not be reconciled with Mg/Ca based DST estimates from the same site. Although there are age model uncertainties, these events appear to correlate with sequences in the NJ record, including step A [*Kominz et al.*, 2008; *Dawber and Tripati*, 2011]. This could suggest that these $\delta^{18}O$ excursions were caused in part by a change in ice volume [*Dawber and Tripati*, 2011].

[100] In the smoothed sea level record used in this review, the period between 44 Ma and 34 Ma shows little sea level variation. However, the raw sea level record does show significant fluctuations [*Kominz et al.*, 2008]. Even if isolated ice caps formed at step A, it is likely that they were ephemeral in this 10 Ma period in order to explain the continued sea level fluctuations in the raw record, whereas step A represents a permanent shift in our DST to sea level crossplot (Figure 16). Additionally, the large sea level fall at the EOT, if it can be explained solely by the formation of ice on Antarctica, requires that there was very little ice on Antarctica before the event [*Miller et al.*, 2009a]. A closer analysis of the $\delta^{18}O$ data suggested that the EOT (step B) also occurred in two steps, representing the isolated ice cap phase prior to full inception of a continental sized East Antarctic Ice Sheet [*Coxall et al.*, 2005]. The two-step function in this review might not represent the noise in the data. In summary, while we are confident that there is a glacioeustatic origin behind step B, there is limited supporting evidence for step A in the middle Eocene being caused by glacioeustasy, although this arguably remains the best explanation for this large and relatively rapid sea level fall in the NJ sea level record.

[101] An independent means of determining the origin of the two steps in our crossplot is the synthetic $\delta^{18}O$ record

created from the sea level and temperature data for comparison with the benthic $\delta^{18}O$ stack (section 5.3). Although there is an increase in the synthetic $\delta^{18}O$ record at step A, there is no obvious increase in the benthic $\delta^{18}O$ record at the same period in the Eocene (Figure 17) [*Zachos et al.*, 2008]. Therefore, the global compilation of benthic $\delta^{18}O$ data do not lend support to step A being caused by glacioeustasy and instead, perhaps, points to either regional tectonic influence on the NJ record or ocean basin changes at this time. When interpreting these steps, it is important to bear in mind the large sources of uncertainty in the NJ sea level record.

6.2. Causes of Nonlinearity in the Temperature to Sea Level Relationship

[102] It is useful to separate the nonlinearities that might be expected in the relationship between temperature and sea level into two types: (1) as seen in some ice sheet modeling studies [*Huybrechts*, 1993; *Pollard and DeConto*, 2005; *Langebroek et al.*, 2009] where a small temperature forcing, near the glacial threshold, generates a large change in ice volume, and (2) caused by the different glacial thresholds of Northern and Southern Hemisphere glaciation and the ice sheet carrying capacity of the Antarctic continent [*de Boer et al.*, 2012]. The steps that are shown in the DST against sea level plots may suggest the first type of nonlinearity, where a small temperature change leads to a large sea level change. However, as we have discussed, it is likely that data artifacts alter, enhance, or even generate these steps. The lack of cooling in the DST record of *Lear et al.* [2000] at the EOT is most likely responsible for the steepness of step B, and there is uncertainty as to whether step A in the Eocene is due to glacioeustasy. Additionally, the EOT step is not seen in the surface temperature plots (Figures 7 and 8). Instead, we suggest that the second type of nonlinearity mentioned above is more evident in the data.

[103] Both the one-step and two-step functions suggest that once a large continental sized EAIS has formed, sea level becomes less sensitive to changing DST; the function asymptotes toward modern sea level and temperature. There is a gap in the sequence stratigraphy sea level data set between 0 and 10 Ma [*Kominz et al.*, 2008], and so the temperature–sea level relationship is not represented in this time period. The sea level record of *Miller et al.* [2005a] uses a calibration of the benthic foraminifera $\delta^{18}O$ record for this time period. Between 3 and 10 Ma in *Miller et al.*'s [2005a] record there is very little sea level variation prior to large sea level fluctuations starting ~3 Ma associated with the formation of the Northern Hemisphere ice sheets and Pleistocene glacial cycles. In the modeling work of *de Boer et al.* [2010, 2012] sea level is also remarkably stable in the period 3–10 Ma, with the majority of variation in the input $\delta^{18}O$ data explained by temperature variation. Therefore, the lack of data for the period of 0–10 Ma does not significantly affect this conclusion, although ideally a complete sea level record for this period is needed.

[104] The relationship between both deep-sea and surface air temperature and sea level has previously been studied for temperatures colder than present [*Rohling et al.*, 2009;

Siddall et al., 2010a, 2010b]. These studies suggest that there is also an asymptotic relationship toward modern sea level from colder temperatures [*Rohling et al.*, 2009; *Siddall et al.*, 2010a, 2010b]. The work on temperature and sea level relationships for temperatures colder than present, in addition to this review and the work of *de Boer et al.* [2010], suggests that the present interglacial state is relatively stable in the context of sea level variations over the past 50 Ma, while supporting the existence of "critical thresholds" within the Earth's climate system. The "warm threshold" corresponds to the early Cenozoic major East Antarctic glaciation, whereas the "cold threshold" corresponds to the major Northern Hemisphere glaciations of the Pleistocene. In between these two large thresholds are the glaciations of the West Antarctic and Greenland, which we cannot resolve in this analysis because of the large errors (>10 m) in the sea level data used.

7. CONCLUSIONS

[105] In this review, the relationship between sea level and DST has been synthesized using the Mg/Ca DST record of *Lear et al.* [2000] and the regional sequence stratigraphy sea level record from the NJ margin [*Kominz et al.*, 2008]. This DST to sea level relationship may differ from the surface temperature to sea level relationship on this long timescale if the surface to DST gradient has changed, which could have occurred because of ocean circulation [*Nong et al.*, 2000; *Najjar et al.*, 2002; *Cramer et al.*, 2009; *Katz et al.*, 2011]. We emphasize the significant sources of error and the regional nature of the currently available long-duration data sets. We have investigated the relationship at the low temporal resolution of the available DST data, ~1 Ma, as such some of the higher-frequency details of the sea level record are not included. In addition to the DST data, we have used SST data across the EOT, as this is a period of major sea level change and a period poorly represented by the current Mg/Ca DST records.

[106] Different functions, justified by previous publications [*Huybrechts*, 1993; *Pollard and DeConto*, 2005; *Archer*, 2006; *de Boer et al.*, 2010], have been fitted to the data. Important constraints, for example, that a function should pass through modern sea level and temperature, mean that it is unlikely that there is a linear relationship between DST and sea level or high-latitude Southern Hemisphere SST and sea level. However, the relationship between low-latitude temperature and sea level remains ambiguous and could be explained by a linear relationship. A linear function is not consistent with ice sheet modeling studies [*Huybrechts*, 1993; *Pollard and DeConto*, 2005; *de Boer et al.*, 2010].

[107] Nonlinear functions, in both one-step and two-step forms, are a more plausible fit to the DST and Southern Hemisphere high-latitude data against sea level plots. It is difficult to determine whether the single-step or two-step function is the most appropriate function given the wide errors in the currently available data. The two-step hypothesis originates from GCM and ice sheet modeling studies where ice build up on Antarctica occurs nonlinearly in a

series of steps in response to declining atmospheric CO_2 and temperature [*Pollard and DeConto*, 2005]. The first step occurs with the formation of isolated ice caps in the mountain regions of Antarctica before the formation of a continent sized ice sheet in the second step. We underline an important caveat of using the NJ sea level record: the long-term sea level change contains thermosteric and ocean basin volume components and potentially regional tectonic effects. The two-step hypothesis is a glacioeustatic concept, yet when it is applied to the DST and sea level data in this review it shows a greater sea level range ($\sim$75 m in the two steps, 100 m in total) than can be explained solely by the formation of the modern ice sheets ($\sim$43–54 m as seen from the NJ margin). Additionally, the first step occurs at $\sim$42–44 Ma, implying that large, permanent Antarctic ice caps formed in the Eocene, for which there is at present limited supporting evidence. The second step at the EOT in the DST against sea level plot is, at least in part, an artifact of the lack of cooling in *Lear et al.*'s [2000] Mg/Ca DST data set across the EOT. A steep step is not apparent for the SST against sea level plots for the EOT.

[108] The asymptotic relationship between modern temperature and sea level relative to glacial temperatures (i.e., cooler than present) [*Rohling et al.*, 2009; *Siddall et al.*, 2010b] or pre-Pleistocene temperatures (i.e., warmer than present, this review) suggests that the present interglacial state is relatively stable compared to the overall sea level change observed for the past 50 Ma. However, the implied nonlinear relationship in the DST and high-latitude Southern Hemisphere SST data suggests there are large sea level thresholds for temperatures warmer and colder than present. These are caused by the different glacial thresholds for Northern Hemisphere and Southern Hemisphere glaciation and the size of the Antarctic continent restricting further growth of the East Antarctic Ice Sheet. Given the significant limitations of the currently available DST data, due in part to uncertainties in the past seawater Mg/Ca concentration, it is difficult to determine precisely the temperatures of these thresholds. Unfortunately, the uncertainties within the sea level and temperature proxy data used here are currently too large to resolve potential thresholds associated with smaller-scale glaciation (e.g., <10 m, which could, for example, include the Greenland Ice Sheet and West Antarctic Ice Sheet).

[109] The sea level to temperature relationships in this review are based on long-term changes (>1 Ma), which, given that the response time of the ice sheets is <1 Ma [*Miller et al.*, 2005a], we assume is representative of the major ice sheets and sea level in near equilibrium with the climate. Therefore, this relationship is not directly applicable to anthropogenic warming on a centennial timescale. In addition, the current uncertainties in the sea level and temperature proxies used in this review precludes an assessment of thresholds that may potentially be associated with today's least stable continental ice sheets (the West Antarctic Ice Sheet and the Greenland Ice Sheet). Hysteresis effects mean that any thresholds are likely to be at higher temperatures

for warming than for cooling; this review uses Cenozoic data that predominantly show cooling. The temperature thresholds visible in the figures should therefore be seen as low estimates. The temperature to sea level relationships investigated in this review use data over a very long time period, which includes significant tectonic change, continental movement, mountain building, and ocean circulation change. All of these effects could have an influence on the paleo-long-term sea level to temperature relationships and are not relevant to short-term future warming. These important caveats are relevant to all attempts at temperature to sea level synthesis on this long timescale, including this review.

8. FUTURE WORK

[110] This review is a tentative attempt at bringing different paleoproxies and modeling studies together. We have identified some interesting relationships in the existing data, and we also highlight significant areas for future work. We have been limited in our ability to define better the DST and SST to sea level relationships on this long timescale given the qualitative and quantitative uncertainties in the sea level and temperature data used in this review and incomplete durations of the data.

[111] Since the publication of *Lear et al.*'s [2000] long-duration, low-resolution DST data set used in this review, improvements to the Mg/Ca temperature proxy and its application have been made, and newer, shorter-duration, higher-resolution data sets have been produced [e.g., *Lear et al.*, 2010; *Pusz et al.*, 2011]. However, further refinement of this proxy is needed, leading to the production of a long-duration, high-resolution data set. This is in addition to the continued development of other temperature proxies such as TEX_{86} and $U^{k'}_{37}$. The potential regional effects in the NJ sequence stratigraphy record mean that additional well-dated records from other regions are needed to determine to what extent this record is representative of global eustatic sea level. This is in combination with work on the tectonic history of the NJ margin during the Cenozoic. More work is needed on reconstructing past ocean circulation changes in order to determine how representative the DST record and multibasinal compilations are of surface climate changes [*Cramer et al.*, 2009]. While this paper was in the late stages of review, a new data synthesis was published that addresses some of these issues [*Cramer et al.*, 2011].

[112] The novel modeling approach of *de Boer et al.* [2010, 2012] and *Bintanja et al.* [2005a] can be developed using more sophisticated 3-D ice sheet models. This may result in the form of the sea level versus temperature relationship showing more similarities to the asynchronous modeling of *Pollard and DeConto* [2005]. Ongoing improvements to the asynchronous ice sheet GCM modeling method will allow more processes and feedbacks to be represented better, such as albedo feedbacks and hysteresis effects. Additional GCM and ice sheet modeling studies are needed to address areas of contention in the proxy record, such as the middle Miocene and the middle to late Eocene. This future work will aid improved understanding of the past temperature versus sea

level relationship as discussed in this review and allow any thresholds to be better defined.

GLOSSARY

Alkenone unsaturation index ($U^{k'}_{37}$):   A proxy of past sea surface temperatures. Alkenones are synthesized by certain species of phytoplankton. The degree of unsaturation displays a relationship with temperature at time of biosynthesis; increasing unsaturation correlates with decreasing temperature.

Asynchronous coupling: A simplified coupling between a general circulation model (GCM) and an ice sheet model that reduces the computational expense of running a GCM. A full coupling would require running the GCM for thousands of years (model time) for the ice sheet model to approach equilibrium, which at present is too computationally expensive. This technique takes advantage of the different timescales that the climate system and the ice sheets take to reach equilibrium: first, by running multiple GCM simulations with different CO_2 and orbital forcings and different ice sheet configurations that are then stored and second, running the ice sheet model for a much longer period (model time) and updating at regular intervals with a new GCM forcing.

Backstripping: A method that progressively removes the effects of compaction, sediment loading, and subsidence from a sediment core to obtain a paleo–water depth estimate.

Biofacies: Bodies of sediment that are distinguished based on the fossil assemblages contained within the sediments.

Biostratigraphy: A stratigraphic technique that uses biological markers to correlate sequences and aid the dating of sediments.

Calcite compensation depth (CCD):   Depth in the ocean where rate of dissolution exceeds supply of calcite. In deep ocean waters, at very low levels of calcite saturation, changes in the CCD and hence the calcite saturation state affect the benthic Mg/Ca proxy.

DST: Deep-sea temperature.

δD: The ratio of deuterium to hydrogen, used as a proxy for atmospheric temperature from the ice in ice cores.

$\delta^{18}O$:   The ratio of the stable oxygen isotopes ^{18}O to ^{16}O; the signal recorded in formainiferal calcite can be used as a climate proxy. A sample and standard are analyzed using a mass spectrometer with the result from the sample conventionally presented using delta (δ) notation relative to the standard. During evaporation of water from the ocean, fractionation occurs because of preferential evaporation of the lighter ^{16}O isotope. Fractionation also occurs during condensation, with the heavier ^{18}O isotope preferentially condensed. As atmospheric vapor is transported away from its source region, condensation during transport means the remaining vapor becomes more and more depleted in ^{18}O. The buildup of ice sheets from isotopically light (depleted in ^{18}O) precipitation, and subsequent storage of ^{16}O in ice sheets, will cause the oceans to become enriched in ^{18}O. In addition to this ice volume component, temperature-dependent fractionation occurs when the oxygen isotopes are incorporated into calcite tests of foraminifera. Increases in benthic foraminiferal $\delta^{18}O$ suggest deep-sea cooling and increased ice storage on land.

East Antarctic Ice Sheet (EAIS):   The larger of the two ice sheets presently in Antarctica, on the eastern side of the continent.

Eocene-Oligocene transition (EOT):   The climate transition between the Eocene and the Oligocene, including the growth of a continental sized ice sheet in the East Antarctic in the earliest Oligocene.

Eustatic sea level: Global sea level with respect to a fixed point, such as the center of the Earth, if seawater were evenly distributed across the ocean volume. In reality, sea level is not evenly distributed because of gravitational and rotational effects.

Foraminifera: A group of microorganisms that often produce a calcium carbonate test (shell), useful in paleoclimatology because of their diversity, abundance, and complex morphology. Foraminifera, or forams, can be used to reconstruct changes in calcium and oxygen isotopes present in seawater, and the fractionation that can occur when these elements are incorporated into their tests. In addition, other elements present in seawater can be incorporated, such as magnesium, strontium, and boron, some of which can be used as paleoclimate proxies.

General circulation model (GCM):   A mathematical representation of the atmosphere and/or ocean system.

Genetic algorithm (GA):   An optimization algorithm that mimics natural evolution, with elements such as a crossover, inheritance, and mutation mechanism, to find a solution. A population of solutions is ranked based on a measure of fitness, with the worst performing members being culled each generation. The average measure of fitness for each generation should therefore increase until a satisfactory solution has been found. The presence of a stochastic (random) element in the algorithm means it may not find the same solution each time it is run.

Highstand: A relatively high period of sea level.

Hyperbolic sine function: A sigmoidal or s-shaped function used here to represent the transition between two quasi-stable states.

Hysteresis: Memory in a system that shows a path dependence, meaning that output of the system cannot be predicted without prior knowledge of the evolution of the system. Used here in specific reference to the different ice volumes and sea levels that can exist at the same temperature depending on the prior state of the climate system. This means that one temperature can be related to several sea level stands depending on, for example, whether the climate system is warming or cooling.

Inverse routine: Used in relation to the modeling work of *Bintanja et al.* [2005a, 2005b] and *de Boer et al.* [2010, 2012] for their method of calculating Northern Hemisphere surface temperature from the difference between modeled $\delta^{18}O$ and observed $\delta^{18}O$ 100 years later.

Ice-rafted debris (IRD):   Material found on the seafloor that was previously embedded in ice on land, transported

by icebergs, and then deposited on the seafloor when the iceberg melts. Therefore, this can be used as a proxy for the past presence of ice on land.

Isostatic sea level change: Local change in sea level as observed from land not caused by a change in volume of water in the ocean or volume of the ocean basin but by displacement of the land, for example, by downward pressure of ice sheets (glacioisostasy) or water (hydroisostasy).

Last Glacial Maximum (LGM): Period of peak ice sheet extent during the last glacial period.

Lithofacies: Bodies of sediment that are distinguished based on their lithic characteristics.

Lowstand: A relatively low period of sea level.

Magnetostratigraphy: A stratigraphic technique that uses the polarity of the magnetic field recorded in sediments to correlate sequences with changes in the polarity of the Earth's magnetic field (of known age) to aid the dating of sediments.

Middle Eocene Climatic Optimum (MECO): A period of peak warmth in the Eocene ~40 Ma, shown as a decrease in $\delta^{18}O$ of benthic foraminifera of ~1.0‰.

Mg/Ca: Used as a proxy for past ocean temperature. Magnesium ions (Mg^{2+}) are incorporated into the calcite tests of foraminifera; the amount incorporated shows a temperature dependent relationship. Both core top samples and culturing experiments show that the Mg/Ca ratio of foraminiferal calcite increases with water temperature. Can be used with both benthic (bottom-dwelling) and planktonic (surface-dwelling) species as a proxy for past deep and surface sea temperatures, respectively.

Middle Miocene Climatic Optimum (MMCO): A period of peak warmth in the Miocene ~15 Ma evident in the benthic $\delta^{18}O$ record as an ~0.5‰ decrease in $\delta^{18}O$.

Orthogonal regression: A fitting method, also known as total least squares, which attempts to account for the instance where there are errors on both axes. By contrast, least squares regression attempts to minimize errors parallel to the y axis (response variable) and assumes that the predictor variable (x axis) has no error. With orthogonal regression, the errors between the data and the function are minimized at right angles.

Passive continental margin: The boundary between a continental and oceanic plate that is not an active plate margin.

Sequence stratigraphy: A geological technique that can be used to infer past changes in depositional environment, changes in local water depth, and hence changes in sea level. Depositional sequences bounded by unconformities show changes in regional sea level. By accurately dating sequences and inferring past water depth during depositional phases from lithofacies and biofacies models, a quantitative estimate of sea level through time can be created.

SST: Sea surface temperature.

Synthetic $\delta^{18}O$: Used here to represent the benthic $\delta^{18}O$ record created from the main constituent components, temperature, and ice volume (from sea level) of the actual benthic $\delta^{18}O$ record. Here we use a calibration for sea level to $\delta^{18}O$ of 0.01‰ per m and temperature to $\delta^{18}O$ of 0.25‰ per °C.

Tetraether index (TEX$_{86}$): The index of tetraethers that consist of 86 carbon atoms is a proxy of past surface sea temperature. The proxy is based on the composition of the membrane lipids of Thaumarchaeota (formerly classed as Crenarchaeota).

Thaumarchaeota: Single celled microorganisms belonging to the Archea domain. The composition of the membrane lipids of Thaumarcheota can be used to estimate past SSTs using the TEX$_{86}$ proxy. Formerly, there were two recognized phylum of Archea (one being Crenarchaeota); Thaumarcheota is a recently proposed third Archaeal phylum distinct from Crenarcheota [*Brochier-Armanet et al.*, 2008].

Thermosteric: Change in sea level caused by the thermal expansion or contraction of seawater.

Unconformity: Surface of nondeposition and/or erosion in the stratigraphic record.

West Antarctic Ice Sheet (WAIS): The smaller of the two ice sheets presently in Antarctica, on the western side of the continent.

REFERENCES

Alley, R. B., P. U. Clark, P. Huybrechts, and I. Joughin (2005), Ice-sheet and sea-level changes, *Science*, *310*(5747), 456–460, doi:10.1126/science.1114613.

Allison, I., R. B. Alley, H. A. Fricker, R. H. Thomas, and R. C. Warner (2009), Ice sheet mass balance and sea level, *Antarct. Sci.*, *21*(05), 413–426, doi:10.1017/S0954102009990137.

Anand, P., H. Elderfield, and M. Conte (2003), Calibration of Mg/Ca thermometry in planktonic foraminifera from a sediment trap time series, *Paleoceanography*, *18*(2), 1050, doi:10.1029/2002PA000846.

Archer, D. (2006), *Global Warming: Understanding the Forecast*, Blackwell, Malden, Mass.

Bamber, J. L., S. Ekholm, and W. B. Krabill (2001), A new high-resolution digital elevation model of Greenland fully validated with airborne laser altimeter data, *J. Geophys. Res.*, *106*(B4), 6733–6745, doi:10.1029/2000JB900365.

Bijl, P. K., S. Schouten, A. Sluijs, G. J. Reichart, J. C. Zachos, and H. Brinkhuis (2009), Early Palaeogene temperature evolution of the southwest Pacific Ocean, *Nature*, *461*(7265), 776–779, doi:10.1038/nature08399.

Bijl, P. K., A. J. P. Houben, S. Schouten, S. M. Bohaty, A. Sluijs, G. J. Reichart, J. S. Sinninghe Damsté, and H. Brinkhuis (2010), Transient middle Eocene atmospheric CO_2 and temperature variations, *Science*, *330*(6005), 819–821, doi:10.1126/science.1193654.

Billups, K., and D. P. Schrag (2003), Application of benthic foraminiferal Mg/Ca ratios to questions of Cenozoic climate change, *Earth Planet. Sci. Lett.*, *209*(1–2), 181–195, doi:10.1016/S0012-821X(03)00067-0.

Bintanja, R., and R. S. W. van de Wal (2008), North American ice-sheet dynamics and the onset of 100,000-year glacial cycles, *Nature*, *454*, 869–872, doi:10.1038/nature07158.

Bintanja, R., R. S. W. van de Wal, and J. Oerlemans (2005a), Modelled atmospheric temperatures and global sea levels over the past million years, *Nature*, *437*, 125–128, doi:10.1038/nature03975.

Bintanja, R., R. S. W. van de Wal, and J. Oerlemans (2005b), A new method to estimate ice age temperatures, *Clim. Dyn.*, *24*(2–3), 197–211, doi:10.1007/s00382-004-0486-x.

Bohaty, S. M., J. C. Zachos, F. Florindo, and M. L. Delaney (2009), Coupled greenhouse warming and deep-sea acidification in the middle Eocene, *Paleoceanography*, *24*, PA2207, doi:10.1029/2008PA001676.

Boon J. J., F. W. van der Meer, P. J. Schuyl, J. W. de Leeuw, P. A. Schenck, and A. L. Burlingame (1978), Organic geochemical analyses of core samples from Site 362, Walvis Ridge, DSDP Leg 40, *Initial Rep. Deep Sea Drill. Proj.*, *38/39/40/41*, supplement, 627–637.

Brassell, S., G. Eglinton, I. Marlowe, U. Pflaumann, and M. Sarnthein (1986), Molecular stratigraphy: a new tool for climatic assessment, *Nature*, *320*, 129–133, doi:10.1038/320129a0.

Brochier-Armanet, C., B. Boussau, S. Gribaldo, and P. Forterre (2008), Mesophilic Crenarchaeota: Proposal for a third archaeal phylum, the Thaumarchaeota, *Nat. Rev. Microbiol.*, *6*(3), 245–252, doi:10.1038/nrmicro1852.

Brown, S. J., and H. Elderfield (1996), Variations in Mg/Ca and Sr/Ca ratios of planktonic foraminifera caused by postdepositional dissolution: Evidence of shallow Mg-dependent dissolution, *Paleoceanography*, *11*(5), 543–551, doi:10.1029/96PA01491.

Browning, J. V., K. G. Miller, and D. K. Pak (1996), Global implications of lower to middle Eocene sequence boundaries on the New Jersey coastal plain: The icehouse cometh, *Geology*, *24*(7), 639–642, doi:10.1130/0091-7613(1996)024<0639:GIOLTM>2.3.CO;2.

Browning, J. V., K. G. Miller, P. J. Sugarman, M. A. Kominz, P. P. McLaughlin, A. A. Kulpecz, and M. D. Feigenson (2008), 100 Myr record of sequences, sedimentary facies and sea level change from Ocean Drilling Program onshore coreholes, US Mid-Atlantic coastal plain, *Basin Res.*, *20*(2), 227–248, doi:10.1111/j.1365-2117.2008.00360.x.

Christie-Blick, N., J. P. Grotzinger, and C. von der Borch (1988), Sequence stratigraphy in Proterozoic successions, *Geology*, *16*(2), 100–104, doi:10.1130/0091-7613(1988)016<0100:SSIPS>2.3.CO;2.

Clark, P. U., A. S. Dyke, J. D. Shakun, A. E. Carlson, J. Clark, B. Wohlfarth, J. X. Mitrovica, S. W. Hostetler, and A. M. McCabe (2009), The Last Glacial Maximum, *Science*, *325*(5941), 710–714, doi:10.1126/science.1172873.

Coggon, R. M., D. A. H. Teagle, C. E. Smith-Duque, J. C. Alt, and M. J. Cooper (2010), Reconstructing past seawater Mg/Ca and Sr/Ca from mid-ocean ridge flank calcium carbonate veins, *Science*, *327*(5969), 1114–1117, doi:10.1126/science.1182252.

Conrad, C. P., C. Lithgow-Bertelloni, and K. E. Louden (2004), Iceland, the Farallon slab, and dynamic topography of the North Atlantic, *Geology*, *32*(3), 177–180, doi:10.1130/G20137.1.

Conte, M. H., A. Thompson, D. Lesley, and R. P. Harris (1998), Genetic and physiological influences on the alkenone/alkenoate versus growth temperature relationship in *Emiliania huxleyi* and *Gephyrocapsa oceanica*, *Geochim. Cosmochim. Acta*, *62*(1), 51–68, doi:10.1016/S0016-7037(97)00327-X.

Covey, C., L. C. Sloan, and M. I. Hoffert (1996), Paleoclimate data constraints on climate sensitivity: The paleocalibration method, *Clim. Change*, *32*(2), 165–184, doi:10.1007/BF00143708.

Cox, S. E., S. N. Thompson, P. W. Reiners, S. R. Hemming, and T. van de Flierdt (2010), Extremely low long-term erosion rates around the Gamburtsev Mountains in interior East Antarctica, *Geophys. Res. Lett.*, *37*, L22307, doi:10.1029/2010GL045106.

Coxall, H. K., and P. N. Pearson (2007), The Eocene-Oligocene transition, in *Deep Time Perspectives on Climate Change: Marrying the Signal From Computer Models and Biological Proxies*, edited by M. Williams et al., pp. 351–387, Geol. Soc., Bath, U. K.

Coxall, H. K., P. A. Wilson, H. Pälike, C. H. Lear, and J. Backman (2005), Rapid stepwise onset of Antarctic glaciation and deeper calcite compensation in the Pacific Ocean, *Nature*, *433*, 53–57, doi:10.1038/nature03135.

Cramer, B. S., J. R. Toggweiler, J. D. Wright, M. E. Katz, and K. G. Miller (2009), Ocean overturning since the Late Cretaceous: Inferences from a new benthic foraminiferal isotope compilation, *Paleoceanography*, *24*, PA4216, doi:10.1029/2008PA001683.

Cramer, B. S., K. G. G. Miller, P. J. Barrett, and J. D. Wright (2011), Late Cretaceous-Neogene trends in deep ocean temperature and continental ice volume: Reconciling records of benthic foraminiferal geochemistry (δ^{18}O and Mg/Ca) with sea level history, *J. Geophys. Res.*, *116*, C12023, doi:10.1029/2011JC007255.

Creech, J. B., J. A. Baker, C. J. Hollis, H. E. G. Morgans, and E. G. C. Smith (2010), Eocene sea temperatures for the mid-latitude southwest Pacific from Mg/Ca ratios in planktonic and benthic foraminifera, *Earth Planet. Sci. Lett.*, *299*(3–4), 483–495, doi:10.1016/j.epsl.2010.09.039.

Crowley, T. (1990), Are there any satisfactory geologic analogs for a future greenhouse warming?, *J. Clim.*, *3*(11), 1282–1292, doi:10.1175/1520-0442(1990)003<1282:ATASGA>2.0.CO;2.

Dansgaard, W. (1964), Stable isotopes in precipitation, *Tellus*, *16*(4), 436–468, doi:10.1111/j.2153-3490.1964.tb00181.x.

Dawber, C. F., and A. K. Tripati (2011), Constraints on glaciation in the middle Eocene (46–37 Ma) from Ocean Drilling Program (ODP) Site 1209 in the tropical Pacific Ocean, *Paleoceanography*, *26*, PA2208, doi:10.1029/2010PA002037.

Dawber, C. F., A. K. Tripati, A. S. Gale, C. MacNiocaill, and S. P. Hesselbo (2011), Glacioeustasy during the middle Eocene? Insights from the stratigraphy of the Hampshire Basin, UK, *Palaeogeogr. Palaeoclimatol. Palaeoecol.*, *300*(1–4), 84–100, doi:10.1016/j.palaeo.2010.12.012.

De Angelis, H., and P. Skvarca (2003), Glacier surge after ice shelf collapse, *Science*, *299*(5612), 1560–1562, doi:10.1126/science.1077987.

de Boer, B., R. S. W. van de Wal, R. Bintanja, L. Lourens, and E. Tuenter (2010), Cenozoic global ice-volume and temperature simulations with 1-D ice-sheet models forced by benthic δ^{18}O records, *Ann. Glaciol.*, *51*(55), 23–33, doi:10.3189/172756410791392736.

de Boer, B., R. S. W. van de Wal, L. J. Lourens, and R. Bintanja (2012), Transient nature of the Earth's climate and the implications for the interpretation of benthic δ^{18}O records, *Palaeogeogr. Palaeoclimatol. Palaeoecol.*, doi:10.1016/j.palaeo.2011.02.001, in press.

DeConto, R. M., and D. Pollard (2003a), A coupled climate ice sheet modeling approach to the early Cenozoic history of the Antarctic ice sheet, *Palaeogeogr. Palaeoclimatol. Palaeoecol.*, *198*, 39–52, doi:10.1016/S0031-0182(03)00393-6.

DeConto, R. M., and D. Pollard (2003b), Rapid Cenozoic glaciation of Antarctica induced by declining atmospheric CO_2, *Nature*, *1317*(2001), 1313–1317.

DeConto, R. M., D. Pollard, and D. Harwood (2007), Sea ice feedback and Cenozoic evolution of Antarctic climate and ice sheets, *Paleoceanography*, *22*, PA3214, doi:10.1029/2006PA001350.

DeConto, R. M., C. Lear, M. Pagani, D. Pollard, P. Wilson, and H. Pälike (2008), Thresholds for Cenozoic bipolar glaciation, *Nature*, *455*, 652–656, doi:10.1038/nature07337.

Dickson, J. A. D. (2002), Fossil echinoderms as monitor of the Mg/Ca ratio of Phanerozoic oceans, *Science*, *298*(5596), 1222–1224, doi:10.1126/science.1075882.

Dowsett, H. J., R. Thompson, J. Barron, T. Cronin, F. Fleming, S. Ishman, R. Poore, D. Willard, and T. Holtz (1994), Joint investigations of the middle Pliocene climate I: PRISM paleoenvironmental reconstructions, *Global Planet. Change*, *9*(3–4), 169–195, doi:10.1016/0921-8181(94)90015-9.

Dupont-Nivet, G., W. Krijgsman, C. G. Langereis, H. A. Abels, S. Dai, and X. Fang (2007), Tibetan plateau aridification linked to global cooling at the Eocene-Oligocene transition, *Nature*, *445*(7128), 635–638, doi:10.1038/nature05516.

Dutton, A., K. C. Lohmann, and R. M. Leckie (2005), Insights from the Paleogene tropical Pacific: Foraminiferal stable isotope and elemental results from Site 1209, Shatsky Rise, *Paleoceanography*, *20*, PA3004, doi:10.1029/2004PA001098.

Elderfield, H., M. Greaves, S. Barker, I. R. Hall, A. Tripati, P. Ferretti, S. Crowhurst, L. Booth, and C. Daunt (2010), A record of bottom water temperature and seawater $\delta^{18}O$ for the Southern Ocean over the past 440 kyr based on Mg/Ca of benthic foraminiferal *Uvigerina* spp, *Quat. Sci. Rev.*, *29*(1-2), 160–169, doi:10.1016/j.quascirev.2009.07.013.

Eldrett, J. S., I. C. Harding, P. A. Wilson, E. Butler, and A. P. Roberts (2007), Continental ice in Greenland during the Eocene and Oligocene, *Nature*, *446*(7132), 176–179, doi:10.1038/nature05591.

Eldrett, J. S., D. R. Greenwood, I. C. Harding, and M. Huber (2009), Increased seasonality through the Eocene to Oligocene transition in northern high latitudes, *Nature*, *459*(7249), 969–973, doi:10.1038/nature08069.

Exon, N. F., et al. (2001), *Proceedings of the Ocean Drilling Program, Initial Reports*, vol. 189, Ocean Drill. Program, College Station, Tex.

Fairbanks, R. G. (1989), A 17,000-year glacio-eustatic sea level record: influence of glacial melting rates on the Younger Dryas event and deep-ocean circulation, *Nature*, *342*, 637–642, doi:10.1038/342637a0.

Fitzgerald, P. (2002), Tectonics and landscape evolution of the Antarctic Plate since the breakup of Gondwana with an emphasis on the West Antarctic Rift System and the Transantarctic Mountains, in *Antarctica at the Close of a Millennium: Proceedings of the 8th International Symposium on Antarctic Earth Sciences, Wellington, 1999*, pp. 453–469, R. Soc. of N. Z., Wellington.

Gebbie, G., and P. Huybers (2011), How is the ocean filled?, *Geophys. Res. Lett.*, *38*, L06604, doi:10.1029/2011GL046769.

Gulsen, M., A. E. Smith, and D. M. Tate (1995), A genetic algorithm approach to curve fitting, *Int. J. Prod. Res.*, *33*(7), 1911–1923, doi:10.1080/00207549508904789.

Haq, B. U., J. Hardenbol, and P. R. Vail (1987), Chronology of fluctuating sea levels since the Triassic, *Science*, *235*(4793), 1156, doi:10.1126/science.235.4793.1156.

Haywood, A. M., A. Ridgwell, D. J. Lunt, D. J. Hill, M. J. Pound, H. J. Dowsett, A. M. Dolan, J. E. Francis, and M. Williams (2011), Are there pre-Quaternary geological analogues for a future greenhouse warming?, *Philos. Trans. R. Soc. A*, *369*, 933–956, doi:10.1098/rsta.2010.0317.

Herbert, T. (2003), Alkenone paleotemperature determinations, in *Treatise on Geochemistry*, vol. 6, *The Oceans and Marine Geochemistry*, edited by H. Elderfield, chap. 15, pp. 391–432, Elsevier, Amsterdam.

Herbert, T. D., L. C. Peterson, K. T. Lawrence, and Z. Liu (2010), Tropical ocean temperatures over the past 3.5 million years, *Science*, *328*(5985), 1530–1534, doi:10.1126/science.1185435.

Hollis, C. J., et al. (2009), Tropical sea temperatures in the high-latitude South Pacific during the Eocene, *Geology*, *37*(2), 99–102, doi:10.1130/G25200A.1.

Huber, M. (2008), A hotter greenhouse?, *Science*, *321*(5887), 353–354, doi:10.1126/science.1161170.

Huber, M., H. Brinkhuis, C. E. Stickley, K. Döös, A. Sluijs, J. Warnaar, S. A. Schellenberg, and G. L. Williams (2004), Eocene circulation of the Southern Ocean: Was Antarctica kept warm by subtropical waters?, *Paleoceanography*, *19*, PA4026, doi:10.1029/2004PA001014.

Huguet, C., J. E. Cartes, J. S. S. Damsté, and S. Schouten (2006), Marine crenarchaeotal membrane lipids in decapods: Implications for the TEX_{86} paleothermometer, *Geochem. Geophys. Geosyst.*, *7*, Q11010, doi:10.1029/2006GC001305.

Huguet, C., A. Schimmelmann, R. Thunell, L. J. Lourens, J. S. S. Damsté, and S. Schouten (2007), A study of the TEX_{86} paleothermometer in the water column and sediments of the Santa Barbara Basin, California, *Paleoceanography*, *22*, PA3203, doi:10.1029/2006PA001310.

Huguet, C., J. Kim, G. de Lange, J. S. Sinninghe Damsté, and S. Schouten (2009), Effects of long term oxic degradation on the $U^{k'}_{37}$, TEX_{86} and BIT organic proxies, *Org. Chem.*, *40*(12), 1188–1194, doi:10.1016/j.orggeochem.2009.09.003.

Huybrechts, P. (1993), Glaciological modelling of the late Cenozoic East Antarctic Ice Sheet: Stability or dynamism?, *Geogr. Ann., Ser. A*, *75*(4), 221, doi:10.2307/521202.

Jaeger, C., H. J. Schellnhuber, and V. Brovkin (2008), Stern's Review and Adam's fallacy, *Clim. Change*, *89*(3–4), 207–218, doi:10.1007/s10584-008-9436-7.

John, C. M., G. D. Karner, E. Browning, R. M. Leckie, Z. Mateo, B. Carson, and C. Lowery (2011), Timing and magnitude of Miocene eustasy derived from the mixed siliciclastic-carbonate stratigraphic record of the northeastern Australian margin, *Earth Planet. Sci. Lett.*, *304*(3–4), 455–467, doi:10.1016/j.epsl.2011.02.013.

Jouzel, J., et al. (2007), Orbital and millennial Antarctic climate variability over the past 800,000 years, *Science*, *317*(5839), 793–796, doi:10.1126/science.1141038.

Karner, M. B., E. F. DeLong, and D. M. Karl (2001), Archaeal dominance in the mesopelagic zone of the Pacific Ocean, *Nature*, *409*(6819), 507–510, doi:10.1038/35054051.

Katz, M. E., K. G. Miller, J. D. Wright, B. S. Wade, J. V. Browning, B. S. Cramer, and Y. Rosenthal (2008), Stepwise transition from the Eocene greenhouse to the Oligocene icehouse, *Nat. Geosci.*, *1*(5), 329–334, doi:10.1038/ngeo179.

Katz, M. E., B. S. Cramer, J. R. Toggweiler, G. Esmay, C. Liu, K. G. Miller, Y. Rosenthal, B. S. Wade, and J. D. Wright (2011), Impact of Antarctic Circumpolar Current development on late Paleogene ocean structure, *Science*, *332*(6033), 1076–1079, doi:10.1126/science.1202122.

Keating-Bitonti, C. R., L. C. Ivany, H. P. Affek, P. Douglas, and S. D. Samson (2011), Warm, not super-hot, temperatures in the early Eocene subtropics, *Geology*, *29*(8), 771–774, doi:10.1130/G32054.1.

Kennett, J. P. (1977), Cenozoic evolution of Antarctic glaciation, the circum-Antarctic Ocean, and their impact on global paleoceanography, *J. Geophys. Res.*, *82*(27), 3843–3860, doi:10.1029/JC082i027p03843.

Kim, J. H., S. Schouten, E. C. Hopmans, B. Donner, and J. S. Sinninghe Damsté (2008), Global sediment core-top calibration of the TEX_{86} paleothermometer in the ocean, *Geochim. Cosmochim. Acta*, *72*(4), 1154–1173, doi:10.1016/j.gca.2007.12.010.

Kim, J. H., J. van der Meer, S. Schouten, P. Helmke, V. Willmott, F. Sangiorgi, N. Koç, E. C. Hopmans, and J. S. S. Damsté (2010), New indices and calibrations derived from the distribution of crenarchaeal isoprenoid tetraether lipids: Implications for past sea surface temperature reconstructions, *Geochim. Cosmochim. Acta*, *74*(16), 4639–4654, doi:10.1016/j.gca.2010.05.027.

Kominz, M. A., J. V. Browning, K. G. Miller, P. J. Sugarman, S. Mizintseva, and C. R. Scotese (2008), Late Cretaceous to Miocene sea-level estimates from the New Jersey and Delaware coastal plain coreholes: An error analysis, *Basin Res.*, *20*(2), 211–226, doi:10.1111/j.1365-2117.2008.00354.x.

Krystek, M., and M. Anton (2007), A weighted total least-squares algorithm for fitting a straight line, *Meas. Sci. Technol.*, *18*(11), 3438–3442, doi:10.1088/0957-0233/18/11/025.

Langebroek, P. M., A. Paul, and M. Schulz (2009), Antarctic ice-sheet response to atmospheric CO_2 and insolation in the middle Miocene, *Clim. Past*, *5*(4), 633–646, doi:10.5194/cp-5-633-2009.

Larson, R. L. (1991), Geological consequences of superplumes, *Geology*, *19*, 963–966, doi:10.1130/0091-7613(1991)019<0963:GCOS>2.3.CO;2.

Lea, D. W., T. A. Mashiotta, and H. J. Spero (1999), Controls on magnesium and strontium uptake in planktonic foraminifera determined by live culturing, *Geochim. Cosmochim. Acta*, *63*, 2369–2379.

Lear, C. H. (2007), Mg/Ca palaeothermometry: A new window into Cenozoic climate change, in *Deep Time Perspectives on Climate Change: Marrying the Signal From Computer Models and Biological Proxies*, edited by M. Williams et al., pp. 313–322, Geol. Soc., Bath, U. K.

Lear, C. H., H. Elderfield, and P. A. Wilson (2000), Cenozoic deep-sea temperatures and global ice volumes from Mg/Ca in benthic foraminiferal calcite, *Science*, *287*(5451), 269, doi:10.1126/science.287.5451.269.

Lear, C. H., Y. Rosenthal, H. K. Coxall, and P. A. Wilson (2004), Late Eocene to early Miocene ice sheet dynamics and the global carbon cycle, *Paleoceanography*, *19*, PA4015, doi:10.1029/2004PA001039.

Lear, C. H., E. Mawbey, and Y. Rosenthal (2010), Cenozoic benthic foraminiferal Mg/Ca and Li/Ca records: Toward unlocking temperatures and saturation states, *Paleoceanography*, *25*, PA4215, doi:10.1029/2009PA001880.

Lear, C. H., T. Bailey, P. N. Pearson, H. Coxall, and Y. Rosenthal (2008), Cooling and ice growth across the Eocene-Oligocene transition, *Geology*, *36*(3), 251–254, doi:10.1130/G24584A.1.

Lemke, P., et al. (2007), Observations: Changes in snow, ice and frozen ground, in *Climate Change 2007: The Physical Science Basis: Working Group I Contribution to the Fourth Assessment Report of the IPCC*, edited by S. Solomon et al., pp. 339–383, Cambridge Univ. Press, New York.

Lisiecki, L. E., and M. E. Raymo (2005), A Pliocene-Pleistocene stack of 57 globally distributed benthic $\delta^{18}O$ records, *Paleoceanography*, *20*, PA1003, doi:10.1029/2004PA001071.

Liu, Z., M. Pagani, D. Zinniker, R. M. DeConto, M. Huber, H. Brinkhuis, S. R. Shah, R. M. Leckie, and A. Pearson (2009), Global cooling during the Eocene-Oligocene climate transition, *Science*, *323*(5918), 1187–1190, doi:10.1126/science.1166368.

Lowenstein, T. K., M. N. Timofeeff, S. T. Brennan, L. A. Hardie, and R. V. Demicco (2001), Oscillations in Phanerozoic seawater chemistry: Evidence from fluid inclusions, *Science*, *294*(5544), 1086–1088, doi:10.1126/science.1064280.

Lythe, M., and D. Vaughan (2001), BEDMAP: A new ice thickness and subglacial topographic model of Antarctica, *J. Geophys. Res.*, *106*, 11,335–11,351, doi:10.1029/2000JB900449.

Markwick, P. (1998), Fossil crocodilians as indicators of Late Cretaceous and Cenozoic climates: Implications for using palaeontological data in reconstructing palaeoclimate, *Palaeogeogr. Palaeoclimatol. Palaeoecol.*, *137*(3–4), 205–271, doi:10.1016/S0031-0182(97)00108-9.

Marlowe, I. T. (1984), Lipids as paleoclimatic indicators, Ph.D. thesis, Univ. of Bristol, Bristol, U. K.

Marlowe, I., S. Brassell, G. Eglinton, and J. Green (1990), Long-chain alkenones and alkyl alkenoates and the fossil coccolith record of marine sediments, *Chem. Geol.*, *88*(3–4), 349–375, doi:10.1016/0009-2541(90)90098-R.

Martin, P. A., D. W. Lea, Y. Rosenthal, N. J. Shackleton, M. Sarnthein, and T. Papenfuss (2002), Quaternary deep sea temperature histories derived from benthic foraminiferal Mg/Ca, *Earth Planet. Sci. Lett.*, *198*(1–2), 193–209, doi:10.1016/S0012-821X(02)00472-7.

Matthews, R. K., and R. Z. Poore (1980), Tertiary $\delta^{18}O$ record and glacio-eustatic sea-level fluctuations, *Geology*, *8*, 501–504, doi:10.1130/0091-7613(1980)8<501:TORAGS>2.0.CO;2.

Medina-Elizalde, M., and D. W. Lea (2005), The mid-Pleistocene transition in the Tropical Pacific, *Science*, *310*(5750), 1009–1012, doi:10.1126/science.1115933.

Miall, A. D. (1992), Exxon global cycle chart: An event for every occasion?, *Geology*, *20*(9), 787–790, doi:10.1130/0091-7613(1992)020<0787:EGCCAE>2.3.CO;2.

Micheels, A., A. A. Bruch, D. Uhl, T. Utescher, and V. Mosbrugger (2007), A late Miocene climate model simulation with ECHAM4/ML and its quantitative validation with terrestrial proxy data, *Palaeogeogr. Palaeoclimatol. Palaeoecol.*, *253*(1–2), 251–270, doi:10.1016/j.palaeo.2007.03.042.

Miller, K. G., R. G. Fairbanks, and G. S. Mountain (1987), Tertiary oxygen isotope synthesis, sea level history, and continental margin erosion, *Paleoceanography*, *2*(1), 1–19, doi:10.1029/PA002i001p00001.

Miller, K. G., G. S. Mountain, J. V. Browning, M. Kominz, P. J. Sugarman, N. Christie-Blick, M. E. Katz, and J. D. Wright (1998), Cenozoic global sea level, sequences, and the New Jersey transect: Results from coastal plain and continental slope drilling, *Rev. Geophys.*, *36*(4), 569–601, doi:10.1029/98RG01624.

Miller, K. G., M. A. Kominz, J. V. Browning, J. D. Wright, G. S. Mountain, M. E. Katz, P. J. Sugarman, B. S. Cramer, N. Christie-Blick, and S. F. Pekar (2005a), The Phanerozoic record of global sea-level change, *Science*, *310*(5752), 1293–1298, doi:10.1126/science.1116412.

Miller, K. G., J. Wright, and J. Browning (2005b), Visions of ice sheets in a greenhouse world, *Mar. Geol.*, *217*(3–4), 215–231, doi:10.1016/j.margeo.2005.02.007.

Miller, K. G., J. Wright, M. Katz, J. Browning, B. Cramer, B. Wade, and S. Mizintseva (2008), A view of Antarctic ice-sheet evolution from sea-level and deep-sea isotope changes during the Late Cretaceous–Cenozoic, in *Antarctica: A Keystone in a Changing World*, pp. 55–70, Natl. Acad., Washington D. C.

Miller, K. G., J. D. Wright, M. E. Katz, B. S. Wade, J. V. Browning, and B. S. Cramer (2009a), Climate threshold at the Eocene-Oligocene transition: Antarctic ice sheet influence on ocean circulation, in *The Late Eocene Earth: Hothouse, Icehouse and Impacts*, *Spec. Pap. Geol. Soc. Am.*, *452*, 169–178.

Miller, K. G., P. J. Sugarman, J. V. Browning, B. P. Horton, A. Stanley, A. Kahn, J. Uptegrove, and M. Aucott (2009b), Sea-level rise in New Jersey over the past 5000 years: Implications to anthropogenic changes, *Global Planet. Change*, *66*(1–2), 10–18, doi:10.1016/j.gloplacha.2008.03.008.

Mitrovica, J. X., M. E. Tamisiea, J. L. Davis, and G. A. Milne (2001), Recent mass balance of polar ice sheets inferred from patterns of global sea-level change, *Nature*, *409*(6823), 1026–1029, doi:10.1038/35059054.

Mitrovica, J. X., N. Gomez, and P. U. Clark (2009), The sea-level fingerprint of West Antarctic collapse, *Science*, *323*(5915), 753, doi:10.1126/science.1166510.

Moran, K., et al. (2006), The Cenozoic palaeoenvironment of the Arctic Ocean, *Nature*, *441*(7093), 601–605, doi:10.1038/nature04800.

Müller, P. J., G. Kirst, G. Ruhland, I. von Storch, and A. Rosell-Melé (1998), Calibration of the alkenone paleotemperature index $U^{k'}_{37}$ based on core-tops from the eastern South Atlantic and the global ocean (60°N–60°S), *Geochim. Cosmochim. Acta*, *62*(10), 1757–1772, doi:10.1016/S0016-7037(98)00097-0.

Müller, R. D., M. Sdrolias, C. Gaina, B. Steinberger, and C. Heine (2008), Long-term sea-level fluctuations driven by ocean basin dynamics, *Science*, *319*(5868), 1357–1362, doi:10.1126/science.1151540.

Najjar, R. G., G. T. Nong, D. Seidov, and W. H. Peterson (2002), Modeling geographic impacts on early Eocene ocean temperature, *Geophys. Res. Lett.*, *29*(15), 1750, doi:10.1029/2001GL014438.

Nong, G. T., R. G. Najjar, D. Seidov, and W. H. Peterson (2000), Simulation of ocean temperature change due to the opening of Drake Passage, *Geophys. Res. Lett.*, *27*(17), 2689–2692, doi:10.1029/1999GL011072.

Notz, D. (2009), The future of ice sheets and sea ice: Between reversible retreat and unstoppable loss, *Proc. Natl. Acad. Sci. U. S. A.*, *106*(49), 20,590–20,595, doi:10.1073/pnas.0902356106.

Nürnberg, D., J. Bijma, and C. Hemleben (1996), Assessing the reliability of magnesium in foraminiferal calcite as a proxy

for water mass temperatures, *Geochim. Cosmochim. Acta*, *60*(5), 803–814, doi:10.1016/0016-7037(95)00446-7.

Oerlemans, J. (1982), Glacial cycles and ice-sheet modelling, *Clim. Change*, *4*(4), 353–374.

Oerlemans, J. (2002), On glacial inception and orography, *Quat. Int.*, *95–96*, 5–10, doi:10.1016/S1040-6182(02)00022-8.

Oerlemans, J. (2004), Correcting the Cenozoic δ^{18}O deep-sea temperature record for Antarctic ice volume, *Palaeogeogr. Palaeoclimatol. Palaeoecol.*, *208*(3–4), 195–205, doi:10.1016/j.palaeo.2004.03.004.

Pagani, M., J. C. Zachos, K. H. Freeman, B. Tipple, and S. Bohaty (2005), Marked decline in atmospheric carbon dioxide concentrations during the Paleogene, *Science*, *309*(5734), 600–603, doi:10.1126/science.1110063.

Pearson, P. N., and M. R. Palmer (2000), Atmospheric carbon dioxide concentrations over the past 60 million years, *Nature*, *406*(6797), 695–699, doi:10.1038/35021000.

Pearson, P. N., B. E. van Dongen, C. J. Nicholas, R. D. Pancost, S. Schouten, J. M. Singano, and B. S. Wade (2007), Stable warm tropical climate through the Eocene Epoch, *Geology*, *35*(3), 211–214, doi:10.1130/G23175A.1.

Pearson, P. N., I. K. McMillan, B. S. Wade, T. D. Jones, H. K. Coxall, P. R. Bown, and C. H. Lear (2008), Extinction and environmental change across the Eocene-Oligocene boundary in Tanzania, *Geology*, *36*(2), 179–182, doi:10.1130/G24308A.1.

Pearson, P. N., G. L. Foster, and B. S. Wade (2009), Atmospheric carbon dioxide through the Eocene–Oligocene climate transition, *Nature*, *461*, 1110–1113, doi:10.1038/nature08447.

Peck, V. L., J. Yu, S. Kender, and C. R. Riesselman (2010), Shifting ocean carbonate chemistry during the Eocene-Oligocene climate transition: Implications for deep-ocean Mg/Ca paleothermometry, *Paleoceanography*, *25*, PA4219, doi:10.1029/2009PA001906.

Pekar, S. F., N. Christie-Blick, M. A. Kominz, and K. G. Miller (2002), Calibration between eustatic estimates from backstripping and oxygen isotopic records for the Oligocene, *Geology*, *30*(10), 903–906, doi:10.1130/0091-7613(2002)030<0903:CBEEFB>2.0.CO;2.

Pekar, S. F., A. Hucks, M. Fuller, and S. Li (2005), Glacioeustatic changes in the early and middle Eocene (51–42 Ma): Shallow-water stratigraphy from ODP Leg 189 Site 1171(South Tasman Rise) and deep-sea δ^{18}O records, *Geol. Soc. Am. Bull.*, *117*(7), 1081, doi:10.1130/B25486.1.

Pekar, S. F., R. M. DeConto, and D. M. Harwood (2006), Resolving a late Oligocene conundrum: Deep-sea warming and Antarctic glaciation, *Palaeogeogr. Palaeoclimatol. Palaeoecol.*, *231*(1–2), 29–40, doi:10.1016/j.palaeo.2005.07.024.

Peltier, W. R. (1974), The impulse response of a Maxwell Earth, *Rev. Geophys.*, *12*(4), 649–669, doi:10.1029/RG012i004p00649.

Peters, S. E., A. E. Carlson, D. C. Kelly, and P. D. Gingerich (2010), Large-scale glaciation and deglaciation of Antarctica during the Late Eocene, *Geology*, *38*(8), 723–726, doi:10.1130/G31068.1.

Petersen, K. D., S. B. Nielsen, O. R. Clausen, R. Stephenson, and T. Gerya (2010), Small-scale mantle convection produces stratigraphic sequences in sedimentary basins, *Science*, *329*(5993), 827–830, doi:10.1126/science.1190115.

Pollard, D. (1982), A simple ice sheet model yields realistic 100 kyr glacial cycles, *Nature*, *296*(5855), 334–338, doi:10.1038/296334a0.

Pollard, D. (2010), A retrospective look at coupled ice sheet–climate modeling, *Clim. Change*, *100*(1), 173–194, doi:10.1007/s10584-010-9830-9.

Pollard, D., and R. M. DeConto (2005), Hysteresis in Cenozoic Antarctic ice-sheet variations, *Global Planet. Change*, *45*(1–3), 9–21, doi:10.1016/j.gloplacha.2004.09.011.

Pollard, D., and R. M. DeConto (2009), Modelling West Antarctic Ice Sheet growth and collapse through the past five million years, *Nature*, *458*(7236), 329–332, doi:10.1038/nature07809.

Prahl, F., and S. Wakeham (1987), Calibration of unsaturation patterns in long-chain ketone compositions for palaeotemperature assessment, *Nature*, *330*, 367–369, doi:10.1038/330367a0.

Prahl, F., R. Collier, J. Dymond, M. Lyle, and M. Sparrow (1993), A biomarker perspective on prymnesiophyte productivity in the northeast Pacific Ocean, *Deep Sea Res., Part I*, *40*(10), 2061–2076, doi:10.1016/0967-0637(93)90045-5.

Prahl, F., C. Pilskaln, and M. Sparrow (2001), Seasonal record for alkenones in sedimentary particles from the Gulf of Maine, *Deep Sea Res., Part I*, *48*(2), 515–528, doi:10.1016/S0967-0637(00)00057-1.

Prahl, F. G., G. V. Wolfe, and M. A. Sparrow (2003), Physiological impacts on alkenone paleothermometry, *Paleoceanography*, *18*(2), 1025, doi:10.1029/2002PA000803.

Pusz, A. E., R. C. Thunell, and K. G. Miller (2011), Deep water temperature, carbonate ion, and ice volume changes across the Eocene-Oligocene climate transition, *Paleoceanography*, *26*, PA2205, doi:10.1029/2010PA001950.

Rahmstorf, S. (2007), A semi-empirical approach to projecting future sea-level rise, *Science*, *315*(5810), 368–370, doi:10.1126/science.1135456.

Raymo, M. E., J. X. Mitrovica, M. J. O'Leary, R. M. DeConto, and P. J. Hearty (2011), Departures from eustasy in Pliocene sea-level records, *Nat. Geosci.*, *4*(5), 328–332, doi:10.1038/ngeo1118.

Rignot, E., G. Casassa, P. Gogineni, W. Krabill, A. Rivera, and R. Thomas (2004), Accelerated ice discharge from the Antarctic Peninsula following the collapse of Larsen B ice shelf, *Geophys. Res. Lett.*, *31*, L18401, doi:10.1029/2004GL020697.

Rohling, E. J., and S. Cooke (1999), Stable oxygen and carbon isotope ratios in foraminiferal carbonate, in *Modern Foraminifera*, edited by B. K. Sen Gupta, chap. 14, pp. 239–258, Kluwer Acad., Dordrecht, Netherlands.

Rohling, E., K. Grant, M. Bolshaw, A. Roberts, M. Siddall, C. Hemleben, and M. Kucera (2009), Antarctic temperature and global sea level closely coupled over the past five glacial cycles, *Nat. Geosci.*, *2*, 500–504, doi:10.1038/ngeo557.

Rohling, E. J., M. Medina-Elizalde, J. G. Shepherd, M. Siddall, and J. D. Stanford (2012), Sea surface and high-latitude temperature sensitivity to radiative forcing of climate over several glacial cycles, *J. Clim.*, doi:10.1175/2011JCLI4078.1, in press.

Rosenthal, Y., and G. P. Lohmann (2002), Accurate estimation of sea surface temperatures using dissolution-corrected calibrations for Mg/Ca paleothermometry, *Paleoceanography*, *17*(3), 1044, doi:10.1029/2001PA000749.

Rosenthal, Y., E. A. Boyle, and N. Slowey (1997), Temperature control on the incorporation of magnesium, strontium, fluorine, and cadmium into benthic foraminiferal shells from Little Bahama Bank: Prospects for thermocline paleoceanography, *Geochim. Cosmochim. Acta*, *61*(17), 3633–3643.

Rosenthal, Y., G. P. Lohmann, K. C. Lohmann, and R. M. Sherrell (2000), Incorporation and preservation of Mg in Globigerinoides sacculifer: Implications for reconstructing the temperature and ^{18}O/^{16}O of seawater, *Paleoceanography*, *15*(1), 135–145, doi:10.1029/1999PA000415.

Rowley, D. B. (2002), Rate of plate creation and destruction: 180 Ma to present, *Geol. Soc. Am. Bull.*, *114*(8), 927–933, doi:10.1130/0016-7606(2002)114<0927:ROPCAD>2.0.CO;2.

Sahagian, D., and M. Jones (1993), Quantified Middle Jurassic to Paleocene eustatic variations based on Russian Platform stratigraphy: Stage level resolution, *Geol. Soc. Am. Bull.*, *105*(8), 1109–1118.

Savin, S. M., and R. G. Douglas (1973), Stable isotope and magnesium geochemistry of recent planktonic foraminifera from the South Pacific, *Geol. Soc. Am. Bull.*, *84*(7), 2327–2342, doi:10.1130/0016-7606(1973)84<2327:SIAMGO>2.0.CO;2.

Scherer, R. P., A. Aldahan, S. Tulaczyk, G. Possnert, H. Engelhardt, and B. Kamb (1998), Pleistocene collapse of the West Antarctic Ice Sheet, *Science*, *281*(5373), 82–85, doi:10.1126/science.281.5373.82.

Schneider von Deimling, T., A. Ganopolski, H. Held, and S. Rahmstorf (2006), How cold was the Last Glacial Maximum?, *Geophys. Res. Lett.*, *33*, L14709, doi:10.1029/2006GL026484.

Schouten, S., E. C. Hopmans, E. Schefuß, and J. S. Sinninghe Damsté (2002), Distributional variations in marine crenarchaeotal membrane lipids: A new tool for reconstructing ancient sea water temperatures?, *Earth Planet. Sci. Lett.*, *204*(1–2), 265–274, doi:10.1016/S0012-821X(02)00979-2.

Sexton, P. F., P. A. Wilson, and P. N. Pearson (2006), Microstructural and geochemical perspectives on planktic foraminiferal preservation: "Glassy" versus "Frosty", *Geochem. Geophys. Geosyst.*, *7*, Q12P19, doi:10.1029/2006GC001291.

Shackleton, N. (1967), Oxygen isotope analyses and pleistocene temperatures re-assessed, *Nature*, *215*(5096), 15–17, doi:10.1038/215015a0.

Shackleton, N., and J. Kennett (1975), Paleotemperature history of the Cenozoic and the initiation of Antarctic glaciation: Oxygen and carbon isotope analyses in DSDP sites 277, 279 and 281, *Initial Rep. Deep Sea Drill. Proj.*, *29*, 743–755.

Shevenell, A. E., J. P. Kennett, and D. W. Lea (2008), Middle Miocene ice sheet dynamics, deep-sea temperatures, and carbon cycling: A Southern Ocean perspective, *Geochem. Geophys. Geosyst.*, *9*, Q02006, doi:10.1029/2007GC001736.

Siddall, M., E. J. Rohling, A. Almogi-Labin, C. Hemleben, D. Meischner, I. Schmelzer, and D. Smeed (2003), Sea-level fluctuations during the last glacial cycle, *Nature*, *423*(6942), 853–858, doi:10.1038/nature01690.

Siddall, M., B. Hönisch, C. Waelbroeck, and P. Huybers (2010a), Changes in deep Pacific temperature during the mid-Pleistocene transition and Quaternary, *Quat. Sci. Rev.*, *29*(1–2), 170–181, doi:10.1016/j.quascirev.2009.05.011.

Siddall, M., M. R. Kaplan, J. M. Schaefer, A. Putnam, M. A. Kelly, and B. Goehring (2010b), Changing influence of Antarctic and Greenlandic temperature records on sea-level over the last glacial cycle, *Quat. Sci. Rev.*, *29*, 410–423, doi:10.1016/j.quascirev.2009.11.007.

Sikes, E. L., J. W. Farrington, and L. D. Keigwin (1991), Use of the alkenone unsaturation ratio $U^{k'}_{37}$ to determine past sea surface temperatures: Core-top SST calibrations and methodology considerations, *Earth Planet. Sci. Lett.*, *104*, 36–47, doi:10.1016/0012-821X(91)90235-A.

Sikes, E. L., J. K. Volkman, L. G. Robertson, and J. J. Pichon (1997), Alkenones and alkenes in surface waters and sediments of the Southern Ocean: Implications for paleotemperature estimation in polar regions, *Geochim. Cosmochim. Acta*, *61*, 1495–1505, doi:10.1016/S0016-7037(97)00017-3.

Sikes, E., W. Howard, C. Samson, T. Mahan, L. Robertson, and J. Volkman (2009), Southern Ocean seasonal temperature and Subtropical Front movement on the South Tasman Rise in the late Quaternary, *Paleoceanography*, *24*, PA2201, doi:10.1029/2008PA001659.

Sinninghe Damsté, J. S., S. Schouten, E. C. Hopmans, A. C. T. V. Duin, and J. A. J. Geenevasen (2002), Crenarchaeol: The characteristic core glycerol dibiphytanyl glycerol tetraether membrane lipid of cosmopolitan pelagic crenarchaeota, *J. Lipid Res.*, *43*, 1641–1651, doi:10.1194/jlr.M200148-JLR200.

Solomon, S., et al. (2007), Technical summary, in *Climate Change 2007: The Physical Science Basis. Contribution of Working Group I to the Fourth Assessment Report of the Intergovernmental Panel on Climate Change*, edited by S. Solomon et al., pp. 18–91, Cambridge Univ. Press, New York.

Sosdian, S., and Y. Rosenthal (2009), Deep-sea temperature and ice volume changes across the Pliocene-Pleistocene climate transitions, *Science*, *325*(5938), 306–310, doi:10.1126/science.1169938.

Spasojević, S., L. Liu, M. Gurnis, and R. D. Müller (2008), The case for dynamic subsidence of the U.S. east coast since the Eocene, *Geophys. Res. Lett.*, *35*, L08305, doi:10.1029/2008GL033511.

Sprengel, C., K. H. Baumann, and S. Neuer (2000), Seasonal and interannual variation of coccolithophore fluxes and species composition in sediment traps north of Gran Canaria (29°N

15°W), *Mar. Micropaleontol.*, *39*, 157–178, doi:10.1016/S0377-8398(00)00019-0.

Stickley, C. E., H. Brinkhuis, S. A. Schellenberg, A. Sluijs, U. Röhl, M. Fuller, M. Grauert, M. Huber, J. Warnaar, and G. L. Williams (2004), Timing and nature of the deepening of the Tasmanian Gateway, *Paleoceanography*, *19*, PA4027, doi:10.1029/2004PA001022.

ten Brink, U. S., R. I. Hackney, S. Bannister, T. A. Stern, and Y. Makovsky (1997), Uplift of the Transantarctic Mountains and the bedrock beneath the East Antarctic Ice Sheet, *J. Geophys. Res.*, *102*(B12), 27,603–27,621, doi:10.1029/97JB02483.

Ternois, Y., M.-A. Sicre, A. Boireau, L. Beaufort, J. C. Miquel, and C. Jeandel (1998), Hydrocarbons, sterols and alkenones in sinking particles in the Indian Ocean sector of the Southern Ocean, *Org. Geochem.*, *28*(7–8), 489–501, doi:10.1016/S0146-6380(98)00008-4.

Thompson, S. L., and D. Pollard (1997), Ice-sheet mass balance at the Last Glacial Maximum from the GENESIS version 2 global climate model, *Ann. Glaciol.*, *25*, 250–258.

Thomsen, C., D. E. Schulz-Bull, G. Petrick, and J. C. Duinker (1998), Seasonal variability of the long chain alkenone flux and the effect on the $U^{k'}_{37}$-index in the Norwegian Sea, *Org. Geochem.*, *28*(5), 311–323, doi:10.1016/S0146-6380(98)00003-5.

Toggweiler, J. R., and H. Bjornsson (2000), Drake Passage and palaeoclimate, *J. Quat. Sci.*, *15*(4), 319–328, doi:10.1002/1099-1417(200005)15:4<319::AID-JQS545>3.0.CO;2-C.

Trommer, G., M. Siccha, M. T. J. van der Meer, S. Schouten, J. S. Sinninghe Damsté, H. Schulz, C. Hemleben, and M. Kucera (2009), Distribution of Crenarchaeota tetraether membrane lipids in surface sediments from the Red Sea, *Org. Geochem.*, *40*, 724–731, doi:10.1016/j.orggeochem.2009.03.001.

Trommer, G., M. Siccha, E. J. Rohling, K. Grant, M. T. J. van der Meer, S. Schouten, U. Baranowski, and M. Kucera (2011), Sensitivity of Red Sea circulation to sea level and insolation forcing during the last interglacial, *Clim. Past*, *7*, 941–955, doi:10.5194/cp-7-941-2011.

Urey, H. C. (1947), The thermodynamic properties of isotopic substances, *J. Chem. Soc.*, *1947*, 562–581, doi:10.1039/jr9470000562.

Utescher, T., B. Erdei, L. François, and V. Mosbrugger (2007), Tree diversity in the Miocene forests of Western Eurasia, *Palaeogeogr. Palaeoclimatol. Palaeoecol.*, *253*(1–2), 226–250, doi:10.1016/j.palaeo.2007.03.041.

Utescher, T., V. Mosbrugger, D. Ivanov, and D. L. Dilcher (2009), Present-day climatic equivalents of European Cenozoic climates, *Earth Planet. Sci. Lett.*, *284*(3–4), 544–552, doi:10.1016/j.epsl.2009.05.021.

Utescher, T., M. Böhme, and V. Mosbrugger (2011), The Neogene of Eurasia: Spatial gradients and temporal trends—The second synthesis of NECLIME, *Palaeogeogr. Palaeoclimatol. Palaeoecol.*, *304*(3–4), 196–201, doi:10.1016/j.palaeo.2011.03.012.

Vail, P. R., R. M. Mitchum Jr., R. G. Todd, J. M. Widmier, S. Thompson III, J. B. Sangree, J. N. Bubb, and W. G. Hatlelid (1977), Seismic stratigraphy and global changes of sea level, in *Seismic Stratigraphy—Applications to Hydrocarbon Exploration*, edited by C. E. Payton, *AAPG Mem.*, *26*, 49–212.

Vermeer, M., and S. Rahmstorf (2009), Global sea level linked to global temperature, *Proc. Natl. Acad. Sci. U. S. A.*, *106*(51), 21,527–21,532, doi:10.1073/pnas.0907765106.

Volkman, J. K., G. Eglinton, E. D. S. Corner, and T. E. V. Forsberg (1980), Long-chain alkenes and alkenones in the marine coccolithophorid *Emiliania huxleyi*, *Phytochemistry*, *19*, 2619–2622, doi:10.1016/S0031-9422(00)83930-8.

Waelbroeck, C., L. Labeyrie, E. Michel, J. C. Duplessy, J. McManus, K. Lambeck, E. Balbon, and M. Labracherie (2002), Sea-level and deep water temperature changes derived from benthic foraminifera isotopic records, *Quat. Sci. Rev.*, *21*(1–3), 295–305, doi:10.1016/S0277-3791(01)00101-9.

Weaver, P., M. Chapman, G. Eglinton, M. Zhao, D. Rutledge, and G. Read (1999), combined coccolith, foraminiferal, and

biomarker reconstruction of paleoceanographic, *Paleoceanography*, 14(3), 336–349, doi:10.1029/1999PA900009.

Weijers, J. W. H., S. Schouten, O. C. Spaargaren, and J. S. Sinninghe Damsté (2006), Occurrence and distribution of tetraether membrane lipids in soils: Implications for the use of the TEX_{86} proxy and the BIT index, *Org. Geochem.*, 37(12), 1680–1693, doi:10.1016/j.orggeochem.2006.07.018.

Wilkinson, B. H., and T. J. Algeo (1989), Sedimentary carbonate record of calcium-magnesium cycling, *Am. J. Sci.*, 289(10), 1158–1194, doi:10.2475/ajs.289.10.1158.

Wilschut, F., R. Bintanja, and R. S. W. van de Wal (2006), Ice-sheet modelling characteristics in sea-level-based temperature reconstructions over the last glacial cycle, *J. Glaciol.*, 52(176), 149–158, doi:10.3189/172756506781828944.

Wilson, D. S., and B. P. Luyendyk (2009), West Antarctic paleotopography estimated at the Eocene-Oligocene climate transition, *Geophys. Res. Lett.*, 36, L16302, doi:10.1029/2009GL039297.

Wright, J. D., R. E. Sheridan, K. G. Miller, J. Uptegrove, B. S. Cramer, and J. V. Browning (2009), Late Pleistocene sea level on the New Jersey Margin: Implications to eustasy and deep-sea temperature, *Global Planet. Change*, 66(1–2), 93–99, doi:10.1016/j.gloplacha.2008.03.013.

Wuchter, C., S. Schouten, L. Coolen, J. Marco, and J. S. S. Damsté (2004), Temperature-dependent variation in the distribution of tetraether membrane lipids of marine Crenarchaeota: Implications for TEX_{86} paleothermometry, *Paleoceanography*, 19, PA4028, doi:10.1029/2004PA001041.

Wuchter, C., S. Schouten, S. G. Wakeham, and J. S. S. Damsté (2005), Temporal and spatial variation in tetraether membrane lipids of marine Crenarchaeota in particulate organic matter: Implications for TEX_{86} paleothermometry, *Paleoceanography*, 20, PA3013, doi:10.1029/2004PA001110.

Wuchter, C., S. Schouten, S. G. Wakeham, and J. S. S. Damsté (2006), Archaeal tetraether membrane lipid fluxes in the northeastern Pacific and the Arabian Sea: Implications for TEX_{86} paleothermometry, *Paleoceanography*, 21, PA4208, doi:10.1029/2006PA001279.

Xu, X., C. Lithgow-Bertelloni, and C. P. Conrad (2006), Global reconstructions of Cenozoic seafloor ages: Implications for bathymetry and sea level, *Earth Planet. Sci. Lett.*, 243(3–4), 552–564, doi:10.1016/j.epsl.2006.01.010.

Yokoyama, Y., K. Lambeck, P. De Deckker, P. Johnston, and L. Fifield (2000), Timing of the Last Glacial Maximum from observed sea-level minima, *Nature*, 406(6797), 713–716, doi:10.1038/35021035.

You, Y., M. Huber, R. D. Müller, C. J. Poulsen, and J. Ribbe (2009), Simulation of the Middle Miocene Climate Optimum, *Geophys. Res. Lett.*, 36, L04702, doi:10.1029/2008GL036571.

Zachos, J. C., L. D. Stott, and K. C. Lohmann (1994), Evolution of early Cenozoic marine temperatures, *Paleoceanography*, 9(2), 353–387, doi:10.1029/93PA03266.

Zachos, J. C., M. Pagani, L. Sloan, E. Thomas, and K. Billups (2001), Trends, rhythms, and aberrations in global climate 65 Ma to present, *Science*, 292(5517), 686–693, doi:10.1126/science.1059412.

Zachos, J. C., G. R. Dickens, and R. E. Zeebe (2008), An early Cenozoic perspective on greenhouse warming and carbon-cycle dynamics, *Nature*, 451(7176), 279–283, doi:10.1038/nature06588.

Zanazzi, A., M. J. Kohn, B. J. MacFadden, and D. O. Terry (2007), Large temperature drop across the Eocene-Oligocene transition in central North America, *Nature*, 445(7128), 639–642, doi:10.1038/nature05551.

E. Gasson and M. Siddall, Department of Earth Sciences, University of Bristol, Wills Memorial Building, Queen's Road, Bristol BS8 1RJ, UK. (e.gasson@bristol.ac.uk)

C. H. Lear, School of Earth and Ocean Sciences, Cardiff University, Main Building, Park Place, Cardiff CF10 3YE, UK.

D. J. Lunt, BRIDGE, School of Geographical Sciences, University of Bristol, University Road, Bristol BS8 1SS, UK.

D. Pollard, Earth and Environmental Systems Institute, College of Earth and Mineral Sciences, Pennsylvania State University, University Park, PA 16802, USA.

O. J. L. Rackham, Bristol Centre for Complexity Sciences, University of Bristol, Merchant Venturers Building, Woodland Road, Bristol BS8 1UB, UK.